DISSERTATION

DEVELOPMENT OF AN ARTIFICIALTEMPOROMANDIBULAR JOINT DISC REPLACEMENT

Submitted by

Jason Paul Kuiper

Department of Mechanical Engineering

In partial fulfillment of the requirements

for the Degree of Doctor of Philosophy

Colorado State University

Fort Collins, Colorado

Summer 2023

Doctoral Committee:

Advisor: Christian M. Puttlitz

David Prawel
Kirk McGilvray
Charles Henry

ABSTRACT

DEVELOPMENT OF AN ARTIFICIAL TEMPOROMANDIBULAR JOINT DISC REPLACEMENT

The temporomandibular joint (TMJ) is a complex bilateral ginglymoarthroidal joint containing a fibrocartilaginous disc and is essential for chewing, speaking, and swallowing. Due to the high loading frequency, small imbalances in joint homeostasis can overcome the natural capacity for adaptation and lead to a cascade of degenerative changes. For progressive TMJ disorders, resection of the TMJ disc is the leading treatment, but disc resection inherently increases stress and friction on the articular cartilage surfaces, leading to a progression to total joint replacement in 11.7% of patients. The current methods of treatment for disorders of the TMJ musculoskeletal complex are predominantly palliative and do not reliably address disorders of arthrogenous origin. Unfortunately, no synthetic TMJ disc replacements currently exist due to profound implant failures in earlier attempts. Introduction of a robust artificial TMJ disc replacement after resection will prevent further joint degradation and improve patient outcomes. Rigorous preclinical evaluation of artificial TMJ disc replacement strategies must be conducted to support future translation to humans. Therefore, the following aims are proposed: (1) Characterize the biomechanical behavior of the ovine temporomandibular joint soft tissues, (2) identify and evaluate a material candidate for a temporomandibular joint disc replacement, (3) develop in silico and in vitro methods for evaluating design candidates for artificial TMJ disc replacement, and (4) implement a temporomandibular joint disc replacement strategy in an ovine model.

ACKNOWLEDGMENTS

Thank you to Dr. Kevin Labus for his direction, thoughtful advice, and patience throughout this project. I sincerely thank Dr. Jeremiah Easley, Dr. Ryan Dobbs, and Dr. Jennifer Rawlinson for their support and feedback throughout the implant design and surgical development. Also, thank you to Grace Kuiper for all her help with editing and figure creation.

DEDICATION

To Grace, my stunning mystery companion.

TABLE OF CONTENTS

LIST OF TABLES

LIST OF FIGURES

LIST OF EQUATIONS

CHAPTER 1 - BACKGROUND

1 The temporomandibular joint

The temporomandibular joint (TMJ) is the bilateral synovial joint between the mandible and skull that is critical for communication and mastication. The articulating surfaces of the TMJ are separated by a fibrocartilage disc which helps to distribute stress in the TMJ.

1.1 Development

Prenatal development of the human temporomandibular joint (TMJ) begins at approximately 7 weeks gestation and stems from a mass of mesenchymal stem cells at the center of the maturing joint [1]. Development of the TMJ is unique from other articular joints because it forms from the convergence of two blastemata, rather than one [2]. Active mouth opening has been observed *in utero* as early as 7-8 weeks gestation and likely involves the articulation of the early TMJ structures by the lateral pterygoid muscle [1, 3]. During the cavitation stage of TMJ gestation (9-10 weeks), the lower joint and synovium of the TMJ begin to form, followed by the formation of the upper joint (11 weeks) which marks the start of the maturation phase. Although the joint capsules and cartilage have already formed, the TMJ is not considered to be fully developed at birth [4]. As with all joints, the development of the TMJ is influenced by genetic and mechanical factors [5]. Mechanical signaling in the maturing TMJ tissues begins with active mouth opening and helps to direct growth and adaptation. Throughout life, changes in mechanical homeostasis stimulate postnatal morphological changes in the TMJ [6-8]. The capability of the TMJ to adapt to its dynamic mechanical environment is critical to lifelong joint function given that changes in dentition/occlusion, diet, and speech patterns are natural disruptions of joint homeostasis which drive development [9].

1.2 Anatomy

The human TMJ is a ginglymoarthroidal joint between the cranium and mandible. The cranium and mandible are both single bones, meaning the joint is most correctly identified as the craniomandibular articulation [10]. However, the term TMJ is widely used to refer to a single side of the joint [10-12]. The TMJ contains a fibrocartilaginous disc that separates superior and inferior synovial joint capsules and acts to distribute stress induced by jaw movements such as mastication and communication (Figure 1) [13]. The TMJ disc is secured to the mandibular condyle and fossa by a circumferential sheath of connective tissue which forms the joint capsule, and its movement is constrained by the shape of the mandibular condyle and articular eminence as well as the dentition [14].

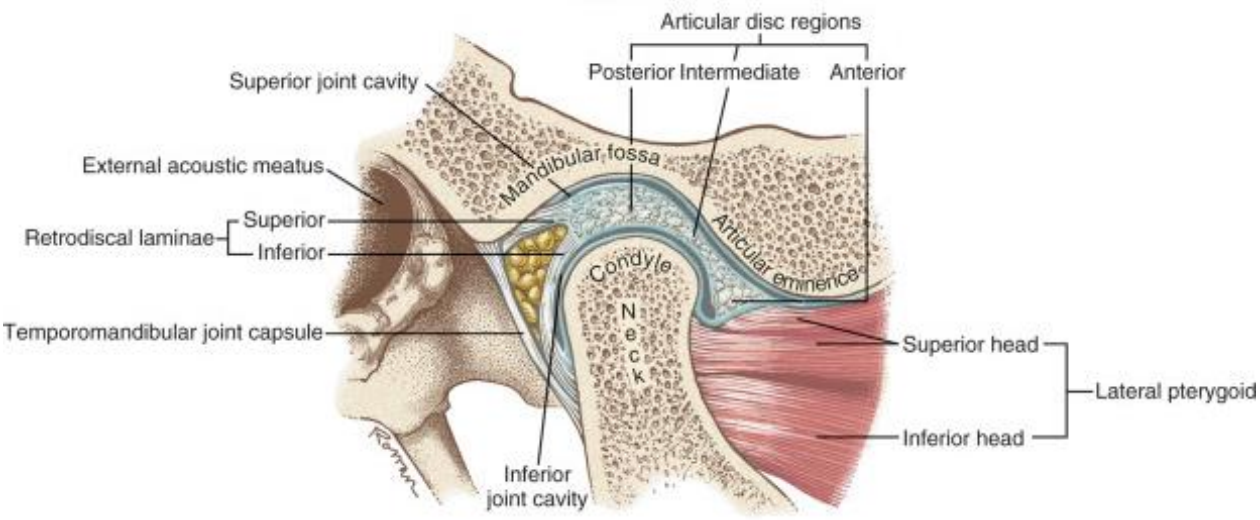

Figure 1: Anatomy of the fully closed right TMJ in anteroposterior cross section. Reprinted from *Comparative Kinesiology of the Human Body* with permission from Elsevier [15].

The masticatory muscles drive the motion of the TMJ. The temporalis, masseter, and medial pterygoid act to close the jaw; the lateral pterygoid muscles close, open, and stabilize the

joint and disc. Although masticatory muscles vary from individual to individual, their general shapes, origins, and insertions can be generalized. The temporalis exhibits a dispersed- and shell-shaped origin on the temporal fossa and a planar, triangular insertion on the coronoid process. The masseter origin is a thin arc along the zygomatic arch, and its insertion on the angle of the mandible is planar and elliptical. The origins of the medial and lateral pterygoids are co-located on the lateral pterygoid plate. The medial pterygoid insertion is on the internal face of the ramus of the mandible near its angle. The lateral pterygoids insert on the condylar neck, TMJ disc, and ramus of the mandible (Figure 1). Although the lateral pterygoids are grouped in name, the superior and inferior heads have been shown to function independently. The superior belly of the lateral pterygoid is involved in jaw closing movements, while the inferior belly is active during jaw opening movements [16].

Branching networks of veins, arteries, and nerves also surround the TMJ. Of particular significance to the TMJ due to their proximity are the trigeminal nerve (particularly the mandibular branch) and the facial nerve which partially control the masticatory muscles [17-19]. The superficial temporal and maxillary vessels provide blood to, and are also closely associated with, the TMJ [20]. Maxillofacial surgeons must be acutely aware of these nerves and vessels during invasive procedures in the TMJ from arthroscopic surgery to total TMJ replacement to protect patients from nerve damage and excessive blood loss.

1.3 Physiology

The physiological environment of the TMJ dictates tissue mechanical behavior and the ability of the cellular components to adapt the extracellular matrix (ECM) composition and geometry to maintain mechanical homeostasis. In terms of cellularity, the TMJ disc appears

fibrocartilaginous with approximately 70% fibroblastic cells and 30% cells with chondrocyte-like morphology dubbed “fibrochondrocytes” [21]. Fibrochondrocytes have been shown to exhibit a fibrocyte-like phenotype in rat, cow, and marmoset TMJ discs [22, 23]. Fibrochondrocytes have also been observed in similar tissues such as the human knee meniscus [24]. The distribution of fibrochondrocytes in the TMJ disc varies regionally, with the central zone expressing the highest relative density [21]. Unlike the disc, the joint capsule of the TMJ is entirely fibroblastic [25-27], containing mainly fibroblast-like cells similar to synovial tissues in other articular joints, as well as macrophage-like cells which increase in number if the synovium is inflamed [28]. The articular cartilage of the TMJ contains a stratified distribution of cells typically seen in hyaline cartilage and fibrocartilage. The articular cartilage contains fibroblasts, osteochondral progenitor cells, and chondrocytes stratified into a superficial fibrocartilage-like layer over a deeper hyaline-like cartilage [26, 27].

Importantly, the TMJ articular cartilage and joint capsule have more readily available nutrient supply than the disc, either through increased vascularity, in the case of the joint capsule [29], or through perfusion of nutrients through the synovial fluid and possibly subchondral bone in the case of the articular cartilage [30]. The TMJ tissues are generally avascular, and their high relative cell density has the potential to create a hypoxic microenvironment. Thus, cells in the TMJ disc are particularly vulnerable to periods with insufficient nutrient supply [31]. Nutrient delivery and waste removal from the synovial fluid is driven by osmotic pressure and mechanical stimulation of the TMJ disc [32]. Accordingly, mechanical stimulation of the TMJ disc is not only critical for cell signaling and tissue adaptation, but also for the survival of the TMJ disc cells.

The biochemical makeup of the TMJ disc [23, 33-36], articular cartilage [29, 37], and joint capsule [28, 38, 39] have been assessed in a number of species. The majority of experiments have

focused on the TMJ disc, which is biochemically distinct from the joint capsule and articular cartilage. The ECM of the TMJ disc is made up primarily of water (~70% wet weight) and type I collagen, as well as regional distributions of elastin, glycosaminoglycans (GAGs), and collagen type II, III, VI, IX, and XI [40]. Regional evaluations of the TMJ ECM have demonstrated a heterogeneous distribution of these constituents throughout the joint, which implies regional variations in biomechanical loading across the joint tissues [34, 40]. Analysis of the TMJ disc attachments, which form the synovial membrane or joint capsule, show a similar water content to the disc (68.5% to 82.2% wet weight) but a lower concentration of collagen per dry weight (71.2% vs. 80.6%) [39]. In the articular cartilage ECM, type I collagen is most prevalent, and proteoglycans, lubricin, GAGs, and types II, IX, and XI collagen also present [29]. This combination of biomolecules is distributed into layers, with a surface layer exhibiting more fibroblastic ECM over a hyaline-like cartilage that transitions into subchondral bone as its depth increases.

1.4 Motion

Efforts to understand the complex motion of the TMJ have utilized a number of mechanical and optical techniques. Tools such as cone beam computed tomography (CT) and magnetic resonance imaging (MRI) can be used to observe the joint morphology and motion for diagnosis of pathological or normal motion [41]. Techniques utilizing dental splints can also be used to track TMJ motion, as well as sensors mounted directly to the dentition [42]. Muscle activity involved in various TMJ motions has been measured using electromyography (EMG) [43, 44]. Through these different sensing modalities, researchers have been able to characterize the range of motion and muscular activity for biomechanical analysis of the TMJ.

TMJ movement can be simplified into the following actions: depression/elevation, retrusion/protrusion, and lateral motion [45]. Normal function of the TMJ requires complex coordination of these movements in order to accomplish functions such as chewing, speaking, and swallowing. During depression/elevation of the joint (mouth opening and closing), the mandible rotates and translates anteriorly, which causes the TMJ disc to slide forward along the articular eminence as the condyle rotates. Healthy individuals will rotate the mandible up to 30° between the fully open and fully closed position, which corresponds to linear translations of the mandible of 15.4 mm - 17.6 mm for men, 12.4 mm – 12.7 mm for women. Optoelectrical measurements have shown sex differences in the linear condylar translation distance, which are dependent on mandible size [46, 47]. Travers *et al.* found that the average maximum incisor opening was highly dependent on condylar rotation in healthy women and also observed high variability in condylar translation for normal opening motions [48]. High person-to-person variability suggests that "normal" function of the TMJ is difficult to define for the general population. Depression/elevation of the mandible induces additional compressive and frictional forces through the joint which translate with condylar movement [49, 50]. The medial and lateral aspects of the joint capsule constrain the disc to a hinge-like motion over the mandibular condyle, while the retrodiscal tissues constrain the forward motion of the disc. In humans, compressive forces in the TMJ are predicted to be up to 94N during biting, which was 13% of the measured bite force [51]. Additionally, chewing and biting typically induce larger forces on the contralateral joint, which may move medially or laterally as a result of deflection in the mandible [49, 51, 52]. Retrusion/protrusion of the mandible allows for alignment of the teeth with maximum displacements of 8 mm to 12 mm [53]. Lateral motion of the jaw in normal patients is limited to about 7 mm to 10 mm [53].

Retrusion/protrusion and lateral motion of the jaw are involved in swallowing and chewing, respectively.

1.5 Mechanical behavior

The TMJ is one of the most frequently loaded joints in the human body [45]. Thus, small disruptions in joint homeostasis may have an accelerated influence on joint health and may initiate a degenerative cascade. The motion of the TMJ is complex, involving simultaneous rotation and translation constrained by the joint capsule, dentition, and contralateral joint [14]. The ranges of motion induced on the TMJ exert dynamic tensile, frictional, and compressive forces on the TMJ disc and articular cartilage. The heterogeneity of cellular makeup across the joint tissues and even regionally within the joint disc emphasizes important differences in tissue function; the TMJ disc and articular cartilage experience more compressive and shear loading, while the joint capsule loading is predominantly tensile. In addition, the joint is configured like a type 3 lever, where the muscle force is applied between the fulcrum (TMJ) and load (gravity, incisal biting forces). Thus, there is a constant passive compressive force through the TMJ articular cartilage and disc [54]. The tensile and compressive behavior of the TMJ soft tissues, particularly those of the TMJ disc and condylar cartilage, have been studied extensively across species [33, 55-63]. The cartilaginous tissues of the TMJ exhibit viscoelastic behavior in compression and tension which correlates with regional collagen and proteoglycan content [61, 64-66]. The friction and wear characteristics of the TMJ disc tissue have also been a primary area of research [67-70]. Coefficients of friction (COF) between the articular cartilage and TMJ disc are similar to those found in other healthy articular joints, reported to be between 0.01 and 0.20 depending on testing the conditions [71, 72]. Taken together, these biomechanical data describe an articular joint that has developed to support

and survive significant and continuous compressive, tensile, and frictional forces in response to frequent and varied articulations.

1.5.1 Temporomandibular joint disc

Tensile evaluations of the TMJ disc reveal anisotropic behavior, with larger elastic moduli in the anteroposterior (AP) direction than mediolateral (ML) direction, with anisotropic ratios of 11.9:1 in ovine TMJ discs [59, 61]. This behavior correlates well with the type I collagen orientation in the TMJ disc, as collagen fibers are arranged predominantly in the AP direction through the central portion of the disc [64]. Tensile elastic moduli for the TMJ disc have been reported from 5 MPa (rabbit) to 250 MPa (ovine) in the AP direction, and from < 1 MPa (bovine) to 20 MPa (ovine) in the ML direction [33, 61]. Values for the elastic moduli of human TMJ discs fall within this range, with central section AP moduli of 8-21 MPa and ML moduli of 5-12 MPa depending on strain magnitude [59]. Biaxial tensile experiments on ovine [61] and human [63] TMJ disc tissues have shown non-linear, viscoelastic, inhomogeneous material behavior [66].

There has been a focus on the compressive properties of whole and partial TMJ disc because the predominant mode of loading in the disc is compressive [33, 56, 63, 65]. Barrientos *et al* performed static and cyclic compressive experiments on whole porcine TMJ discs to develop a streamlined method for assessing the whole TMJ [56]. These experiments highlighted the importance of the viscoelastic behavior of the disc in compressive studies and identified a range of relaxed compressive moduli of the discs from 40-100 kPa. Further cyclic compressive testing on porcine TMJ discs has demonstrated an increase in the tangent modulus with increased loading frequency, and higher moduli in the posterior aspect of the disc for all loading conditions [73]. Allen and Athanasiou measured a range of instantaneous compressive moduli from 371 ± 435 kPa

(lateral-inferior region) to 1924 ± 2390 kPa (posterior-inferior region) and relaxed moduli from 99 ± 59 (lateral-inferior region) to 173 ± 151 kPa (medial-inferior region) using a single strain step viscoelastic model fitting of compressive data collected from submersed porcine discs at a physiologically relevant temperature (37 ± 1.5 °C) [65]. Overall, compressive experiments on the TMJ disc demonstrate regionally variable non-linear viscoelastic behavior with significantly lower compressive moduli than tensile moduli.

Indentation has been used to evaluate the TMJ disc material properties in ovine [61], human [55], and porcine [74] tissues. In ovine tissues, there was regional variation in the instantaneous and relaxed moduli, with averages of 1200 ± 800 kPa and 200 ± 190 kPa, respectively. The highest indentation moduli were observed in the anterior and posterior bands. In porcine discs, the average indentation modulus was 36.17 ± 19.43 kPa [74]. Indentation experiments on human TMJ discs investigated the dynamic regional tissue properties, finding the highest tissue stiffness in the intermediate zone rather than the anterior and posterior bands. Hysteresis was observed with increasing loading cycles in all locations, with 50% relaxation occurring within the first 10 cycles [55].

The COF for the TMJ disc have been reported from 0.0145 ± 0.0027 [70] to 0.074 (no standard deviation provided) [68]. In one experiment, the COF between the TMJ articular surfaces increased from 0.0177 ± 0.0021 to 0.0361 ± 0.0063 after porcine TMJ disc excision [69]. Frictional and wear evaluations of the TMJ disc surface exhibit wide variation due to differences in experimental protocol [70]. The COF in the TMJ are dependent on the movement speed and magnitude of the applied load, the duration of the friction test, and the type and presence of lubrication [67]. However, all measured COF data fall within the range of values reported for normal articular cartilage (0.001-0.1) [71]. For a joint that experiences high rates of loading, a

sufficiently low COF must exist to reduce wear and degradation of the continuously loaded articular cartilage and disc surfaces.

The aforementioned mechanical evaluations of the TMJ disc emphasize the significant role that the viscoelastic component plays in the tissue's tensile and compressive behavior, which is linked to its regionally variable ECM composition. Thus, time-dependent analyses are necessary for full characterization of the native tissues. In addition, the COF of the TMJ are on the order of COF values that have been reported for other articular joints. Published values for the tensile, compressive, indentation, and friction analyses of the TMJ disc tissues vary due to differences in experimental protocol and the inherent dynamic nature of the TMJ disc tissue. Since the mechanical behavior of the TMJ disc is dependent on many factors, paired experiments utilizing standardized experimental protocols should be used to draw appropriate comparisons between the TMJ disc, joint tissues, and candidate materials for tissue replacement.

1.5.2 Articular cartilage

The mandibular and fossa cartilage have also been mechanically evaluated through tensile, compressive, indentation, and frictional experiments [75]. The tensile and compressive properties of the porcine condylar cartilage superficial layer demonstrated non-linearity, with tensile and compressive moduli of 30.73 ± 12.97 MPa and 0.023 ± 0.016 MPa, respectively. The more internal, hyaline-like condylar cartilage exhibited relatively reduced tensile moduli of 2.43 ± 1.75 MPa and compressive moduli of 0.14 ± 0.09 MPa [76]. Singh and Detamore also studied the tensile properties of the porcine TMJ condylar cartilage, which exhibited a 2.4 times higher elastic moduli in the AP than ML direction and no statistically significant differences in the regional tensile properties [57]. Stribeck curve analysis of the TMJ condylar cartilage on glass measured COF

between 0.009 and 0.19 depending on anatomic location, fluid pressurization, and sliding direction, with the lowest values observed in the posterior aspect [60]. Atomic force microscopy-nanoindentation techniques were used to evaluate the regional distribution in the indentation properties of murine TMJ discs [77]. These experiments showed the surface of the murine condylar cartilage exhibited higher elastic moduli (306 ± 84 kPa) as compared to the TMJ disc surfaces (85 ± 23 kPa superior, 45 ± 12 kPa inferior).

1.5.3 Temporomandibular joint capsule

The purpose of the TMJ capsule is to maintain the synovial fluid and constrain motion of the TMJ disc during dynamic mandibular motions [14]. The joint capsule does not experience direct compressive or frictional loading during normal function. Thus, the geometric and tensile properties of the joint capsule are most pertinent to the overall joint function. Histological analyses of the TMJ attachments reveal a higher proportion of aligned collagen fibers than in the disc, suggesting tensile loading in the joint capsule is a more dominant mode of loading than in the TMJ disc [39]. Six distinct sections (medial, lateral, posterior-inferior, posterior-superior, anterior-inferior, and anterior-superior) of the porcine TMJ disc attachments were evaluated by Willard *et al.*, who found an anisotropic distribution in collagen fiber alignment in all but the anterior inferior section [58]. Elastic moduli of the distinct regions ranged from 1.4 MPa (medial and anterior-superior sections) to 16.3 MPa (posterior-superior section). One group investigated the failure strength of the human inferior lateral joint capsule and found an average load of 54N was necessary for attachment failure [78]. However, failure strength in other sections of the human TMJ capsule have not been investigated.

1.6 Pathology

The tissues of the TMJ are subject to persistent mechanical stresses to which the TMJ ECM must adapt geometrically and biochemically to maintain healthy function. Even small disturbances in joint homeostasis can progress to temporomandibular joint disorders (TMDs) when mechanical stresses exceed the limit of adaptability of the TMJ tissues [79, 80]. The term TMD encompasses a wide range of signs and symptoms and is not a diagnosis, but rather a classification of symptoms including pain, and muscle and joint dysfunction that may lead to chronic joint disorders [81]. Mechanisms for the degeneration of TMJ health are complex and poorly understood, involving multiple pathways for deterioration that advance simultaneously. For instance, bruxism (jaw clenching) may be the result or the cause of myofascial pain, and only intermittently lead to chronic degenerative joint disease (DJD) [9]. In addition, individuals will respond differently to disruptions like internal derangement, with some cases progressing towards pain or joint disorder and others returning to normal function [82]. Of course, disorders and malformities of the TMJ can also arise during development [83] or as the result of traumatic injury [84-86]. Research has also shown that psychological factors such as stress may predispose individuals to TMDs and orofacial pain [87, 88]. A 2016 meta-analysis estimated that the prevalence of clinical signs of TMDs is 16% among children and adolescents [89]. Further research reveals the incidence rate for orofacial pain is 4% per year for adults aged 18-44 years [90]. A study conducted in 2018 found that 11.2 to 12.4 million U.S. adults experienced TMJ pain over a three month period [91]. Of individuals suffering from TMJ pain, approximately 42% report high pain intensity [92]. Despite the high incidence TMDs, the TMJ and related disorders are relatively under-studied as compared to other articular joints such as the knee, which has a six-fold higher published article count [93].

The complex and poorly understood etiology of TMDs has led to some controversy over TMD classification methods and even the term TMD itself [94]. The classification method proposed by Dimitroulis forms the basis for the following discussion [95]. TMDs have been classified into three major categories: myofascial pain and dysfunction (MPD), TMJ functional derangement, and TMJ degenerative/inflammatory joint disease. Subclassifications of these categories include ankylosis (bone growth), dislocation, multiple types of arthritis, and localized and dispersed pain in the TMJ tissues. Some of the most common TMDs are MPD and internal derangement (ID) of the TMJ disc [96]. Cases involving arthritis typically involve degeneration and inflammation, while joint structural changes are associated with growth disorders, which may occur through natural tissue adaptations [84].

MPD is believed to originate in the masticatory muscles and can be the result of myriad external factors and behaviors [97]. This type of pain presents clinically as an intermittent or continuous dull ache or, more infrequently, as a sharp radiating pain in the masticatory muscles that is exacerbated by muscular activation [98]. For patients with TMDs, approximately 45.3% experience some form of pain in the masticatory muscles [99]. Myofascial pain is poorly correlated with pathological changes in the TMJ. For 75 – 90% of patients, MPD can be treated with therapy or dietary changes [95].

ID of the TMJ disc is also prevalent, with the most common derangements occurring anteriorly [100]. To summarize the progression of ID, initial signs of TMJ disc ID begin with a clicking or popping noise emanating from the disc space as the TMJ disc travels forward off of the condyle. Further progression of ID can lead to a “closed lock” of the jaw, where the TMJ disc is displaced anteriorly, preventing jaw opening. If left untreated, it is possible for the disc to adhere to the condyle or articular eminence leading to ankylosis and tearing of the disc [101]. If the joint

disc begins to adhere, minimally invasive surgical treatments such as arthroscopic lysis and lavage will be pursued [102]. However, most patients with ID exhibit only preliminary stages, which may not progress beyond simple TMJ noise such as clicking or popping [97]. In fact, ID was observed in 33% of otherwise asymptomatic individuals in one cohort of 76 volunteers [103]. Stages of ID have been broken down to inform diagnosis and treatment initially by Wilkes in 1989 [104] and further built upon by Dimitrulious in 2013 [105] and Hegab *et al.* in 2021 [106] for surgical and non-surgical interventions, respectively. Where less invasive treatments are not successful, a disc excision will likely be performed [107, 108].

2 Treatments for temporomandibular joint disorders

TMD severity and responsiveness to treatment can be difficult to predict. Understanding the factors that lead to pathological changes in a patient's TMJ are critical for choosing an appropriate treatment [79, 80]. Wright and Klasser have published an updated "Manual for Temporomandibular Disorders", which serves as a resource to help surgeons correctly identify TMDs with formal diagnostic criteria and treat them using the most effective therapies [109]. Perhaps the most widely adopted criteria for identifying TMD is the "Diagnostic Criteria for Temporomandibular Joint Disorders" (DC/TMD) which was developed by an international consortium of specialists [110]. Typically, more conservative non-surgical treatment options are preferred [111, 112], particularly for MPD [113]. However, these approaches are typically only palliative, or they do not address the underlying cause of joint dysfunction [114, 115]. Figure 2 shows a flowchart for surgeons to identify the appropriate treatment, based on patient symptoms [116]. This figure emphasizes the conservative approach to TMD treatment, for which surgery is considered an undesirable and final option in traumatic cases, or when conservative treatments do not successfully prevent joint deterioration.

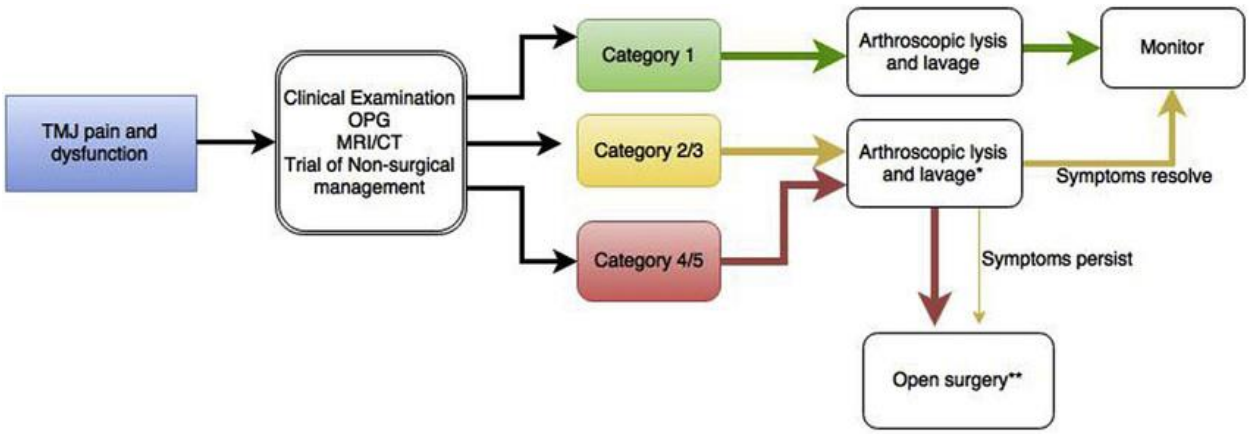

Figure 2: Flow-chart of suggested diagnosis and treatment strategies for TMJ pain and dysfunction based on categorized severity. Reprinted from *Temporomandibular joint (TMJ) arthroscopic lysis and lavage: Outcomes and rate of progression to open surgery,* with permission from Elsevier [116].

Conservative treatments for TMDs include pharmacotherapy, occlusal splints, and physical therapy [87, 117-121]. The purpose of pharmacotherapy is primarily to reduce pain, typically utilizing non-steroidal anti-inflammatory drugs, which may take several weeks to provide a full benefit [122]. Occlusal splints are a controversial TMD treatment; their benefit is served under the assumption that the root cause of TMJ dysfunction is "incorrect" occlusion [123]. Meta-analyses have demonstrated a reduction in pain and increased maximum mouth opening as the result of occlusal splint therapy [124]. However, most evidence supporting the use of occlusal splints and physical therapy for TMDs is of moderate to low quality or limited in scope [125, 126] . Likewise, there is a lack of high-quality studies on the efficacy of pharmacological treatments [117].

If mild TMDs do not resolve on their own or in response to conservative treatments, more invasive arthroscopic treatments may be employed to halt disease progression. Arthroscopic lysis and lavage is a minimally invasive method to remove osteophytes growing on the bony surfaces of the TMJ, to prevent ankylosis, and to reduce friction [127]. Arthroscopic surgery has been shown to increase TMJ range of motion and reduce pain for patients [102, 128]. Long-term success

rates of 77.7% (cases requiring no further surgery) for arthroscopic lysis and lavage procedures have been reported [116]. Arthroscopic injection of platelet-rich plasma [129] and hyaluronic acid [130] have only been shown to be slight to moderately effective treatments. In cases of ID of the TMJ disc, the disc may be repositioned using surgical techniques, which may be performed arthroscopically [131]. Repositioning the disc requires that sutures be passed through the posterior (for anterior displacement) aspect of the disc, and a small anchor to be inserted into the posterior aspect of the mandibular condyle in order to draw the disc tissue posteriorly in an effort to aid the TMJ ligament in resisting further anterior displacement [132-134] (Figure 3).

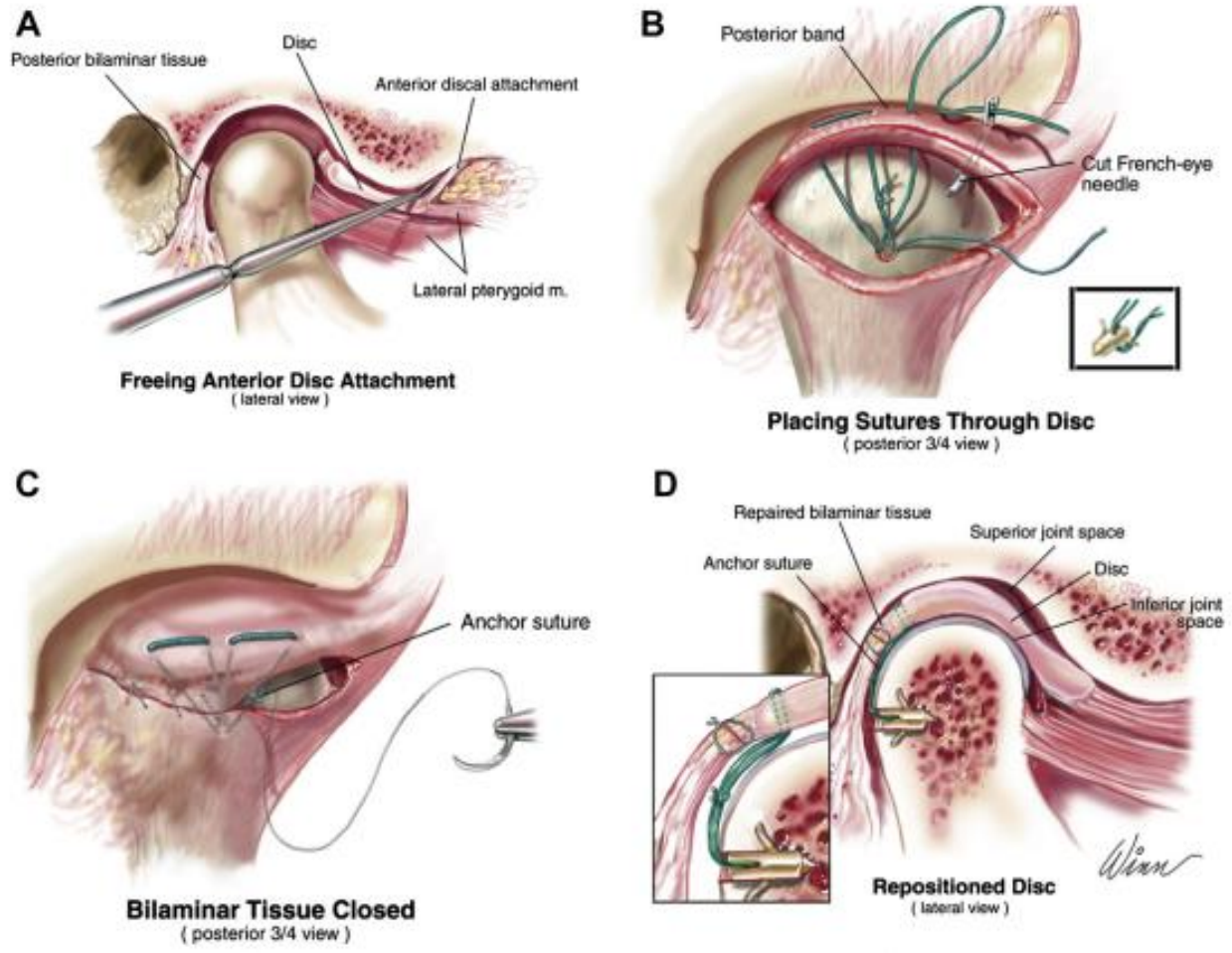

Figure 3: Stages of TMJ disc repositioning surgery using sutures and a mini anchor. Reprinted from *Disc Repositioning Does it Really Work?,* with permission from Elsevier [135]

Discectomy, or disc excision, is currently the most common treatment for advanced TMDs [95, 104], with some surgeons using skin, fat, or temporalis muscle tissues as an interpositional material between the joint surfaces following disc removal. These tissues are intended to reduce wear on the articular surfaces of the joint, which would otherwise be in direct contact [136-138]. Discectomy is shown to be effective in reducing acute pain [111, 136], but it inherently increases friction in the joint [69] , which can cause or exacerbate osteoarthritis, sclerosis, adverse condylar remodeling, and/or ankylosis [108, 139, 140]. Unfortunately, there are currently no artificial TMJ disc replacements approved for human use [141], and discectomy failure rates (progression to total

joint replacement) of 11.9% have been reported [142, 143]. In these instances, highly invasive surgeries such as total joint replacement become necessary [142]. Although total TMJ replacements are relatively rare and only necessary for treating a small number of TMDs [144], these procedures are highly invasive, requiring tissue removal and reshaping of bone near the brain, facial nerves, and facial/cranial blood supply [12, 145]. Fortunately, global revision rates for custom total TMJ replacements are low, with approximately 1.19 per 100 prosthesis-years [146].

3 Animal models for TMJ research

Numerous animal species have been utilized for preclinical TMJ research including ovine, caprine, canine, primate, bovine, porcine, leporine**,** and murine models. Investigation in murine and leporine models has been the focus in earlier research [147]. Murine models are good for studying osteoarthritis [148], pain [149], and genetic factors [150] in basic research, but translation of surgical procedures and mechanical characterization is limited [147]. Leporine models have been used to study TMDs [151-153] and TMJ regenerative strategies [154]. Low cost and simple access to the TMJ are advantages of leporine models. However, forces in the leporine TMJ are substantially lower than they are in the human TMJ, with the ipsilateral joint experiencing negligible loading during chewing motions [147, 155]. Thus, murine and leporine models are not ideal models for studying relevant stresses experienced by TMJ implants. Porcine (particularly Yucatán minipigs) and ovine species are more translatable to humans for basic science and preclinical research purposes [33, 156-158]. Due to their omnivorous diet, as wells as genetic and biomechanical similarities to humans, porcine species have been suggested as an excellent model for TMJ research [159, 160]. Porcine models have been used extensively to study TMJ biomechanics [56, 161-163], ECM composition [34, 39, 40, 164], cellular composition and

signaling [21, 165, 166], as well as numerous surgical [69, 167, 168] and tissue engineering strategies [169-171]. However, porcine species never reach skeletal maturity, and they possess a zygomatic arch which folds over the TMJ disc space that complicates lateral access to the joint [158]. Ovine and caprine models have not been studied as extensively [160]. However, lateral surgical access to the ovine TMJ approximates the optimal approach in human TMJ surgery [158, 172], suggesting that they may be a more appropriate model for preclinical surgical and implant development. In addition, ovine and caprine species chew approximately 30,000 -50,000 times a day [173] due to their ruminate behavior, which allows for accelerated studies of wear in implant development. Ovine models have been used to investigate TMJ biomechanics [61], joint morphology [157], TMDs [140, 174, 175], and surgical strategies [176-178].

4 Finite element modeling of the temporomandibular joint

Finite element (FE) models are widely accepted tools for mechanical evaluation of articular joints, artificial implants, and surgical procedures *in silico* [179-182], including for the TMJ [183, 184]. Such models provide a method for assessing joint mechanics in simulations of diseased and healthy joints and are used to predict the mechanical behavior of implanted structures. Wu *et al.* used a FE model to assess the biphasic properties of the TMJ disc tissue, emphasizing the importance of fluid pressurization as a key loading support mechanism of the TMJ disc [185]. FE studies of TMJ internal derangement have shown increased stress for displaced discs over normally placed discs [186], with highest stresses measured for posterior disc displacement [187], particularly in the contralateral side [188]. *In silico* studies also showed that stress in the TMJ disc tissues increased with joint COF [189]. Models focused on the mandibular condylar cartilage demonstrated the importance of the load distribution capability of the TMJ disc tissue, which was aided by the fibrocartilage surface layers [190]. A review of FE modeling of off-the-shelf and

patient-specific total TMJ disc replacements demonstrated a decrease in stresses for more customized implants [184]. Overall, FE models have been successfully used in the study of TMJ biomechanics, disorders, and implant design.

5 Summary

The TMJ is a complex bilateral ginglymoarthroidal joint that is critical for human function. Dynamic stresses are induced in the TMJ during activities such as chewing and communication, which act to distribute nutrients to the TMJ cellular components as well as to drive normal adaptation of the joint. Mixed cell phenotypes and regional distribution of biochemical constituents, paired with unique motion profiles, differentiate the TMJ from most other articular joints. Mechanical behavior of the TMJ soft tissues has been well characterized across species with a focus on more translatable porcine and ovine models. Disorders of the TMJ are complex, and the root cause may be difficult to identify as symptoms and severity can range significantly and may be poorly correlated. FE modeling has also been used to study the normal and pathologic TMJ states, as well as the effect of artificial implants introduced in the TMJ space. In the field of TMJ research and artificial TMJ disc replacement there is great potential for reducing human suffering and economic burden.

6 Specific aims

The purpose of this research project is to design and implement an artificial TMJ disc replacement strategy, and to develop methods for implant evaluation. The goal of TMJ disc replacement is to arrest degenerative changes in the TMJ after disc excision by successfully replacing the TMJ disc with a robust artificial replacement. The following specific aims are proposed to support this objective.

Specific Aim 1: Characterize the biomechanical behavior of the ovine temporomandibular joint soft tissues. In depth mechanical investigation of the TMJ disc tissues is paramount in setting design targets for an artificial TMJ disc replacement. The soft tissues of the TMJ comprise articular fibrocartilage, a circumferential ligamentous joint capsule, and a fibrocartilaginous disc which act to constrain motion, reduce friction, and distribute joint stresses. A rigorous mechanical characterization of the ovine joint capsule, articular cartilage, and disc will be performed. Tension, indentation, unconfined compression, and friction experiments will be performed on freshly harvested ovine TMJ discs. The regional biomechanics of the TMJ capsule and articular cartilage will also be investigated though uniaxial tensile tests to failure, and indentation-stress relaxation testing, respectively. These data will inform FE modeling efforts and be used to set design targets for an artificial TMJ disc implant.

Specific Aim 2: Identify and evaluate a material candidate for a temporomandibular joint disc replacement. A literature review of numerous biocompatible polymeric material candidates for disc replacement will be completed. Cursory evaluation of candidates will be performed through indentation-stress relaxation experiments. The leading material candidate will undergo a comprehensive mechanical analysis. Specifically, unconfined compression, uniaxial tension, and friction experiments will be completed using the same experimental protocol used for the TMJ discs. Specific aim 2 will be achieved through an in-depth literature review focused on non-degradable, biocompatible polymers, followed by mechanical analysis of promising material candidates leading to a primary material candidate for TMJ disc replacement. The data from the mechanical characterization will be used to determine if the material candidate is suitable for implantation as an artificial TMJ disc replacement.

Specific Aim 3: Develop *in silico* and *in vitro* methods for evaluating design candidates for artificial TMJ disc replacement. A FE model of the ovine TMJ will be developed utilizing the mechanical properties determined in Specific Aims 1 and 2. Simulation of jaw clenching will be used to compare the contact area and stress response between the native tissue and an artificial TMJ disc replacement. The model will be validated by *ex vivo* experiments mimicking jaw clenching on freshly excised ovine TMJs. The FE model predictions of stress with respect to applied clenching load for both the native and artificial TMJ discs will support the further refinement of implant design. Additionally, a mechanism for *ex vivo* evaluation of implant candidates simulating the *in vivo* conditions will be designed. The apparatus will replicate the chewing motion in a cadaveric skull using a four-bar linkage. Motion capture of ovine mastication will be used to design the four-bar linkage motion. This will allow for expedited, *ex vivo* comparison of tensile- or compressive-based implant failure in a simulated *in vivo* condition. The accomplishment of Specific aim 3 will provide tools for evaluating TMJ disc replacement design candidates *in silico* and *ex vivo* to expedite future development of a successful TMJ disc replacement.

Specific Aim 4: Implement a temporomandibular joint disc replacement strategy in an ovine model. First, an iterative approach to implant design will focus on creating a finalized implant geometry and surgical strategy with the help of maxillofacial and veterinary surgeons. The finalized implant geometry will be implanted in a cohort (n=1 control, n=2 implant) of otherwise healthy sheep to investigate the efficacy of the surgical strategy, fixation technique, and native tissue response in a six-week pilot study. Patient-specific TMJ discs will be implanted in two of three sheep following unilateral disc resection, contralateral joints will be left intact. Prior to implantation, clinical CT scans will be used to define the artificial TMJ disc replacement geometry.

Throughout the pilot study, the body weight, masticatory motion, and rate of mastication of each specimen will be recorded. At study conclusion, indentation-stress relaxation experiments and histological evaluation will be performed on bilateral TMJ tissue samples and evaluated by a trained veterinary pathologist. Completion of a pilot study will allow for refinement of *in vivo* and *ex vivo* experiments to determine the success of a TMJ disc replacement strategy.

CHAPTER 2 - BIOMECHANICAL ANALYSIS OF THE OVINE TEMPOROMANDIBULAR JOINT TISSUES

The mechanical properties of the TMJ soft tissues have been extensively evaluated in several species, demonstrating regional, anisotropic, and viscoelastic behavior in tension and compression. These properties are inherently linked to the ECM composition arrangement as described in Chapter 1. However, further analyses of ovine TMJ tissue properties are needed to establish ovine-specific targets for preclinical study of an artificial disc replacement and to inform a FE model for *in silico* analysis. Previously, Labus *et al.* have performed uniaxial and biaxial tensile experiments, as well as regional indentation-stress relaxation tests of the ovine TMJ disc [61]. This chapter describes additional efforts to characterize the ovine TMJ, including: (1) unconfined compression and frictional evaluation of the TMJ disc, (2) tensile testing of the TMJ capsule, and (3) indentation-stress relaxation experiments on the TMJ articular cartilage. For all tests, TMJ tissues were harvested from skeletally mature female Columbian Rambouillet sheep that were euthanized for unrelated studies and obtained via a tissue sharing protocol governed by Colorado State University (CSU) Institutional Animal Care and Use Committee (IACUC) protocol KR104.

1 Temporomandibular joint disc

Unconfined compression experiments were performed on cylindrical samples of 10 excised ovine TMJ discs (n=5 right, n=5 left). A cylindrical sample was removed from the central portion of each TMJ disc using a 2 mm diameter biopsy punch. TMJ disc samples were mounted in a hydraulic testing system between two parallel compressive platens (Model 858, MTS, Eden Prairie, MN) outfitted with a 220 N load cell (661.09 B-21, MTS, Eden Prairie, MN). Each sample was loaded to a minimum of 60% strain at a strain rate of 0.005 s^{-1}, and paired force-displacement

data were collected. MATLAB (MATLAB 2019, MathWorks, Natick, MA) was used to analyze the force-displacement data. Stress was calculated as the axial force divided by the sample cross-sectional area, and stretch was calculated as the displacement of the upper platen divided by the initial height of the sample. Incompressibility was assumed due to the high water content of the TMJ discs [191]. The experimental stress-stretch data between $\lambda = 1.00$ and $\lambda = 0.56$ were fit to a 2-term Yeoh model:

$$\psi = C_1(I_1 - 3) + C_2(I_1 - 3)^2 \qquad \textit{Equation 2.1}$$

where ψ is the strain energy density, C_1 and C_2 are material constants, and I_1 is the first invariant of the right Cauchy-Green deformation tensor:

$$I_1 = \lambda_1^2 + \lambda_2^2 + \lambda_3^2 \qquad \textit{Equation 2.2}$$

where λ_1, λ_2, and λ_3, are the principal stretches. For the purposes of fitting, all materials were assumed to be transversely isotropic. Thus, for unconfined compression, $\lambda_1 = \lambda$, $\lambda_2 = \lambda_3 = \lambda^{-1/2}$, and $\sigma_{22} = \sigma_{33} = 0$. Therefore, the axial Cauchy stress (σ_{11}) can be related to the axial stretch (λ) according to the following equation:

$$\sigma_{11} = 2\left(\lambda - \frac{1}{\lambda^2}\right)\left[C_1 + 2C_2\left(\lambda^2 + \frac{2}{\lambda} - 3\right)\right] \qquad \textit{Equation 2.3}$$

The values of C_1 and C_2 were determined using a least-squares fit of *Equation 2.3* to the stress-stretch data. In addition, the tangent moduli at stretch values from $\lambda = 1.00$ to $\lambda = 0.96$ and from $\lambda = 0.60$ to $\lambda = 0.56$ were calculated using a localized linear regression. Stretch ranges were chosen to represent an initial tangent modulus ($\lambda = 1.00$ to $\lambda = 0.96$) and tangent modulus at a physiologically relevant maximum strain based on FE modeling of the human TMJ while

clenching ($\lambda = 0.60$ to $\lambda = 0.56$) [192]. A t-test, assuming unequal variance, was used for statistical comparison of the calculated tangent moduli.

The COF of freshly harvested ovine TMJ discs were tested against a bearing surface of ovine TMJ fossa cartilage. Six (n=3 right, n=3 left) ovine TMJ discs were excised for friction testing. A cylindrical osteochondral plug with a 3.2 mm radius was extracted from an ovine TMJ fossa using a drill-press mounted hole saw and kept hydrated with phosphate buffered saline (PBS). The same osteochondral specimen was used for all tests to keep protocols consistent and comparable. This osteochondral plug was mounted in a hydraulic testing machine (MTS Bionix™, MTS, Eden Prairie, MN) with an offset of 90 mm from the center of rotation (Figure 4). A mass was applied above the cylindrical plug to induce a uniform pressure of 100 kPa throughout the test to match a physiologically relevant joint pressure [193]. All samples were fixed to a polished brass surface with a cyanoacrylate adhesive and immersed in artificial synovial fluid consisting of 30g/L newborn calf serum diluted with PBS, 2g/L sodium azide, 3g/L Ethylenediaminetetraacetic acid, and 3g/L hyaluronic acid [194].

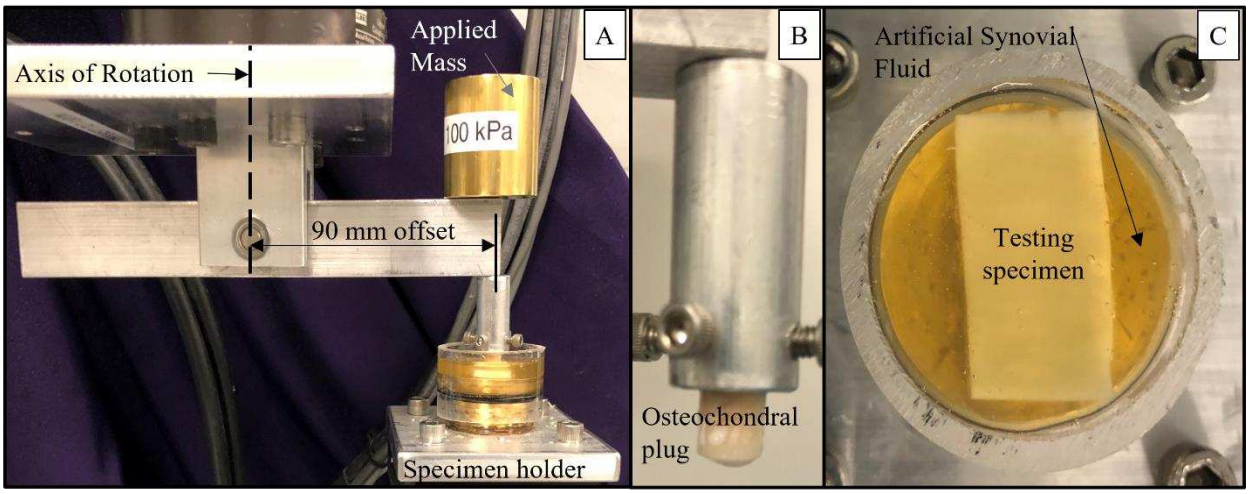

Figure 4: Experimental setup for friction experiments showing (A) the entire apparatus, (B) the installed osteochondral plug, and (C) a testing specimen submerged in artificial synovial fluid.

The fossa cartilage was drawn back and forth across the TMJ disc sample surface five times at rates of 0.4 mm/s, 4.0 mm/s, and 40 mm/s to match speeds expected for mandibular motion [195, 196]. The normal and transverse forces were measured using an axial and torsional load cell (Model 661.19H-03, MTS, Eden Prairie, MN). MATLAB was used to calculate the sample COF. The COF was calculated as the absolute value of the transverse force, divided by the normal force. The average COF was calculated over the central 90% of the total stroke length for the five cycles at each speed. A one-way ANOVA was performed on COF values for each speed to determine if there was any significant difference in the COF across testing speeds. A logarithmic transformation was applied to the data to satisfy assumptions of normality and equal variance.

The C_1 and C_2 terms from fitting the unconfined compression data of the TMJ discs were 80.6 ± 41.8 kPa and 75.0 ± 58.7 kPa, respectively. The percent root mean squared error (%RMSE) for the 2-term Yeoh model fits of the unconfined compression data was 3.5% for the TMJ disc. The difference between the initial (λ = 1.00 to λ = 0.96) and physiological (λ = 0.60 to λ = 0.56) tangent moduli was significantly different ($p < 0.001$), demonstrating nonlinearity in the

compressive behavior of the ovine TMJ disc. The measured tangent moduli in these experiments compare well with published values for TMJ discs of other species [33, 65, 197]. The average tangent moduli for unconfined compression in the TMJ disc at higher values of stretch exceeded the indentation moduli found by Labus *et al.* [61]. The observed non-linearity and discrepancies between unconfined compression and indentation values are attributed to the collagen fiber component in the TMJ disc, which suggests that the sample stiffness will increase to a greater extent in macro-scale unconfined compression as compared to micro-scale indentation [198].

The friction experimental conditions approximate the *in vivo* environment by including ovine TMJ cartilage as the contacting material and lubrication with artificial synovial fluid. However, hydration, applied pressure, translation speed, and contacting material can all influence measured COF [199, 200]. These factors underscore the motivation for comparative experiments that can be repeated on candidate materials for artificial implants. These friction experiments showed a lower average COF (0.058 ± 0.047) between the TMJ fossa cartilage and disc than what was reported by Zimmerman *et al.* [68] and greater than those measured by Tanaka *et al.* [69, 70] in porcine discs. No significant differences in COF were observed for the three different translation speeds used in this evaluation, despite the fact that these speeds spanned two orders of magnitude. Results from the friction and unconfined compression experiments are shown in Figure 5.

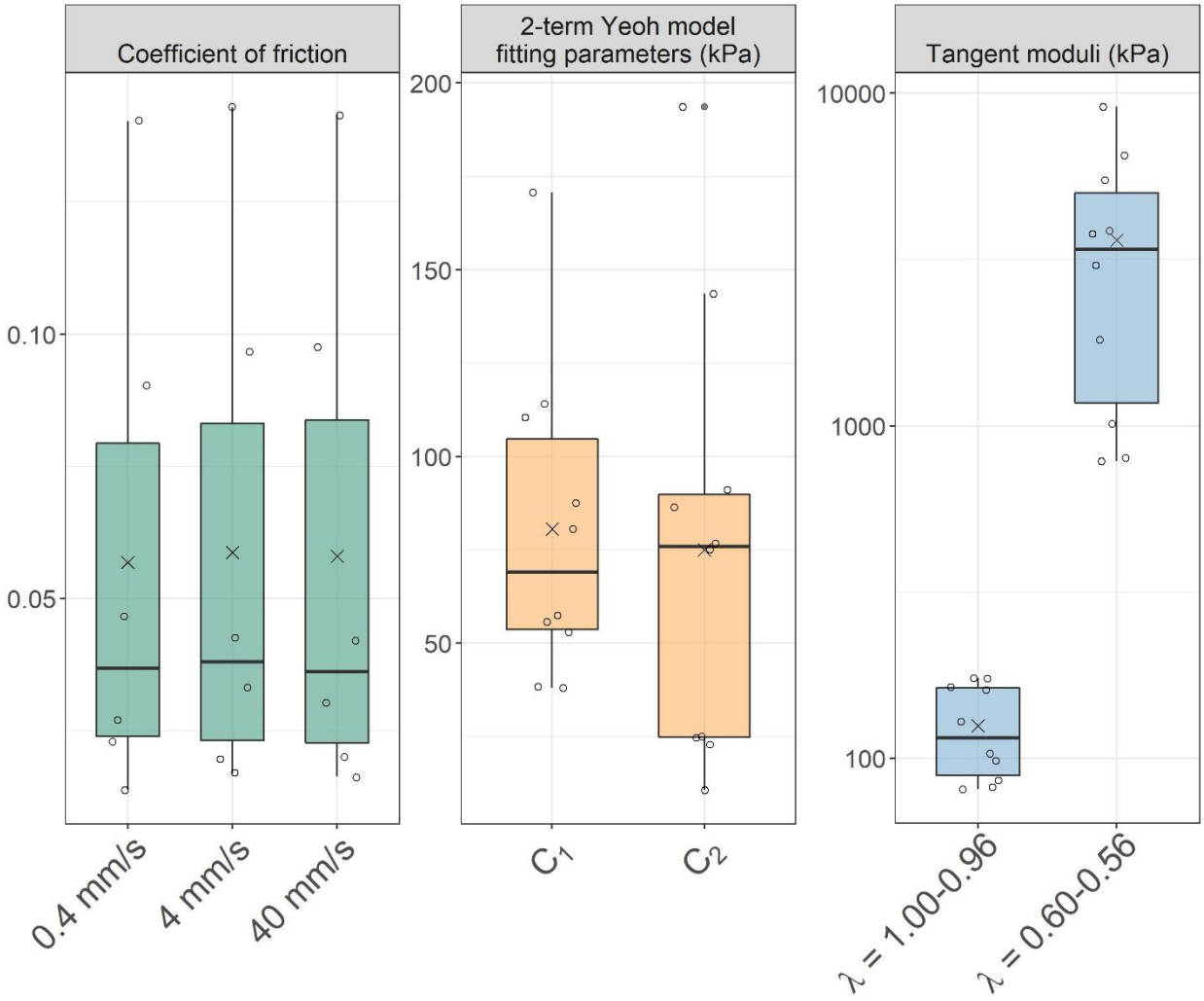

Figure 5 : Summary of and frictional and unconfined compression data of TMJ disc tissues.

2 Temporomandibular joint capsule

To assess the geometry and tensile behavior of the TMJ capsule, six TMJs (n=3 left, n=3 right) were excised *en bloc* and meticulously dissected into eight distinct regions based on anatomic position. The following sections were isolated: anterior superior (AS), inferior lateral (IL), superior lateral (SL), inferior medial (IM), superior medial (SM), posterior inferior medial (PIM), posterior inferior lateral (PIL), and posterior superior lateral (PSL). Each capsule section

was gripped in a custom uniaxial loading system comprising a linear actuator and load cell mounted on a rigid frame (Figure 6).

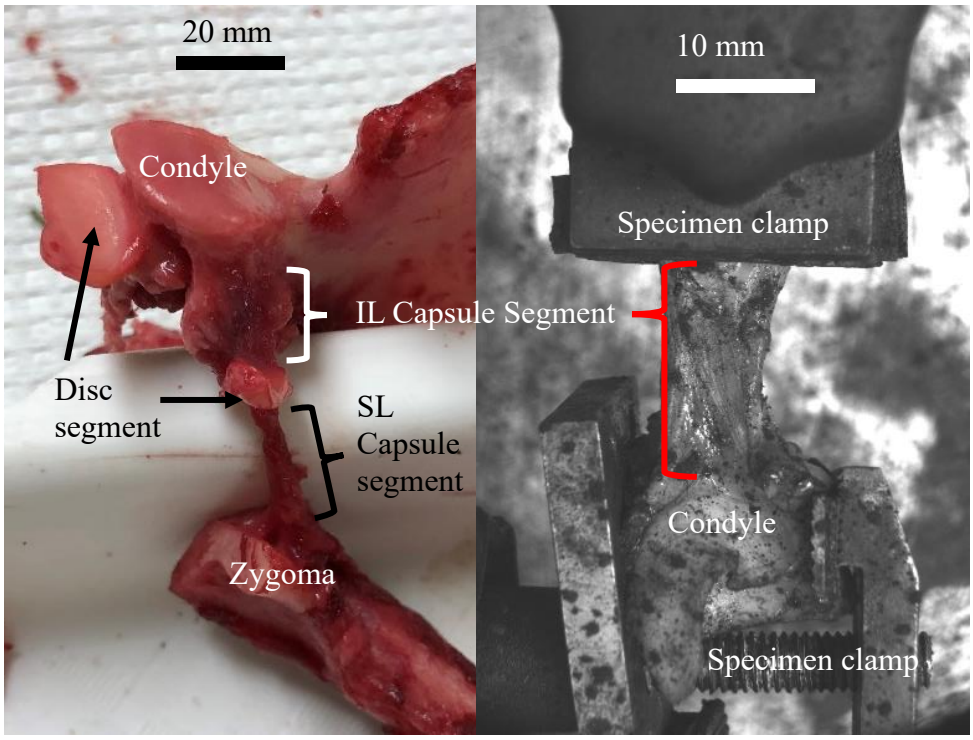

Figure 6 : Lateral joint capsule sections of the dissected TMJ capsule (left) and testing setup used to perform uniaxial tensile analysis on distinct anatomical regions of the TMJ capsule (right).

All samples were kept hydrated with phosphate-buffered saline and refrigerated; all testing occurred within 36 hours of animal sacrifice. Physical measurements of the length, width, and thickness of each capsule section were made using digital calipers (Series 500, Mitutoyo America Corporation, Aurora, IL). Samples were pre-cycled 20 times to 5% strain at 1 Hz and then loaded uniaxially to 100% strain at a rate of 1% strain/s using a calculation of strain based on the measured initial, unloaded length. Force and displacement data were collected throughout the uniaxial tensile test. Sample stiffness was defined as the slope of the linear portion of the force-displacement curve for each sample. The regional stiffness values were compared using a one-way ANOVA.

A summary of tensile testing results, including representative median stiffness force-displacement curves for each location is shown in Figure 7. Of the joint capsule components tested, the stiffest was the SM region, and the least stiff was the IM region. Some regional variation in the joint capsule mechanical properties was expected based on biochemical analyses [39], however no statistically significant ($p < 0.05$) differences in regional stiffnesses were found in this experiment.

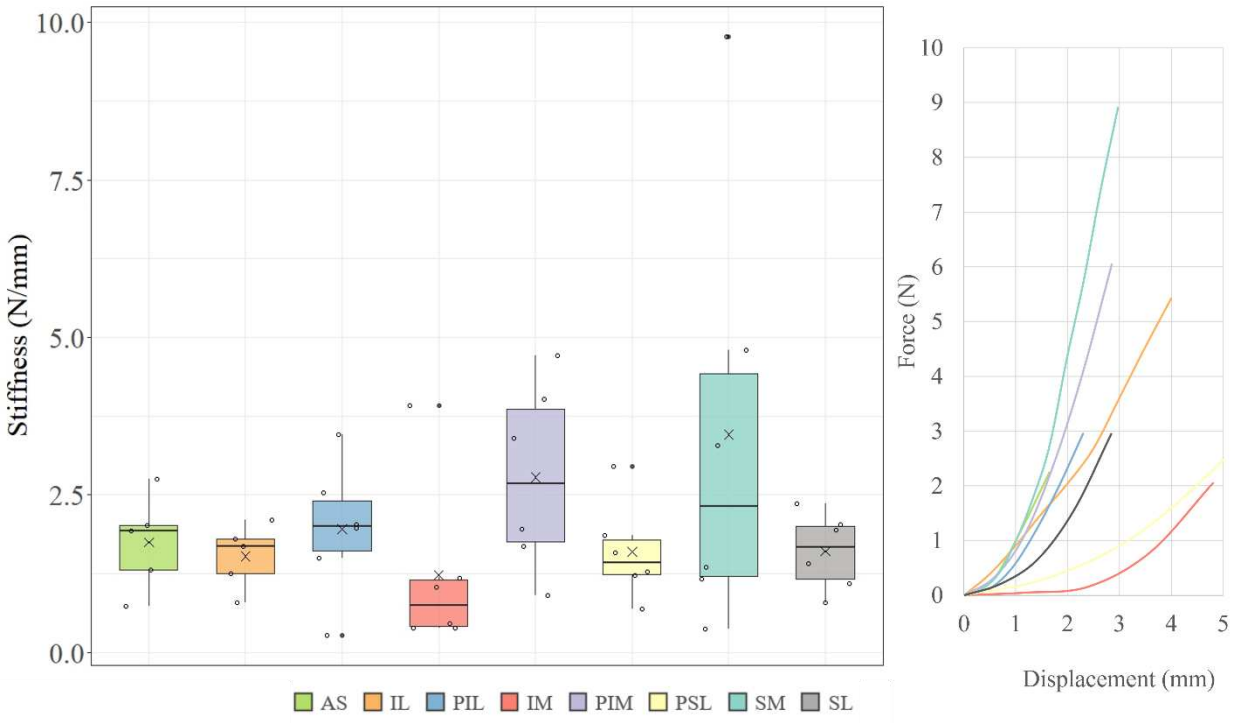

Figure 7: Capsule section stiffness (left), and representative median stiffness force-displacement curves for TMJ capsule sections (right).

3 Articular cartilage

Fresh ovine TMJs (n=3 left, n=3 right) were excised *en bloc*; joint capsules were opened, and their articular discs were removed to expose the fossa and condylar cartilage regions (Figure 8). During indentation, cartilage surfaces were submerged in PBS at room temperature (20°C) and mounted perpendicular to the indenter motion using an adjustable clamp. Indentation testing was

performed using the MTS Bionix™ system outfitted with a calibrated 2 lb load cell (Futek, Irvine,CA). A stainless-steel indenter tip with a 0.4 mm radius was used to indent the cartilage surface in five locations spaced equally across the width of the sample surface. A preload of 5mN was used to confirm contact with the cartilage surface. The specimens were then indented in each location to a 0.2 mm depth at a rate of 0.2 mm/s to approximate the rate of mastication [201, 202], followed by a 100 s hold to allow for tissue relaxation before indenter retraction. Force and displacement data were collected during the stress-relaxation test. MATLAB was used to analyze the force displacement data collected during indentation testing according to the method described by Labus *et al.* [61]. The instantaneous and equilibrium elastic moduli (E) were calculated using Hertzian contact mechanics (*Equation 2.4*) [203]:

$$E = \frac{1 - v^2}{\frac{4R^{\frac{1}{2}}d^{\frac{3}{2}}}{3F} - \frac{1 - v_i{}^2}{E_i}} \qquad \textit{Equation 2.4}$$

Where υ is the Poisson's ratio of the sample, υ_i is the Poisson's ratio of the indenter tip, E_i is the Young's modulus of the indenter tip, F is the measured force, and d is the indenter tip displacement. For this analysis, E_i = 210 GPa and υ_i = 0.29 were assigned to represent the stainless-steel indenter tip, and υ = 0.49 was ascribed to the TMJ articular cartilage to simulate near-incompressibility. The instantaneous modulus was calculated using a least-squares fit of *Equation 2.4* to the loading portion of the force-displacement data. Force-displacement data from the end of the 100 s hold period was used to calculate the equilibrium modulus using *Equation 2.4*. Any indentations for which the %RMSE for the least-squares fit was greater than 5% were ignored. Two-sample t-tests were used to compare equilibrium and instantaneous moduli of the condyle and fossa, and a one-way ANOVA with *post hoc* Tukey test was performed to investigate statistical differences in the

regional properties of the fossa and condylar cartilage. For these analyses, $p < 0.05$ was considered significant.

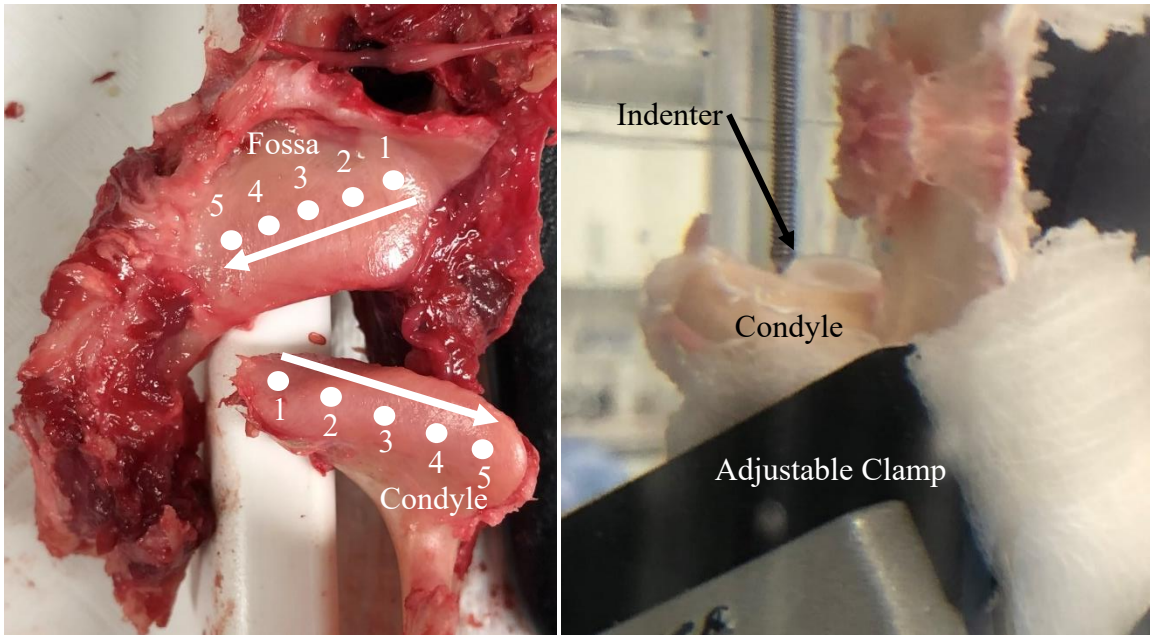

Figure 8: Cartilage surfaces of the ovine TMJ disc (left) and indentation testing apparatus (right)

The average instantaneous and equilibrium moduli for all cartilage indentations were 1200 ± 800 kPa (n=27) and 200 ± 190 kPa (n=23), respectively. No statistically significant differences between regions in the fossa or regions in the condyle were found for equilibrium or instantaneous moduli (Figure 9). However, the central portion (location 3) of the condyle and fossa tended to have higher indentation moduli than the peripheral regions (locations 1 and 5). Moduli calculated from indentation data are comparable in magnitude to compressive moduli for condylar cartilage that have been reported for other species [33, 75, 197].

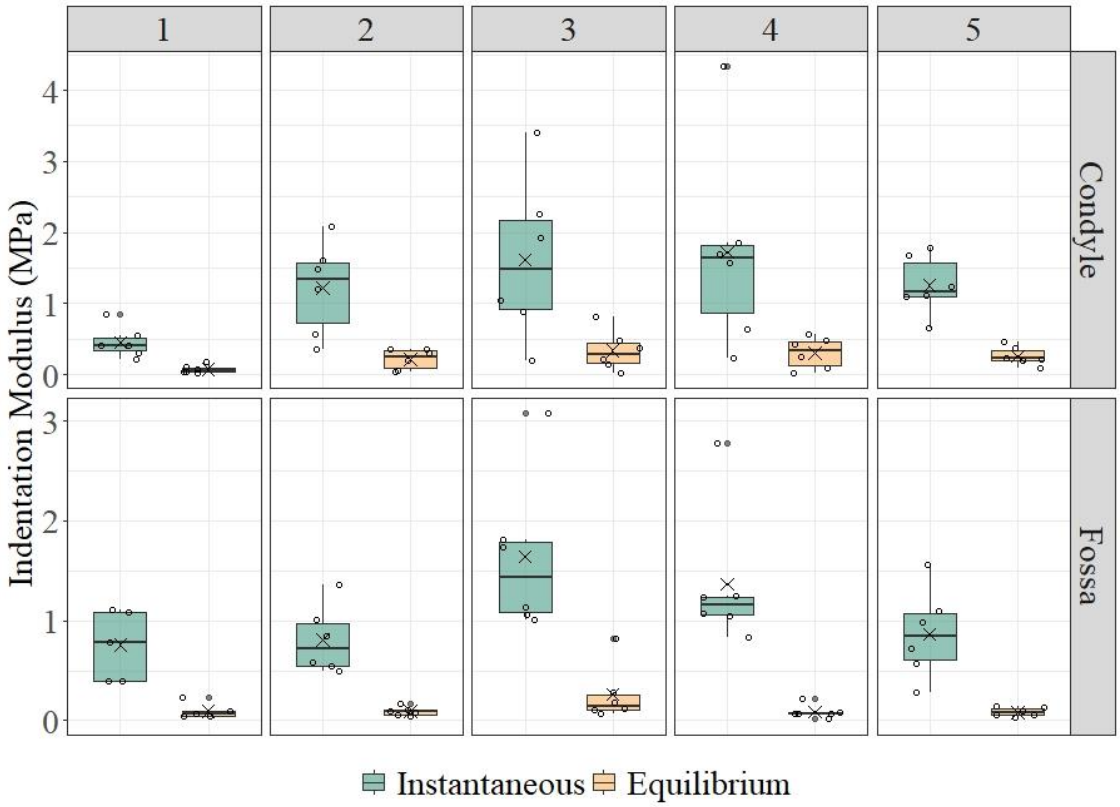

Figure 9: Summary of regional instantaneous and equilibrium moduli from indentation of the TMJ fossa and condylar cartilage.

4 Summary

A robust characterization of the mechanical behavior of the ovine TMJ discs using unconfined compression and friction experiments has been performed, which complements the indentation and tensile evaluation of Labus *et al* [61]. Data on the tensile behavior of joint capsule regions was collected and stress-relaxation experiments on the mandibular and fossa cartilage were also performed. This in-depth analysis of the ovine TMJ soft tissues provides the requisite inputs for FE model development, which will play a key role in the successful development of TMJ disc replacement strategies. In addition, the mechanical properties of the TMJ disc, articular cartilage, and joint capsule have been defined, providing target values for implant development to support long-term implant survival.

CHAPTER 3 - IDENTIFICATION OF BIOMATERIAL CANDIDATES FOR TMJ DISC REPLACEMENT

1 Polymers

The term polymer refers to a broad class of materials characterized by chains of smaller monomer subunits that are chemically linked with covalent bonds. Classification and design of polymers is complex, as the structure and size of each molecule can vary significantly, which results in a wide range of properties from the same monomer subunit. Some of the important features to consider are the polymer molecular weight and hierarchical architecture. The molecular weight of a polymer is the sum of the molecular mass of the monomer constituents. Polymers with high molecular weight typically exhibit greater failure properties and melting temperatures. The architecture of a polymer refers to both the nature of its individual molecules as well as the structure of its assembled molecules. Placement of repeated monomer groups within a polymer may be random (atactic), alternating (syndiotactic), or uniform (isotactic). Assembled polymer molecules may have linear or branched structures that can be random (amorphous), highly ordered (crystalline), or a combination of these two arrangements. Polymers may be assembled from single monomers (homopolymers) or multiple monomers (copolymers). Molecular weight and architecture can be controlled during synthesis to create a wide variety of structures from the same monomer or monomers [204, 205].

Polymers are ubiquitous in biomedical applications due to their versatility and tunability. Recent applications include tissue engineering, tissue replacement [206-213], and targeted drug delivery [214-217]. Regardless of application, implanted polymeric materials must be biocompatible, have predictable degradation behavior, and possess sufficient mechanical strength

to survive *in vivo*. By definition, a biocompatible material should not cause damage to the surrounding cells and tissues [218]. For this reason, the target for most long-term implantable materials is chemical and biological inertness [219, 220]. Poorly biocompatible materials will elicit an immune response in the surrounding cells in an attempt to isolate or remove the foreign object from the body [221]. The definition of biocompatibility, however, must be expanded when considering bioactive or multi-material implants for which a tissue response is intended. Thus, biocompatibility is a function of the desired *in vivo* response [222].

Mechanical strength is also an important consideration in implant design. In this discussion, the term mechanical strength is used broadly, referring to the ability of an implanted device to withstand appropriate physiologic loading throughout its *in vivo* lifecycle. The necessary strength varies based on application; orthopedic materials such as total hip and total knee replacements must withstand significant and frequent loading without failure [223, 224], whereas subcutaneous drug-eluting implants may only experience slight and infrequent loading [225]. As previously discussed, the TMJ experiences relatively large and frequent stresses, suggesting that high mechanical strength is an important factor in material selection. A deep understanding of the native tissue behavior can be used to set target values for implant mechanical properties to ensure an implant will not be destroyed prematurely.

Degradability of an implanted material refers to the rate of, and mode by which, an implant will be dissociated naturally in the body. Degradation rate of a polymeric material can typically be modified through manipulation of synthesis conditions and implant geometry, which allows for controlled release of molecules like degradation byproducts or encapsulated drugs [226, 227]. Long term implantation of materials requires exceptionally low degradation rates. The primary *in vivo* degradation mechanisms are hydrolytic and enzymatic in nature [228-230]. In some cases,

particularly as the result of a significant immune response, oxidative degradation may also occur [231, 232]. Most polymeric materials are susceptible to oxidative degradation, but numerous artificial polymers are not susceptible to hydrolytic or enzymatic degradation, which makes them highly resistant to *in vivo* degradation in the absence of a pronounced tissue immune response [231]. Biocompatibility, degradability, and mechanical strength are also intimately related: degradable materials will not maintain mechanical strength and may create toxic concentrations of wear particles; materials with low mechanical strength may fragment and degrade sooner than intended; and poorly biocompatible materials can elicit a significant immune response resulting in accelerated degradation. Therefore, biocompatibility, mechanical strength, and degradability of an implanted material must be appropriately understood and balanced in the design of polymeric implants.

For replacing the TMJ disc, a polymeric implant should be sufficiently robust to survive the natural environment as effectively as possible, but biological tissues are incredibly complex and dynamic structure of biomolecules and cells that may not be possible to replicate with a single material. As a result, some implant design targets may need to exceed the natural tissue properties to be a successful solution. Thus, the dominant role of biological materials must be identified in order to prioritize target materials for tissue development. Beyond biocompatibility and general mechanical strength, the frictional and compressive properties of the TMJ disc are primary design targets for artificial implant development. A non-degradable implant or a bioactive degradable scaffold should possess appropriate mechanical strength and appropriate degradation rate to allow for the surrounding tissue to recover and, in the case of a bioactive scaffold, replace the scaffold over time.

Several polymer candidates for artificial TMJ disc replacement have been identified, including polyvinyl alcohol (PVA), polyethylene glycol diacrylate (PEGDA), and gelatin methacrylate (GelMA). Polycaprolactone (PCL) and Polypropylene (PP) have also been considered as structural reinforcement for PEGDA, GelMA, and PVA hydrogels. Figure 10 shows the skeletal formulae of these polymer candidates.

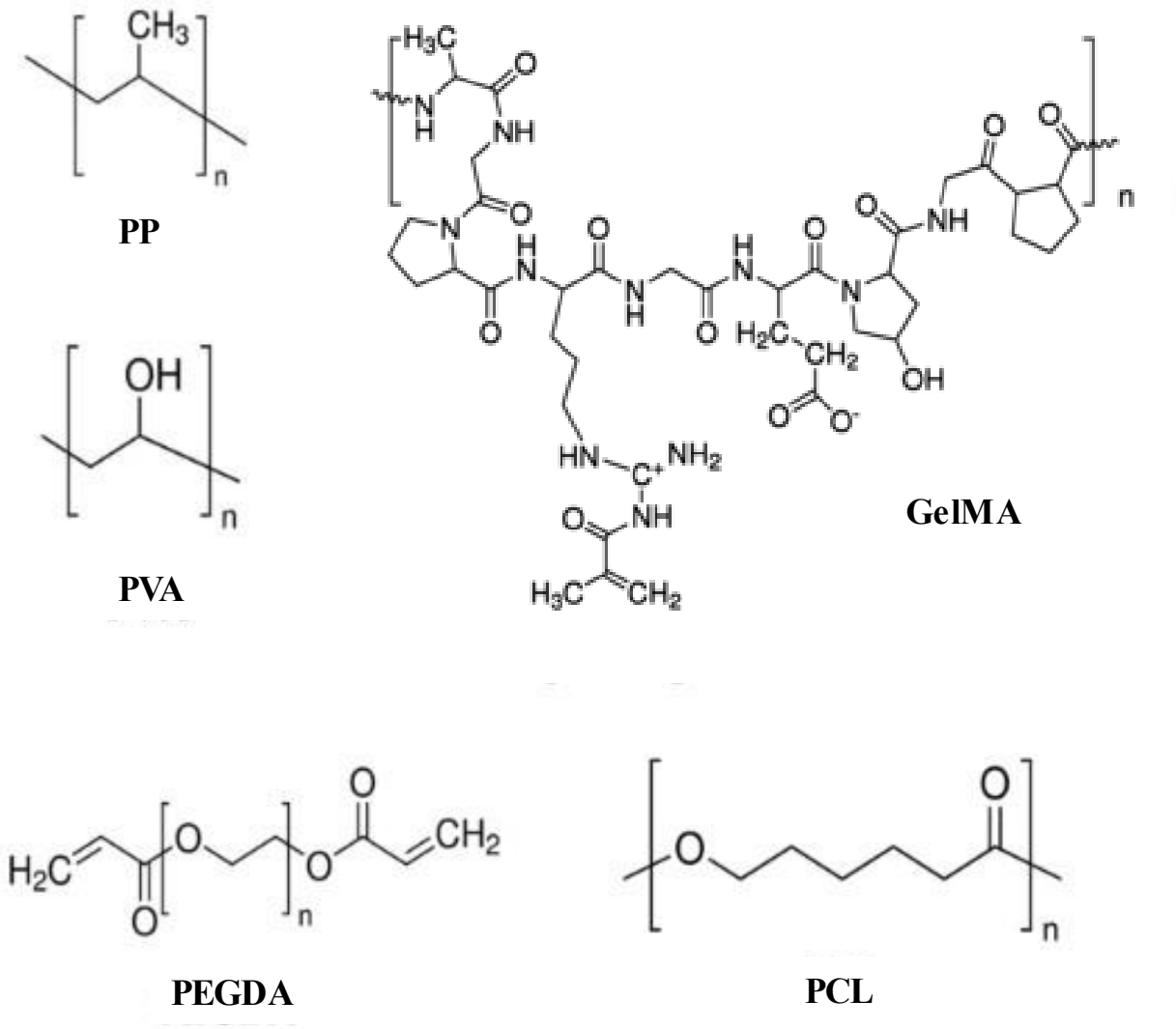

Figure 10*:* Monomer skeletal formulae of candidate TMJ disc replacement candidates

1.1 Polyethylene glycol diacrylate

PEGDA is synthesized from polyethylene glycol monomers by replacing the polyethylene glycol hydroxyl end groups with two acrylate groups [233]. PEGDA and PEGDA hydrogels have been used in biomedical applications of both photosensitive and functionally graded materials [234-236]. PEGDA monomers are polymerized through covalent bonding at acrylate ends through chain polymerization facilitated by a catalyst such as a thermal or photo initiator [237]. The primary *in vivo* degradation method of PEGDA is via hydrolytic degradation, although oxidative degradation is also possible in the presence of a tissue immune response [238, 239]. Unbonded PEGDA monomers are not biocompatible. In polymer form, however, PEGDA and PEGDA hydrogels exhibit good biocompatibility given that excess unbonded PEGDA and catalyst molecules are removed [240].

1.2 Gelatin methacrylate

Gelatin, the backbone of GelMA, is a product of collagen degradation and has excellent biocompatibility [241, 242]. Methods of GelMA synthesis vary, but reacting gelatin with methacrylic anhydride is one common approach [243]. Similar to PEGDA, acrylate groups on the GelMA molecules may be utilized to create covalent bonds between GelMA molecules through catalyzed chain polymerization [244]. This technique can also be used to create GelMA hydrogels when GelMA is dissolved in water prior to polymerization. It also allows for the creation of complex geometries from liquid GelMA via digital light projection 3D printing techniques [245, 246]. Without reinforcement, however, structures synthesized with GelMA possess relatively low mechanical strength [247]. In addition, GelMA is rapidly degraded both hydrolytically and enzymatically, contributing to a short *in vivo* lifespan [244]. Thus, GelMA is typically used for

cell transplantation [248] in tissue engineering approaches that are focused on short-term therapeutics for the regeneration of native tissues (such as skin and blood vessels [244]), rather than long-term implantation [248].

1.3 Polyvinyl alcohol

PVA is synthesized through hydrolysis of polyvinyl acetate, rather than through the assembly of vinyl alcohol monomers, which are inherently unstable [249]. The solubility of PVA is inversely related to the degree of hydrolysis, with high degrees of hydrolysis (96%-99%) exhibiting lower solubility [250]. Hydrogels may be synthesized from PVA by dissolving PVA molecules in water at elevated temperatures (~80°C, for high degrees of hydrolysis). Once dissolved, PVA is poured into molds and put through freeze-thaw (FT) cycling during which physical crosslinking of the PVA molecules occurs due to ice crystal expansion [251]. PVA hydrogels have been identified as a promising candidate for musculoskeletal soft tissue replacement [252]. They can also be formulated to exhibit low friction, retain biomimetic water content, and possess mechanical properties similar to a range of cartilaginous tissues [252-255]. Furthermore, PVA is considered non-degradable *in vivo* [256, 257]. PVA hydrogels and associated wear particles exhibit excellent biocompatibility and hemocompatibility [258], and they have been shown to exhibit a lower tissue immune response than ultra-high molecular weight polyethylene [259]. Among other applications, PVA hydrogels have been investigated as a replacement for intervertebral discs [260], meniscus [261], vasculature [262], and articular cartilage in load bearing joints [263-265]. To our knowledge, PVA hydrogels have only recently been investigated application in the TMJ. Jiang *et al* demonstrated the ability to maintain stability of the TMJ and prevent cartilage and bone damage associated with disc resection using a partial disc repair patch comprising PVA hydrogel reinforced with a PCL mesh [266].

1.4 Polycaprolactone

PCL is a polymer with well documented biocompatibility that has been used to develop tissue engineering scaffolds and implantable devices [267, 268]. PCL has a relatively low melting temperature (60° C) and excellent processability, which makes it facile to implement in additive manufacturing technologies [268-270]. PCL is synthesized through ring opening polymerization of epsilon-caprolactone, which can be facilitated by a broad range of catalytic systems [271]. Degradation rates of PCL are well documented *in vitro* and *in vivo* and are related to implant structure and PCL molecular weight [272]. PCL is hydrolytically degraded *in vivo* at an exponential rate through scission of the polymer backbone leading to a loss in molecular weight and mechanical strength over time [273]. Thus, PCL is not recommended for long-term (> 3 years) implantable devices, but it is an excellent candidate for the development of tissue engineering strategies [274].

1.5 Polypropylene

PP is a polymer created from propylene monomers that are joined using a metallocene catalyst under controlled temperatures and pressures [275]. Propylene is a gas produced during petroleum refinement and contains only carbon and hydrogen molecules [275]. Most commercially available PP is linear and isotactic [275]. Biomedical uses of PP include sutures [276, 277] and meshes for hernia and pelvic organ prolapse repair [278, 279]. PP, a petroleum-based polymer, is considered non-degradable *in vivo*, but it can be susceptible to oxidative degradation [232, 280]. Biocompatibility of PP implants can be influenced by molecular weight and implant structure [281]. In the case of implanted meshes, lower molecular weight PP is typically more biocompatible

than higher molecular weight blends [282]. Surface coatings and functionalization have been shown to effectively reduce immune response to implanted PP structures [276, 283].

2 Mechanical properties of polymer candidates

The relationship between synthesis conditions, molecular architecture, and mechanical strength is well documented for PCL [284] and PP [275, 285]. The use of PVA, PEGDA, and GelMA hydrogels in biomedical engineering, however, is relatively limited and therefore, they have not been characterized as extensively. The goal of this evaluation was to characterize relevant properties of PEGDA, GelMA, and PVA to evaluate their suitability for an artificial TMJ disc replacement. Preliminary evaluation of PEGDA, GelMA, and PVA hydrogels was performed through indentation stress-relaxation experiment. During their synthesis and molding prior to indentation testing, the low mechanical strength of PEGDA and GelMA hydrogels was apparent, which may explain the lack of published mechanical data available for these hydrogels without additives [286-288] or structural reinforcement [289, 290]. In contrast, PVA hydrogels demonstrated excellent toughness, were simple to produce, and were less costly. It was intractable to study the frictional, compressive, and tensile properties of PEGDA and GelMA hydrogels according to the same method used for ovine TMJ tissues due to their low mechanical strength. Thus, we focused additional mechanical investigation of frictional, compressive, and tensile properties on the PVA hydrogels.

2.1 Hydrogel synthesis

PVA hydrogels were synthesized with 15%, 20%, or 25% initial polymer weight concentrations at mixing. PVA (molecular weight 89,000-98,000, 99+% hydrolyzed) was mixed with deionized water in a sealed beaker and heated to 80°C for at least two hours while being

stirred. Sheets of PVA hydrogel were molded between two glass microscope slides with a thickness of 2 mm for friction testing specimens and 1 mm for compressive, indentation, and tensile testing specimens. All groups were subjected to 6 FT cycles (12 hours at -18°C, 3 hours at 20°C). After cycling, gels were removed from their molds and submerged in PBS for at least 24 hours prior to testing. Molded PVA sheets were cut to the appropriate geometries immediately before testing. PEGDA (Mn = 700) hydrogels with polymer concentrations of 10%, 20%, and 30% and GelMA (degree of substitution: 60%) hydrogels with 10% and 20% polymer concentrations were mixed with DI water and 1% phenylbis(2,4,6-trimethylbenzoyl)phosphine oxide photoinitiator. GelMA and PEGDA hydrogel formulations were injected into 24 well plates in 2 ml aliquots, then fully cured with an ultraviolet light source (Exakt 402, Exakt Technologies, Oklahoma City, OK) for one hour. Prior to testing, all PEGDA and GelMA hydrogels were kept hydrated in deionized water. All chemicals were purchased from Sigma-Aldrich (Merck KGaA, Darmstadt, Germany).

2.2 Indentation

Indentation stress-relaxation testing was performed using the same method described for the TMJ articular cartilage in Chapter 2. Briefly, a stainless-steel indenter tip with a 0.4 mm radius was used to indent hydrogel surfaces to a depth of 0.2 mm at a rate of 0.2 mm/s, followed by a 100 s hold to allow for tissue relaxation before indenter retraction. Force and displacement data were collected and used to calculate the instantaneous and equilibrium elastic moduli using Hertzian contact mechanics (*Equation 2.4*). The total number of indentations varied between groups due to initial sample size and the number of indentations which met the inclusion criteria (< 5% RMSE of loading data). Table 1 shows the number of indentations used for analysis for each hydrogel group. Data collected from the TMJ discs were non-normal and exhibited higher variation than the

hydrogel groups. Thus, a Kruskal-Wallis test with *post hoc* Wilcoxon rank-sum tests at significance level $\alpha = 0.05$ were implemented to compare instantaneous and equilibrium moduli between the hydrogel groups and TMJ disc (Figure 11). Previously published indentation data collected regionally on the ovine TMJ disc [61] were grouped for these comparisons.

Table 1: Summary of indentation number for each hydrogel group

	GelMA		PEGDA			PVA		
polymer concentration (weight %)	10	20	10	20	30	15	20	25
number of indentations	5	5	10	63	48	17	19	18

The instantaneous and equilibrium moduli of all hydrogels increased with polymer concentration, and mean equilibrium moduli were smaller than mean instantaneous moduli for all hydrogels. There were statistically significant differences between the TMJ disc and all GelMA hydrogels for both the instantaneous and equilibrium moduli. The instantaneous moduli of both the 10% and 20% PEGDA hydrogels were significantly different from that of the TMJ disc, and only the 10% PEGDA approximated the TMJ disc equilibrium modulus. The indentation properties measured for the 10% and 20% PEGDA hydrogels fell within the range of TMJ disc values (Figure 11). Therefore, PEGDA formulations between 10% and 20% may approximate the TMJ disc tissue's mechanical behavior.

The instantaneous moduli of both the 15% and the 20% PVA hydrogels were similar to that of the TMJ disc. Additionally, the 15% PVA group was not significantly different from the TMJ disc for equilibrium modulus. These results suggest that the 15% PVA most closely matches the behavior of the TMJ discs in indentation. However, the ratios of instantaneous to equilibrium modulus for the PVA hydrogels were 2.9 (15% PVA) to 4.3 (25% PVA) times greater than the

ratio for the TMJ disc tissue (0.19 ratio). This discrepancy emphasizes the high degree of relaxation observed in the native TMJ disc tissue as compared to the PVA hydrogels. However, all experimental groups fell within the range of observed instantaneous moduli of the TMJ disc. Activities such as chewing or talking induce larger dynamic stresses on the TMJ disc than more static, distributed forces such as those that occur during clenching [56]. The dynamic mechanical behavior of the TMJ disc is primarily governed by its instantaneous properties rather than its equilibrium properties. Therefore, it may be argued that the instantaneous modulus may be a more relevant consideration for a TMJ disc replacement material than the equilibrium modulus.

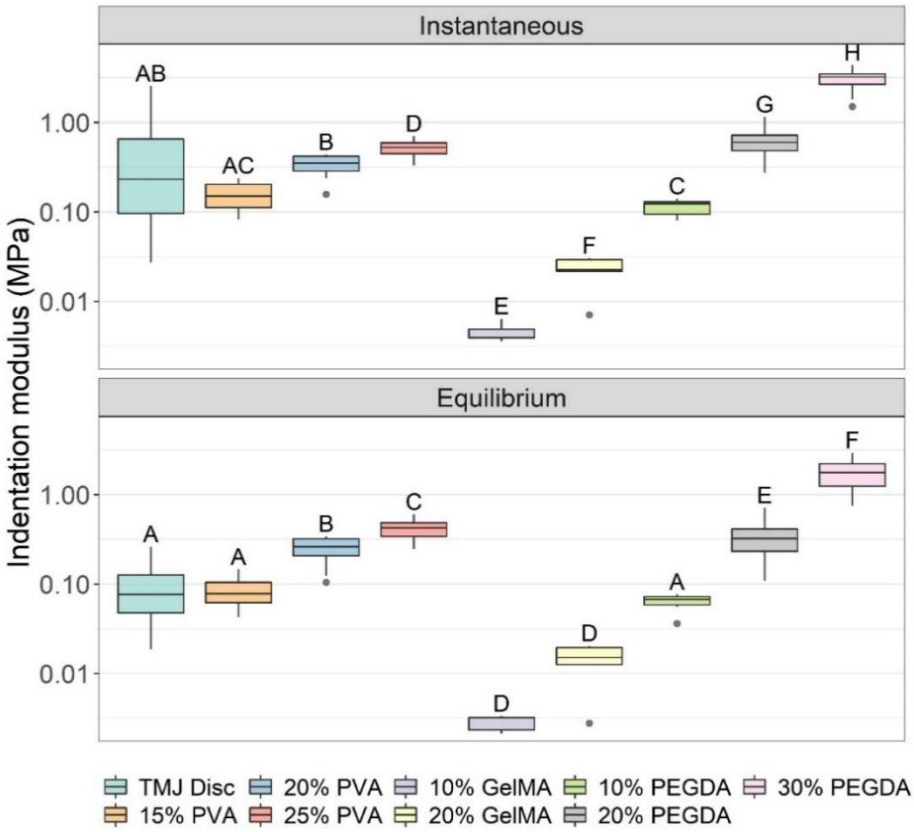

Instantaneous Modulus [MPa]								
p-values	15% PVA	20% PVA	25% PVA	10% GelMA	20% GelMA	10% PEGDA	20% PEGDA	30% PEGDA
TMJ Disc	0.10	0.31	**0.03**	**<0.001**	**<0.001**	**0.04**	**<0.001**	**<0.001**
15% PVA		**<0.001**	**<0.001**	**<0.001**	**<0.001**	0.07	**<0.001**	**<0.001**
20% PVA			**<0.001**	**<0.001**	**<0.001**	**<0.001**	**<0.001**	**<0.001**
25% PVA				**<0.001**	**<0.001**	**<0.001**	**0.02**	**<0.001**
10% GelMA					**0.008**	**<0.001**	**<0.001**	**<0.001**
20% GelMA						**<0.001**	**<0.001**	**<0.001**
10% PEGDA							**<0.001**	**<0.001**
20% PEGDA								**<0.001**

Equilibrium Modulus [MPa]								
p-values	15% PVA	20% PVA	25% PVA	10% GelMA	20% GelMA	10% PEGDA	20% PEGDA	30% PEGDA
TMJ Disc	0.80	**<0.001**	**<0.001**	**<0.001**	**<0.001**	0.33	**<0.001**	**<0.001**
15% PVA		**<0.001**	**<0.001**	**<0.001**	**<0.001**	0.13	**<0.001**	**<0.001**
20% PVA			**<0.001**	**<0.001**	**<0.001**	**<0.001**	**0.02**	**<0.001**
25% PVA				**<0.001**	**<0.001**	**<0.001**	**0.009**	**<0.001**
10% GelMA					0.06	**<0.001**	**<0.001**	**<0.001**
20% GelMA						**<0.001**	**<0.001**	**<0.001**
10% PEGDA							**<0.001**	**<0.001**
20% PEGDA								**<0.001**

Figure 11: Box-and-whisker plots of the calculated instantaneous and equilibrium elastic moduli from indentation of the PVA, GelMA, PEGDA hydrogels, and the pooled TMJ data from Labus et al [61]. Groups that do not share a letter were significantly different. All p-values for post hoc Wilcoxon rank-sum comparisons are provided in the associated table (below).

2.3 Friction

The coefficient of friction (COF) of PVA hydrogels was tested against a bearing surface of ovine TMJ fossa cartilage according to the same protocol described in Chapter 2 for TMJ disc samples. Briefly, an osteochondral plug was drawn back and forth across the surface of each sample five times at rates of 0.4 mm/s, 4.0 mm/s, and 40 mm/s. Samples were immersed in artificial synovial fluid. The normal and transverse forces were measured, and MATLAB was used to calculate the sample COF defined as the absolute value of the transverse force, divided by the normal force. Eight PVA hydrogel samples from each group were cut to an approximate size of 40 mm by 20 mm. A Kruskal-Wallis statistical test with *post hoc* Wilcoxon rank-sum tests at significance level $\alpha=0.05$ were performed to compare COF between the hydrogel groups and TMJ disc (Figure 16). No statistically significant differences in COF were found between the TMJ disc and any of the PVA hydrogel groups at any of the testing speeds. Although there were no differences in COF between the three PVA hydrogel concentrations at the 0.4 mm/s speed, the COF of the 15% PVA hydrogel was significantly lower than the 20% and 25% PVA hydrogels at 4 mm/s and 40 mm/s speeds (Figure 12).

Sardinha *et al.* demonstrated similar COF values for PVA-based hydrogels to those measured during this study under similar loading conditions [254]. However, hydration, applied pressure, translation speed, hydrogel concentration, hydrogel molecular weight, and contacting material all influence the apparent friction coefficient [199, 200]. At moderate (4 mm/s) and high (40 mm/s) speeds, the 15% PVA hydrogel exhibited significantly lower friction than the 20% and 25% PVA hydrogels, suggesting that lower polymer concentrations may exhibit better frictional properties at higher speeds. However, this trend may not be consistent for different applied loads. Experiments on PVA/polyvinylpyrrolidone hydrogels have shown a decrease in COF with

increasing polymer concentration at lower applied loads and the opposite trend at higher applied loads [291]. Importantly, the friction experiments in the current study showed no statistical difference in COF between the ovine TMJ disc and PVA hydrogels regardless of translation speed or polymer concentration.

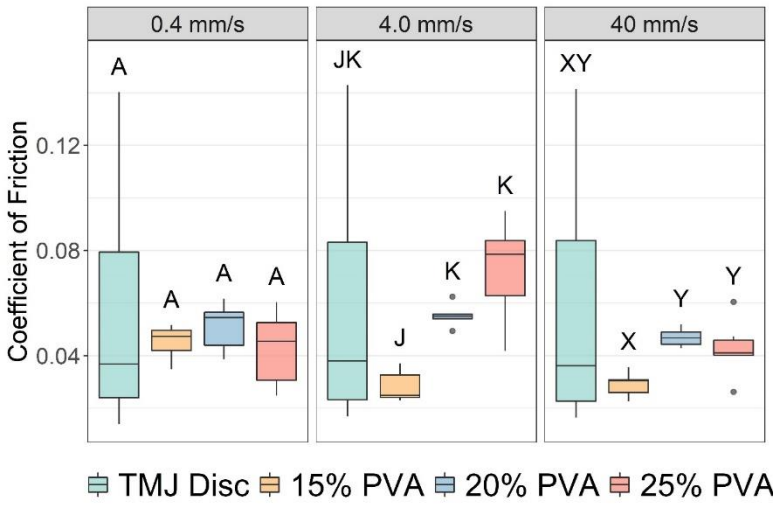

0.4 mm/s			
p-values	20% PVA	25% PVA	TMJ Disc
15% PVA	0.18	0.94	0.70
20% PVA		0.39	0.59
25% PVA			1.0

4.0 mm/s			
p-values	20% PVA	25% PVA	TMJ Disc
15% PVA	**0.002**	**0.002**	0.59
20% PVA		0.09	0.39
25% PVA			0.38

40 mm/s			
p-values	20% PVA	25% PVA	TMJ Disc
15% PVA	**0.002**	**0.03**	0.70
20% PVA		0.18	0.39
25% PVA			0.94

Figure 12: (left) Box-and-whisker plots of the average COF at each speed from friction evaluation of the PVA hydrogels and ovine TMJ discs. Groups that do not share a letter were significantly different. (right) All p-values from post hoc Wilcoxon rank-sum comparisons are provided in the associated table.

2.4 Compression

Unconfined compression tests were performed on cylindrical samples of the PVA hydrogels using the protocol described in Chapter 2 for ovine TMJ discs. A 2 mm diameter cylindrical sample was removed from the central portion of each TMJ disc with a biopsy punch. Each sample was loaded to a minimum of 60% strain at a strain rate of 0.005 s^{-1} between two compressive platens. Paired force-displacement data were collected, and MATLAB was used to calculate the sample stress as the axial force divided by the sample cross-sectional area. Stretch was calculated as the displacement of the upper platen divided by the initial height of the sample.

2-term Yeoh model fitting and localized linear fitting were used to determine the Yeoh model fitting and tangent moduli, respectively, using the same method described in Chapter 2. The values of C_1 and C_2 were determined using a least-squares fit of *Equation 2.3* to the stress-stretch data, and the tangent moduli at stretch values from $\lambda = 1.00$ to $\lambda = 0.96$ and from $\lambda = 0.60$ to $\lambda = 0.56$ were calculated using a localized linear regression.

Eight samples from each PVA hydrogel concentration were designated for use in unconfined compression experiments. Similar to the analysis of friction and indentation testing data, a Kruskal-Wallis statistical test with *post hoc* Wilcoxon rank-sum tests (α=0.05) was implemented to compare compressive tangent moduli and 2-term Yeoh model fitting coefficients between the hydrogel groups and TMJ disc (Figure 13). The stress-stretch behavior was similar between the PVA hydrogels and the TMJ disc samples under small deformations. However, the TMJ disc data exhibited a greater degree of nonlinearity under larger deformations. For small deformations (stretch values approaching 1.00), the TMJ disc tangent modulus was not statistically different from the 20% PVA and 25% PVA. However, for greater compressive stretches ($\lambda < 0.90$), the TMJ disc tangent modulus was significantly larger than all PVA hydrogels. The mean tangent moduli and fitted C_1 parameter increased with increasing PVA concentration. The %RMSE for the 2-term Yeoh model fits of the unconfined compression data was 0.60% for the PVA hydrogels. The values of C_1 and C_2 for the TMJ disc were significantly higher than those of the PVA hydrogels (Figure 13).

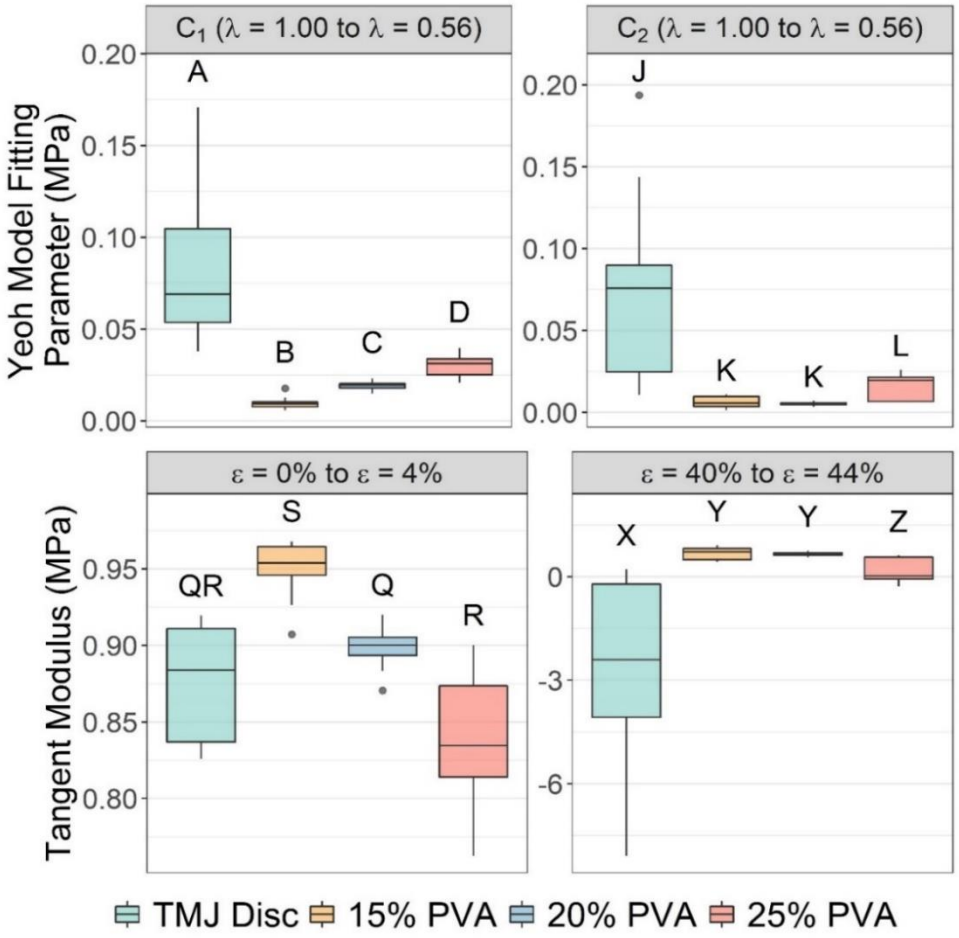

C_1 (λ = 1.00 to λ = 0.56) [MPa]			
p-values	20% PVA	25% PVA	TMJ Disc
15% PVA	**< 0.001**	**< 0.001**	**< 0.001**
20% PVA		**0.001**	**< 0.001**
25% PVA			**< 0.001**

C_2 (λ = 1.00 to λ = 0.56) [MPa]			
p-values	20% PVA	25% PVA	TMJ Disc
15% PVA	0.88	**0.04**	**< 0.001**
20% PVA		**0.003**	**< 0.001**
25% PVA			**0.003**

Tangent Modulus (λ = 1.00 to λ = 0.96) [MPa]			
p-values	20% PVA	25% PVA	TMJ Disc
15% PVA	**< 0.001**	**< 0.001**	**< 0.001**
20% PVA		**0.005**	0.32
25% PVA			0.07

Tangent Modulus (λ = 0.60 to λ = 0.56) [MPa]			
p-values	20% PVA	25% PVA	TMJ Disc
15% PVA	0.72	**0.01**	**< 0.001**
20% PVA		**< 0.001**	**< 0.001**
25% PVA			**0.02**

Figure 13 : (top) Box-and-whisker plots of the calculated 2-term Yeoh model fitting parameters (C_1, C_2) from λ = 1.00 to λ = 0.56, and the tangent moduli from λ = 1.00 to λ = 0.96 and from λ = 0.60 to λ = 0.56. (bottom) Groups that do not share a letter were significantly different. All *p*-values for *post hoc* Wilcoxon rank-sum comparisons are provided in the associated table.

The unconfined compression results reveal a disproportionate increase in tangent modulus with increasing stretch magnitude for the TMJ disc compared to the PVA hydrogels. At lower levels of stretch, the tangent modulus of the TMJ disc was not significantly different from the 20% and 25% PVA hydrogel. However, at higher ($\lambda = 0.60$ to $\lambda = 0.56$) compressive stretch magnitudes, the tangent modulus of the TMJ disc was significantly higher than the PVA hydrogels. These findings are explained by the non-linear behavior of the TMJ disc tissue, which has been documented across species [66]. In addition, the tangent moduli for unconfined compression in the TMJ disc at higher values of stretch also exceeded the indentation moduli. This behavior is likely due to the significant collagen fiber component in the TMJ disc, which can contribute to its stiffness to a greater degree in macro-scale unconfined compression than in micro-scale indentation [198]. Thus, we have demonstrated that the PVA hydrogels do not fully mimic the non-linear behavior of the TMJ disc. These results suggest that transversely aligned tensile reinforcement may be required to increase the compressive stiffness of PVA hydrogel materials at higher physiological strains (estimated up to 44%) to mimic the compressive behavior of the TMJ disc [192].

2.5 Tension

PVA hydrogel tensile specimens were tested following the protocol described by Labus *et al.* for ovine TMJ discs [61]. Specifically, PVA hydrogel specimens were cut to a dog-bone shape with width 3.48 ± 0.14 mm and thickness 1.44 ± 0.10 mm (mean ± standard deviation) using a scalpel and 3D printed cutting jig. The initial distance between grips was measured after a preload of 0.05 N was applied. Graphite powder was applied to the top surface of each sample to enhance the texture for measuring strain via digital image correlation. Each sample was preconditioned for 10 cycles to 8% strain at a displacement rate of 8% strain/second. Once preconditioned, samples

were loaded to failure at a rate of 0.01 s^{-1}. The initial grip-to-grip distance was used to define the strain rate for each test. A MATLAB-based digital image correlation algorithm was used to calculate the average stretch of a central region of interest of each sample up to a stretch of $\lambda = 1.4$ [61, 292]. The stress-stretch data were used to determine a tensile elastic modulus using a linear fit of the data between $\lambda=1.1$ to $\lambda = 1.2$, matching the range used for TMJ disc samples. The failure stretch for each sample was calculated by measuring fiducial markers placed on the sample surface using ImageJ (Version 1.52s, National Institute of Health, Bethesda, MD) [293]. PVA ultimate strength was defined as the maximum stress observed for each sample, and PVA sample toughness was estimated as the ultimate strength multiplied by the failure strain divided by two due to the highly linear stress-stretch behavior. A one-way ANOVA with *post hoc* Tukey test ($\alpha=0.05$) was used to compare the PVA hydrogel and TMJ disc tensile moduli, failure stretch, ultimate tensile strength, and toughness (Figure 14). A logarithmic transformation was applied to all tensile data before statistical evaluation in order to satisfy the assumptions of normality and equal variance.

The average elastic modulus, failure stretch, ultimate tensile strength, and toughness increased with PVA concentration. The elastic modulus, ultimate tensile strength, and toughness were all greater in the anteroposterior (AP) direction (predominant fiber direction) than in the mediolateral (ML) direction (transverse to the fibers) for the TMJ disc as demonstrated by Labus *et al*. The mean elastic moduli of the TMJ disc tissue in the AP and ML directions were 630 and 53 times greater, respectively, than the mean elastic modulus of the 25% PVA hydrogel. The ultimate tensile strength of the TMJ disc in the ML direction was not significantly different from the 20% or 25% PVA hydrogels. In the AP direction, the TMJ disc ultimate strength was significantly greater than all PVA hydrogel materials. The failure stretches for the 20% PVA and

25% PVA were significantly greater than the TMJ disc, regardless of direction. A summary of findings from these tensile experiments is provided in Figure 14.

The most disparate material property between the PVA hydrogels and TMJ disc is the tensile modulus. Previous tensile characterization of unmodified PVA hydrogels with the same molecular weight and degree of hydrolysis report tensile moduli from 0.23 MPa [294] to 7.6 MPa [295]. This broad range can be attributed to differences in synthesis methods and PVA concentration. In our evaluation, the tensile modulus of the 25% PVA group (0.40 MPa) was 53 to 630 times smaller than that of the ovine TMJ disc. These results suggest that mimicking the tensile stiffness of the ovine TMJ disc would require reinforcement of the PVA hydrogels. Attempts to reinforce PVA hydrogel networks have been attempted [252]. Introduction of additional polymers into the PVA hydrogel networks has increased tensile moduli to approximately 200 MPa [296]; Holloway *et al.* measured a tensile modulus of 258.1 ± 40.1 MPa for a PVA hydrogel reinforced with melt-blown ultra-high molecular weight polyethylene and PP fibers [294].

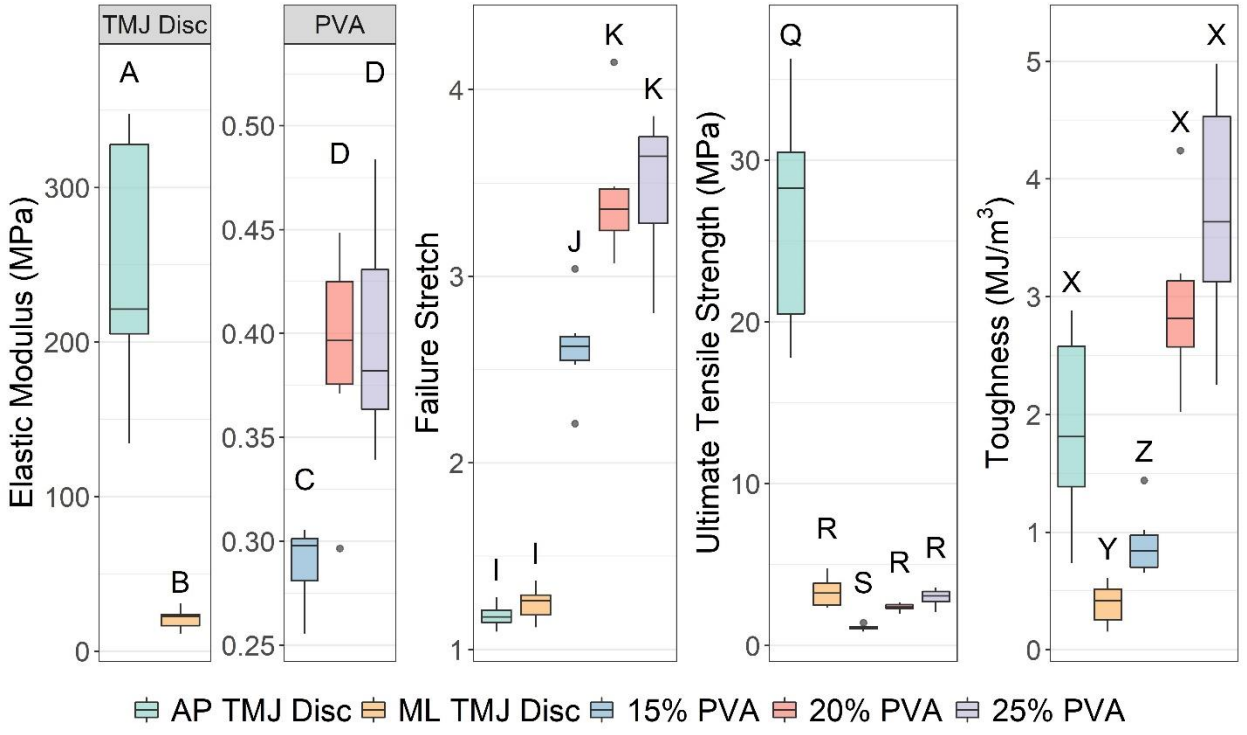

Tensile Modulus [MPa]				
p-values	20% PVA	25% PVA	TMJ Disc AP	TMJ Disc ML
15% PVA	**< 0.001**	**< 0.001**	**< 0.001**	**< 0.001**
20% PVA		0.94	**< 0.001**	**< 0.001**
25% PVA			**< 0.001**	**< 0.001**
TMJ Disc AP				**< 0.001**

Failure Stretch				
p-values	20% PVA	25% PVA	TMJ Disc AP	TMJ Disc ML
15% PVA	**< 0.001**	**< 0.001**	**< 0.001**	**< 0.001**
20% PVA		0.99	**< 0.001**	**< 0.001**
25% PVA			**< 0.001**	**< 0.001**
TMJ Disc AP				0.68

Toughness [MJ/m^3]				
p-values	20% PVA	25% PVA	TMJ Disc AP	TMJ Disc ML
15% PVA	**0.001**	**< 0.001**	0.95	**0.001**
20% PVA		0.89	0.47	**< 0.001**
25% PVA			0.082	**< 0.001**
TMJ Disc AP				**< 0.001**

Ultimate Tensile Strength [MPa]				
p-values	20% PVA	25% PVA	TMJ Disc AP	TMJ Disc ML
15% PVA	**< 0.001**	**< 0.001**	**< 0.001**	**< 0.001**
20% PVA		0.45	**< 0.001**	0.078
25% PVA			**< 0.001**	0.92
TMJ Disc AP				**< 0.001**

Figure 14 : (top) Box-and-whisker plots of the elastic modulus, failure stretch, ultimate tensile strength, and failure stretch from the tensile evaluation of the PVA hydrogels and ovine TMJ discs [61, 297]. Groups that do not share a letter were significantly different. (bottom) All p-values for post hoc Tukey's HSD tests are provided in the associated table.

2.6 Summary

These experiments provide a broad analysis of the mechanical behavior of PVA, GelMA, and PEGDA hydrogels with a direct comparison to the ovine TMJ disc. Overall, trends in these data show increasing elastic moduli measured for indentation, tension, and unconfined

compression with increasing polymer concentration. Table 2 shows a brief summary of measured material properties of the ovine TMJ disc, condylar cartilage, and joint capsule in comparison to relevant material properties for PCL, PP, 20% PEGDA hydrogel, 20% GelMA hydrogel, and 20% PVA hydrogel [61, 284, 298-304]. For cases in which regional values were measured for the TMJ tissues, a mean value is provided for the sake of simplicity.

Table 2: Summary of candidate polymer mechanical properties in indentation, compression, friction, and tension in comparison to the ovine TMJ tissues.

Sample	Indentation Properties			Author
	E_I (kPa)	E_E (kPa)	E_E/E_I	
Ovine TMJ Disc	485 ± 560	94 ± 58	0.19	Labus (2021) [61]
Ovine TMJ Articular Cartilage	1200 ± 800	200 ± 190	0.17	Novel data
PVA (25% Hydrogel)	510 ± 110	415 ± 101	0.81	Novel data
PP	$7.0 \times 10^5 – 1.2 \times 10^6$ (nanoindentation)		-	Tranchida (2005) [303]
PCL	1.17×10^6		-	Lin (2017) [299]
PEGDA (20%)	610 ± 190	330 ± 130	0.54	Novel data
GELMA (20%)	22 ± 9	14 ± 7	0.64	Novel data
	Compressive Properties			
	E'_0 (kPa)	E'_{max} (kPa)	C_1 (kPa)	C_2 (kPa)	
Ovine TMJ Disc	125 ± 40.0	3610 ± 2750	80.5 ± 41.8	66.4 ± 58.7	Novel data
Ovine TMJ Articular Cartilage	363 ± 169	1677 ± 538	-	-	Hagandora (2011) [301]
PVA (25% Hydrogel)	162 ± 46.2	827 ± 358	30.0 ± 6.5	15.9 ± 8.2	Novel data
PP	1380×10^3		-	-	Matweb [285]
PCL	$455 \times 10^3 \pm 2 \times 10^3$		-	-	Ragaert (2014) [284]
PEGDA (20%, P700)	259 ± 4		-	-	Kotturi (2017) [300]
GELMA (20%, GMAB180)	113 ± 15		-	-	Gu (2020) [298]
	Coefficient of Friction			
	0.4 mm/s	4 mm/s	40 mm/s	
Ovine TMJ Disc	0.057 ± 0.049	0.059 ± 0.050	0.058 ± 0.050	Novel data
Ovine TMJ Articular Cartilage	Tested against TMJ disc, see above			Novel data
PVA (25% Hydrogel)	0.043 ± 0.015	0.073 ± 0.020	0.043 ± 0.011	Novel data
	Tensile Properties			
	E (MPa)	UTS (MPa)	λ_f	Toughness (MJ/m^3)	
Ovine TMJ Disc (AP)	251 ± 81	25.6 ± 4.6	1.18 ± 0.07	1.82 ± 0.53	
Ovine TMJ Disc (ML)	21.5 ± 6.7	3.7 ± 0.4	1.25 ± 0.06	0.40 ± 0.12	
Ovine TMJ Capsule	4.1 ± 4.1	2.29 ± 1.64	-	-	Novel data
PVA (25% Hydrogel)	0.40 ± 0.06	2.79 ± 0.62	3.55 ± 0.27	3.62 ± 1.12	Novel data
PP	1,750 - 2,500	25 - 32	10 - 44	-	Tordjeman (2001) [304]
PCL	440 ± 3	17.8 ± 5	1.024 ± 0.006 – 1.031 ± 0.002	-	**E and UTS:** Ragaert (2014) [284] **λ_f :** Eshraghi (2010) [302]

3 Polymer selection and reasoning

The objective of these experiments was to provide a broad mechanical comparison between polymer candidates and the ovine TMJ disc to identify a suitable candidate for a TMJ disc replacement. Indentation served as a screening method for PEGDA, GelMA, and PVA hydrogels. These tests revealed that PVA and PEGDA hydrogel instantaneous and equilibrium moduli were nearest to the TMJ discs. Through manual manipulation, it was evident that the GelMA and PEGDA hydrogels lacked the necessary mechanical strength to endure friction or tensile testing and were therefore determined to be too weak to survive *in vivo* without additives or structural reinforcement. Though a tissue engineering solution for TMJ disc replacement is warranted [305], understanding of healthy TMJ adaptation is poor. The hypoxic environment of the TMJ disc further complicates the application of a degradable, bioactive scaffold for TMJ disc replacement at this time. Initial efforts in this field should be targeted toward restoring joint health and preventing further disease progression in the pathologic TMJ. We believe that a non-degradable PVA hydrogel-based TMJ disc replacement will provide an opportunity to arrest TMD progression as well as prevent or delay the need for total TMJ replacement in some cases.

PVA hydrogels are tough, simple to produce, and inexpensive. They also show promise for TMJ disc replacement due to their biomimetic frictional, tensile failure, and compressive properties. Of the concentrations tested, the 25% PVA group is the most promising candidate for TMJ disc replacement from a holistic view of the collected data. The 25% PVA hydrogel was most similar to the TMJ discs in initial compressive modulus, ultimate tensile strength, and toughness, and it exhibited higher failure stretch than the TMJ discs. The indentation results demonstrated better agreement between the 15% PVA and the TMJ disc, but the instantaneous modulus of the

25% PVA hydrogel group was within the range of values calculated for the TMJ disc. Additionally, the COF of 25% PVA was not significantly different from the ovine TMJ disc at any speed.

The disparity between the tensile modulus and high-stretch compressive modulus of the 25% PVA hydrogel and ovine TMJ disc demonstrates a need for tensile reinforcement of the PVA hydrogel structure to achieve or exceed the natural tensile behavior. Both PCL and PP exhibit sufficiently high tensile properties and could be implemented as a structural reinforcement for PVA hydrogels in order to more closely resemble the TMJ tensile properties. However, the value of mimicking the tensile characteristics of the ovine TMJ disc must be balanced with the importance of the frictional and compressive properties of the native tissue. The importance of low friction in articular joint replacements is well understood, and the compressive properties of articular cartilage replacements are also essential, as the primary mode of loading in the TMJ is compression. For dynamic activity, physiologically relevant compressive strains in articular cartilage can range from 15% to 35% [306], while tensile characterizations of the canine TMJ disc have reported physiological *in vivo* tensile strains of 4% [307]. This disparity in strain magnitude suggests that sufficiently high frictional and compressive properties in a joint replacement strategy are necessary.

This mechanical evaluation was limited in scope, focusing PVA of a single molecular weight and degree of hydrolysis. The mechanical behavior of PVA hydrogels is highly tunable, influenced by a multitude of synthesis conditions and polymeric characteristics [308]. PVA hydrogel properties may also be optimized through other strategies, including reinforcement from additional polymers [309, 310], directional freezing [295], and thermal annealing [311, 312]. However, this study does provide a baseline for comparison between one PVA hydrogel

formulation and the ovine TMJ disc. Overall, these experiments further support development of PVA hydrogels for TMJ disc replacement in an ovine preclinical model.

CHAPTER 4 - FINITE ELEMENT MODELING OF THE OVINE TEMPOROMANDIBULAR JOINT

A FE model of the ovine TMJ was developed for *in silico* evaluation of artificial TMJ disc replacement strategies. This model was validated using *ex vivo* data collected during jaw clenching experiments of ovine TMJ tissues. Results from the validation experiments were not statistically different from the FE model predictions, which suggests that this model has the predictive accuracy for performing quasistatic compressive evaluations of TMJ disc replacement strategies.

1 Geometry and 3D modeling

One left ovine TMJ was used to define the FE model geometry. The TMJ was fixed in the fully closed position with a titanium screw passed through the zygoma and into the coronoid process. The fixed TMJ was excised *en bloc* and excess muscle and fat was removed. Next, an incision was made in the posterior aspect of both joint capsules. Finally, the sample was immersed in a 30% Lugol's iodine - 70% PBS solution for 72 hours. This solution increased the radiopacity of the TMJ disc, which improved its visibility in micro-computed tomography (μCT) images [313]. The TMJ sample was placed in a μCT sample holder and secured in place using a dense foam to ensure that the joint would stay in the fully closed configuration after the external fixator pin was removed. A μCT scan was taken of the TMJ specimen with a voxel size of 74 μm. Figure 15 shows a representative image from the μCT scan before and after soaking in the Lugol's iodine solution.

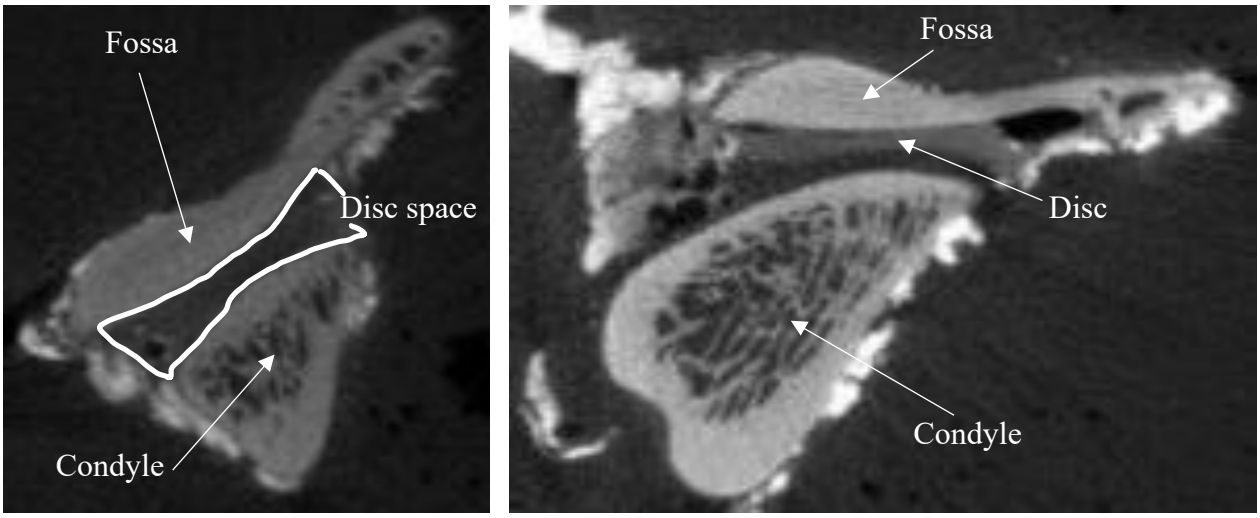

Figure 15: Comparison of TMJ disc visibility before (left) and after (right) soaking in Lugol's iodine solution.

Segmentation of the 3D geometry of the fossa, condyle, and TMJ disc was completed using ITK-snap, an automatic segmentation software for processing medical images [314]. Separate surface model geometries of the fossa, condyle, and TMJ disc were exported as .STL files. Meshmixer® (Autodesk Inc., San Francisco, CA) was used to patch holes in the mesh files, remove superfluous bone and internal voids, smooth articular cartilage surfaces, and reduce the number of facets used to define the geometry. The condyle and fossa models were imported into Solidworks® (3DS Dassault Systèmes, Vélizy-Villacoublay, France), which was used to create condylar and fossa cartilage plates defined as 0.25 mm thick extrusions offset from the subchondral bone surfaces. The disc geometry was meshed with quadratic tetrahedral elements (C3D10), and the fossa and condylar cartilage geometries were meshed with two layers of hexahedral (C3D8R) elements. The condyle and fossa bones were also meshed with tetrahedral elements and used to define the joint capsule attachment locations, but these elements were otherwise not included in the FE model for the sake of simplicity. All meshing was accomplished using Coreform Cubit™ (Coreform LLC, Orem, UT). Abaqus (Abaqus/CAE 2021, 3DS Dassault Systèmes, Vélizy-Villacoublay, France) was used to conduct all FE modeling simulations/computations.

The joint capsule and disc attachments were modeled as nonlinear spring elements with attachment locations defined by *in-situ* measurements of the ovine TMJ. Each joint capsule section was divided into six evenly spaced spring elements with length and width equal to the average dimensions measured during joint capsule tensile testing, using methods previously described in Chapter 2. The meshed fossa and condyle bone models were used to define the location of attachment for the joint capsule. These locations were imported into the soft-tissue only model. The regions of joint capsule attachment to the TMJ disc were defined in the soft-tissue model (Figure 16).

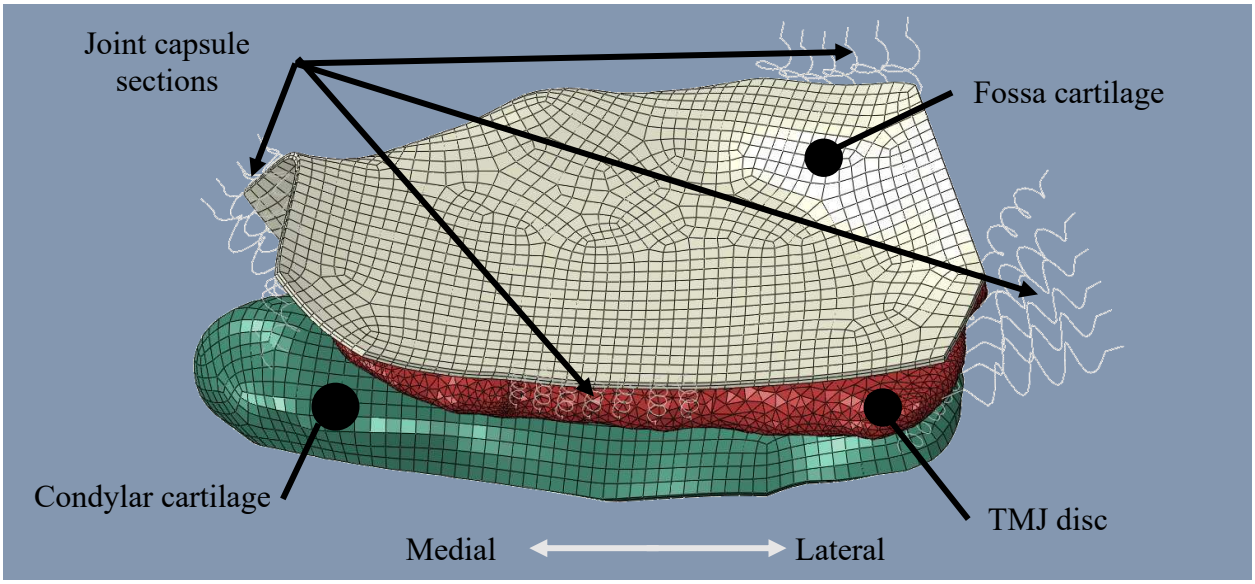

Figure 16: Initialized soft-tissue FE model demonstrating the fossa cartilage, condylar cartilage, TMJ disc, simplified joint capsule sections, and joint capsule attachment points.

The superior surface of the TMJ fossa cartilage and the superior joint capsule attachment points were assigned a fixed boundary condition. The center of mass (COM) of the TMJ condylar cartilage was determined, and the internal condylar cartilage nodes and inferior ligament attachment points were coupled to the condyle COM with multi-point constraint beam elements.

This configuration allowed for simplified motion of the condyle relative to the fixed fossa position through constraint and manipulation of the COM control point.

2 Model initialization

Material properties for the TMJ disc, condylar cartilage, fossa cartilage, and joint capsule sections were obtained from the *ex vivo* measurements of ovine specimens as described in Chapter 2, and experiments on the 25% PVA hydrogels described in Chapter 3. Specifically, the TMJ disc material properties were defined using the 2-term Yeoh model parameters captured through unconfined compression of the TMJ discs and 25% PVA hydrogels. The condylar and fossa cartilage, on the other hand, were defined as homogeneous linearly elastic materials using data collected during the *ex vivo* indentation testing. For the quasistatic simulations, the mean equilibrium modulus was used to define the cartilage material property. The force-displacement behavior of each joint capsule section was defined directly from its corresponding force-displacement curve with the median elastic modulus. Contact between the TMJ discs and the articular cartilage was defined with a contact stiffness derived from relaxed moduli from indentation stress-relaxation experiments. The COF for contact was defined as the average COF measured from friction experiments. Table 3 provides a summary of the material property definitions for each TMJ FE model component.

Table 3: Summary of material property definitions for each component of the TMJ FE model

	Material Property Definition	*Source*
TMJ disc component	2 -term Yeoh model (incompressible)	Unconfined compression
Ovine TMJ	C_1 = 80.5 kPa C_2 = 75.0 kPa	
25% PVA hydrogel	C1 = 30.1 kPa C2 = 15.9 kPa	
Fossa and Condylar cartilage	Linear, isotropic material 200 kPa	Indentation stress-relaxation
Joint Capsule	Imported force-displacement data	Tensle testing
Cartilage - Disc Contact	COF	Friction
Ovine TMJ	0.058	
25% PVA hydrogel	0.043	
	Contact stiffness (linear) 200 kPa	Indentation stress-relaxation

3 Jaw clenching simulation

Initial investigations utilizing the TMJ FE model were focused on quasistatic compression of the TMJ components to mimic jaw clenching. A linearly ramped compressive load of 50N was applied through the condyle COM. This force acted to close the TMJ and applied compressive forces that were distributed by the TMJ disc. Motion of the condyle was constrained to prevent AP and ML motion as well as rotation about the AP and ML axes. The average centroidal pressure of surface elements within 2.5 mm of the peak pressure was captured at 20 intervals during the force

ramp. The slope of the average contact force with respect to the applied load was calculated for the FE model prediction. Figure 17 shows the motion of the TMJ condyle and disc throughout a jaw clenching simulation with corresponding stress distributions in the TMJ disc. The area of contact with the TMJ disc was also collected at each loading interval. Contact area was defined as the as the area of nodes with a contact pressure (CPRESS) greater than 0.1 MPa.

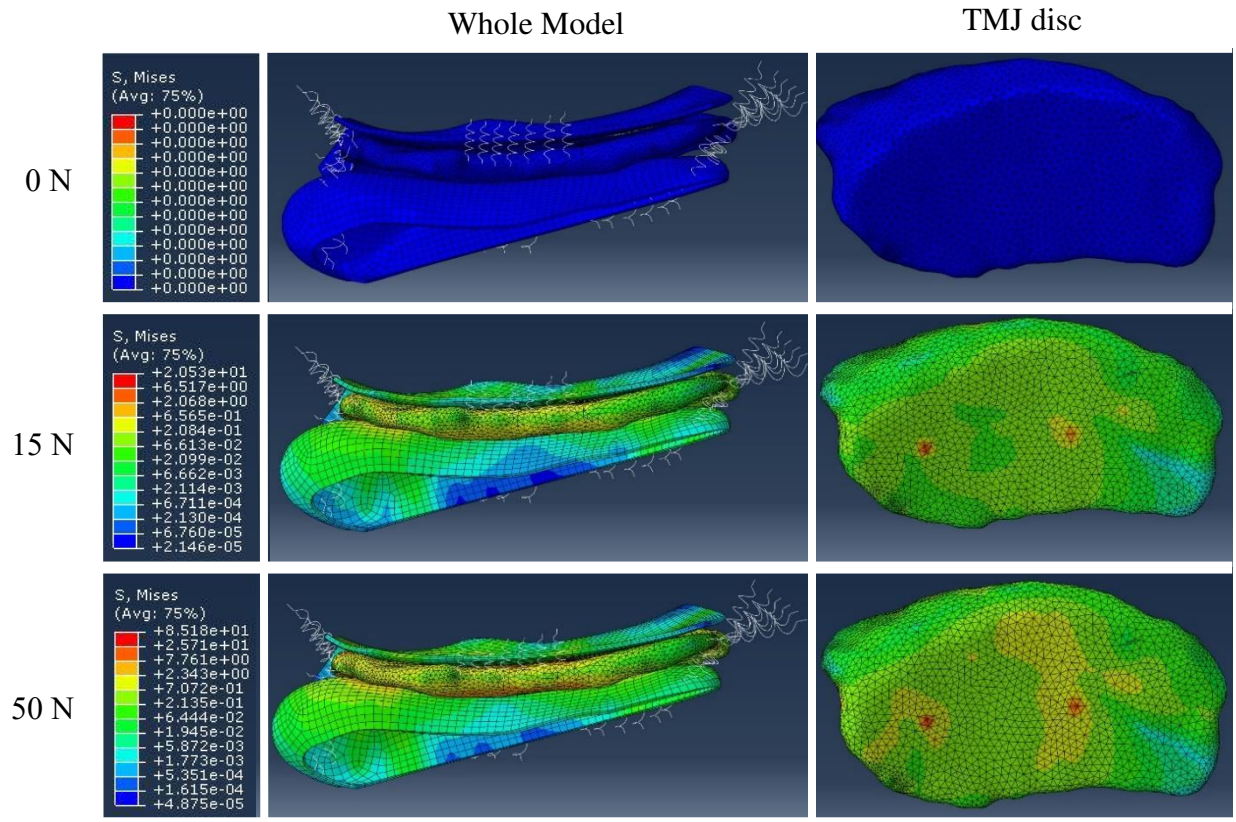

Figure 17: Stages of motion in the TMJ FE model showing the stress distribution in the anterior view of the whole joint (center column) and superior view of the TMJ disc (right column)

3.1 Validation

Ex vivo experiments to simulate jaw clenching were performed for validation of the FE model simulation results. Seven TMJs (n=4 left, n=3 right) were excised *en bloc* and fixed in the fully closed position using external fixator pins. The specimen ends were embedded in a 2-part

epoxy resin and mounted in a servo-hydraulic material testing machine (Model 858, MTS, Eden Prairie, MN). An incision was made in the posterior aspect of the superior TMJ capsule, and a flexible pressure-mapping sensor was inserted between the TMJ disc and fossa (Figure 18a). The pressure distribution between the TMJ disc and fossa was collected at 5N increments up to the pressure sensor stress limit (1.21 MPa). The average pressure within 2.5 mm of the measured peak pressure was calculated for each increment of applied load to compare between the FE model and pressure sensor readings. The slope of the peak stress-applied force curve was compared between experimental data and model predictions under commensurate loading using a one-sample t-test. The contact area was also collected for each loading step as the area of the pressure sensor or FE model surface with a measured pressure greater than 0.1 MPa.

The FE model prediction fell within one standard deviation of the experimental mean and was not significantly different from the mean experimental validation data (p = 0.50). The predicted contact area fell within the 95% confidence interval of the experimental data for an applied force of 7.5 N, but underpredicted the experimental contact area at higher loads (Figure 18). These data demonstrate general agreement between the FE model and comparable *ex vivo* compression experiments on the ovine TMJ in terms of contact stress, but the FE model underestimates the contact area at higher applied loads. Further mesh refinement in the contact area may lead to a more accurate estimation of the contact area. However, the discrepancy between the contact area in the model compared to the measured contact area from the validation experiments is also influenced by the use of the isotropic 2-term Yeoh model. Though the 2-term Yeoh model can successfully capture the non-linear material stress response, it does not explicitly account for the transverse anisotropy due to the collagen fiber component in the native disc.

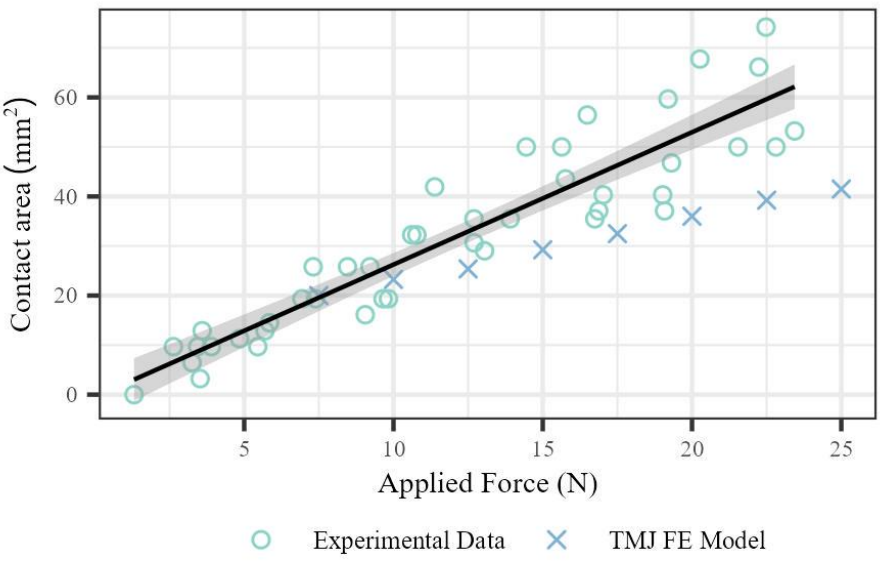

Figure 18: Comparison between FE model and experimental contact area with respect to applied load.

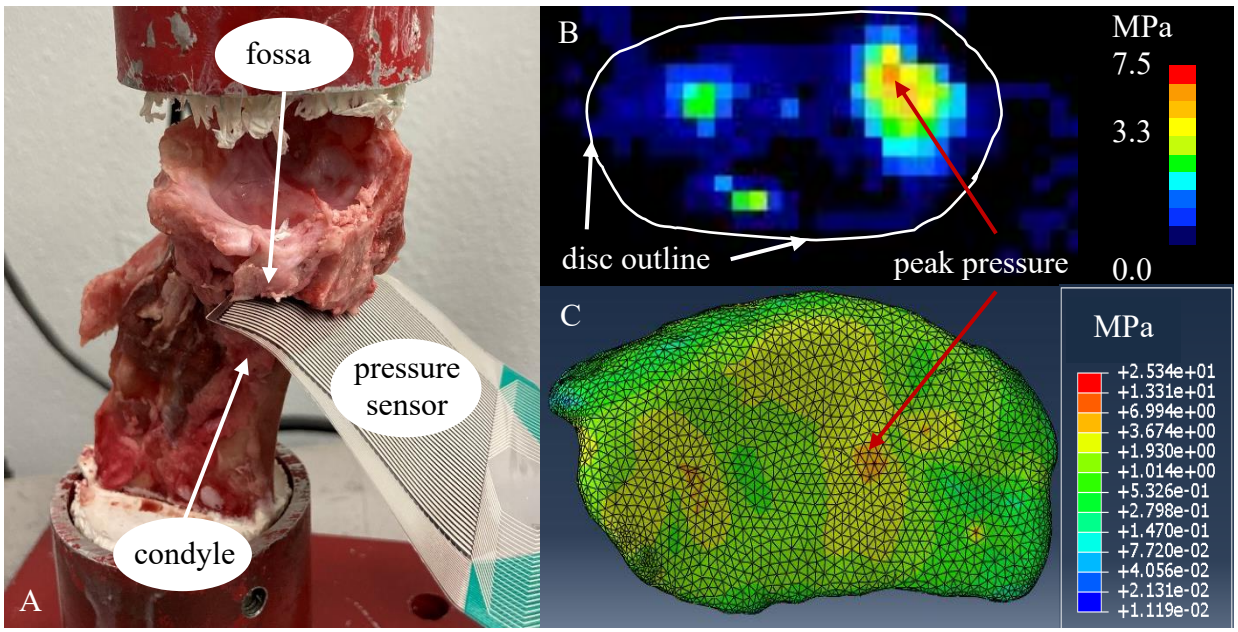

Figure 19: (A) TMJ jaw clenching experimental setup, (B) example pressure map of the joint under 50 N compressive load, (C) FE results under 25 N compressive load.

3.2 Study of model sensitivity

An investigation of the TMJ FE model sensitivity to the mechanical properties of the TMJ disc was also performed to determine the importance of the TMJ disc properties on the FE model predictions. Separate simulations were conducted in which the TMJ disc was defined as a linearly elastic, isotropic material with an elastic modulus of 0.01 E, 0.1 E, 1 E, 10 E, 100 E, 1,000 E, and 10,000 E where E was the instantaneous modulus of the TMJ disc from indentation stress-relaxation experiments (E = 400 kPa) [61]. Results of these simulations show that the slope of the peak stress versus applied force curve was sensitive to the TMJ disc elastic modulus between 0.01 E and 100 E (Figure 20).

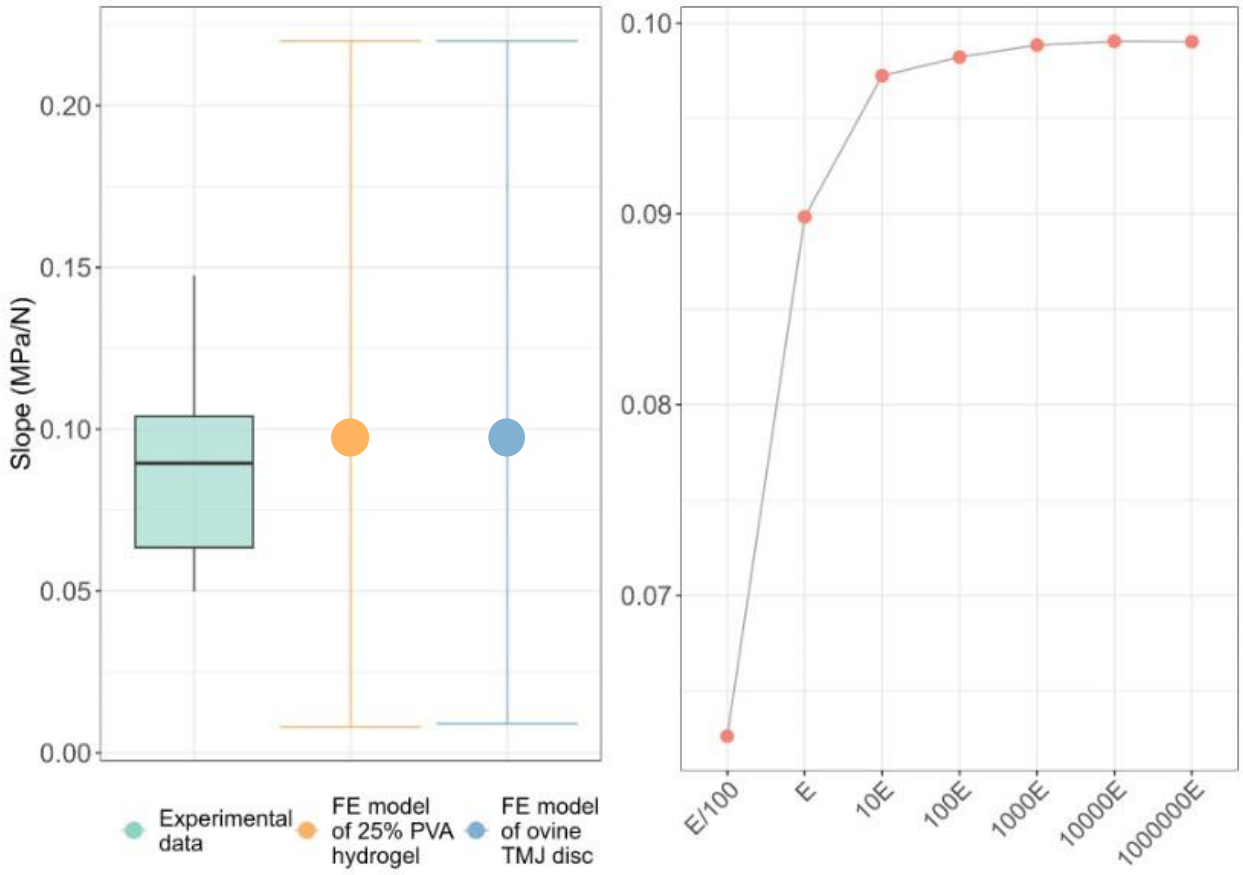

Figure 20: Summary of experimental data and FE model predictions for the TMJ disc and 25% PVA hydrogel (left) and model sensitivity experiments (right).

3.3 Performance of PVA hydrogels

After successful validation of the FE model, it was also implemented to study the TMJ behavior with a 25% PVA hydrogel artificial disc replacement in a simulated jaw clenching experiment. The properties of the TMJ disc component were defined according to the 2-term Yeoh model fitting parameters from unconfined compression of the 25% PVA hydrogels, which is described in Chapter 3. All other constraints, loads, and material property definitions were kept consistent with the previous jaw clenching simulations of the native TMJ disc. A one-sample t-test was used to compare the slope of the peak pressure versus applied force between the simulated 25% PVA hydrogel and the experimental *ex vivo* validation data. The model prediction for the

25% PVA hydrogel fell within one standard deviation of the experimental mean. Furthermore, the model prediction for the 25% PVA hydrogel TMJ disc replacement was not significantly different from the mean experimental validation data ($p = 0.51$).

4 Summary

A FE model of the ovine TMJ disc was developed based on *ex vivo* mechanical evaluation of ovine tissues with geometry derived from μCT scans of one left ovine TMJ. The FE model stress predictions for jaw clenching were validated against *ex vivo* experimental data collected from a group of seven freshly harvested ovine TMJs. The behavior of a 25% PVA hydrogel artificial disc replacement was also evaluated and compared against the experimental data. Model predictions for both the native ovine TMJ disc and the PVA hydrogel disc replacement showed excellent agreement with the experimental data. These results suggest that the FE model is able to accurately predict stresses that result from jaw clenching. They also demonstrate that a 25% PVA hydrogel experiences similar internal stresses that the native TMJ disc experiences in this mode of loading. Future efforts will target the development and validation of a FE model to simulate the masticatory motions of the ovine TMJ; this dynamic model will further inform the selection of a material candidate for the development of an effective TMJ disc replacement strategy.

CHAPTER 5 - *EX VIVO* EVALUATION OF TMJ DISC REPLACEMENT STRATEGY

Timely evaluation of TMJ disc replacement candidates throughout their development can be facilitated by *ex vivo* experiments. The nature of implant failure is an especially important factor in long-term implant stability, particularly in the replacement of articular joints. This chapter describes a method for assessing the failure mechanisms of artificial TMJ disc replacement strategies. An apparatus that manipulates a cadaveric specimen through repetitive chewing motions has been designed and implemented to study artificial TMJ disc replacement candidates under near *in vivo* conditions. This simulated chewing apparatus (SCA) has been used to successfully replicate the observed modes of failure seen in the TMJ disc replacements used in the pilot experiment described in Chapter 6.

1 Design

3D motion capture of ovine chewing motions was completed as part of the pilot experimental protocol and is described in more detail in Chapter 6. All *in vivo* procedures were approved by the Colorado State University IACUC (protocol #3999, approved November 28, 2022). Briefly, reflective markers were affixed to each sheep's nose and chin using flexible 3D printed structures. A multiple-camera stereophotogrammetry system (Motion Analysis Corp., Santa Rosa, CA) was used to capture pilot experiment animals' chewing motions before and after surgical intervention. Individual chewing cycles were identified through post-processing in the Motion Analysis software. MATLAB was used to remove superfluous translation and rotation due to whole skull movements from the motion of a single mandible-mounted marker throughout each chewing cycle. The unrelated skull translation was subtracted from each corresponding increment directly using the motion of the skull-mounted markers. The rotation of the mandible marker related to whole skull rotation was removed by calculating a rotation matrix for the skull marker

movement, multiplying the rotation matrix by the vector between the skull marker and mandible marker, and subtracting the resultant vector between the initial and rotated skull-mandible vector from the subsequent mandible marker position. A representative curve was selected from the chewing data collected prior to surgical intervention and used in the SCA design.

A crank-rocker, four-bar linkage was designed to replicate the selected chewing motion from a single motor input. A crank-rocker four-bar linkage can repeatably reproduce a planar motion by revolving one link (the crank), which causes the remaining links to articulate in a predictable manner (Figure 21).

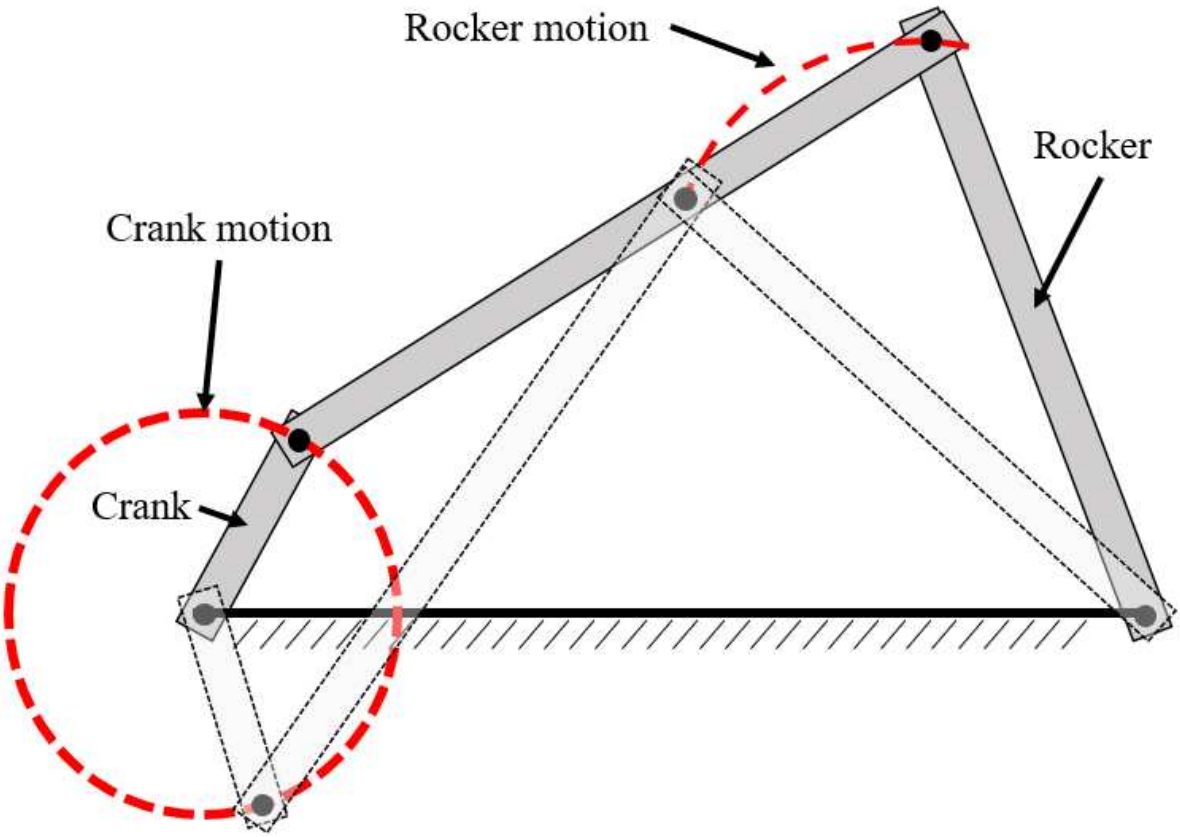

Figure 21: Crank-rocker 4 bar linkage configuration depicting crank and rocker motions.

MATLAB was used to determine the dominant plane of the chewing motion by minimizing the absolute value of the out-of-plane motion for the selected chewing cycle. 3D motion data for the chosen chewing cycle was transformed into this dominant plane, resulting in a maximum out-of-plane displacement of 1.21 mm, which was 3.0% of the cycle range of motion. This process maximized the amount of 2D motion throughout the chewing cycle, which allows for the most accurate reproduction of the chosen cycle possible by a four-bar linkage. A 2D recapitulation of the TMJ chewing motion captured by the mandible-mounted reflector was deemed appropriate due to the small ratio of in-plane to out-of-plane motion. The resulting 2D curve was used for four-bar linkage design. MATLAB was used to compare the measured chewing motion to the motion of an arbitrary point (Q) on the middle link of a crank-rocker four-bar linkage with the following link lengths: $L_1 = 15$ mm, $L_2 = 45$ mm, $L_3 = 35$ mm, $L_4 = 40$ mm. The location of point Q on the center link (L_2) was defined using a distance (r) and angle (θ) defined from the pivot point connecting the crank and center link (Figure 22).

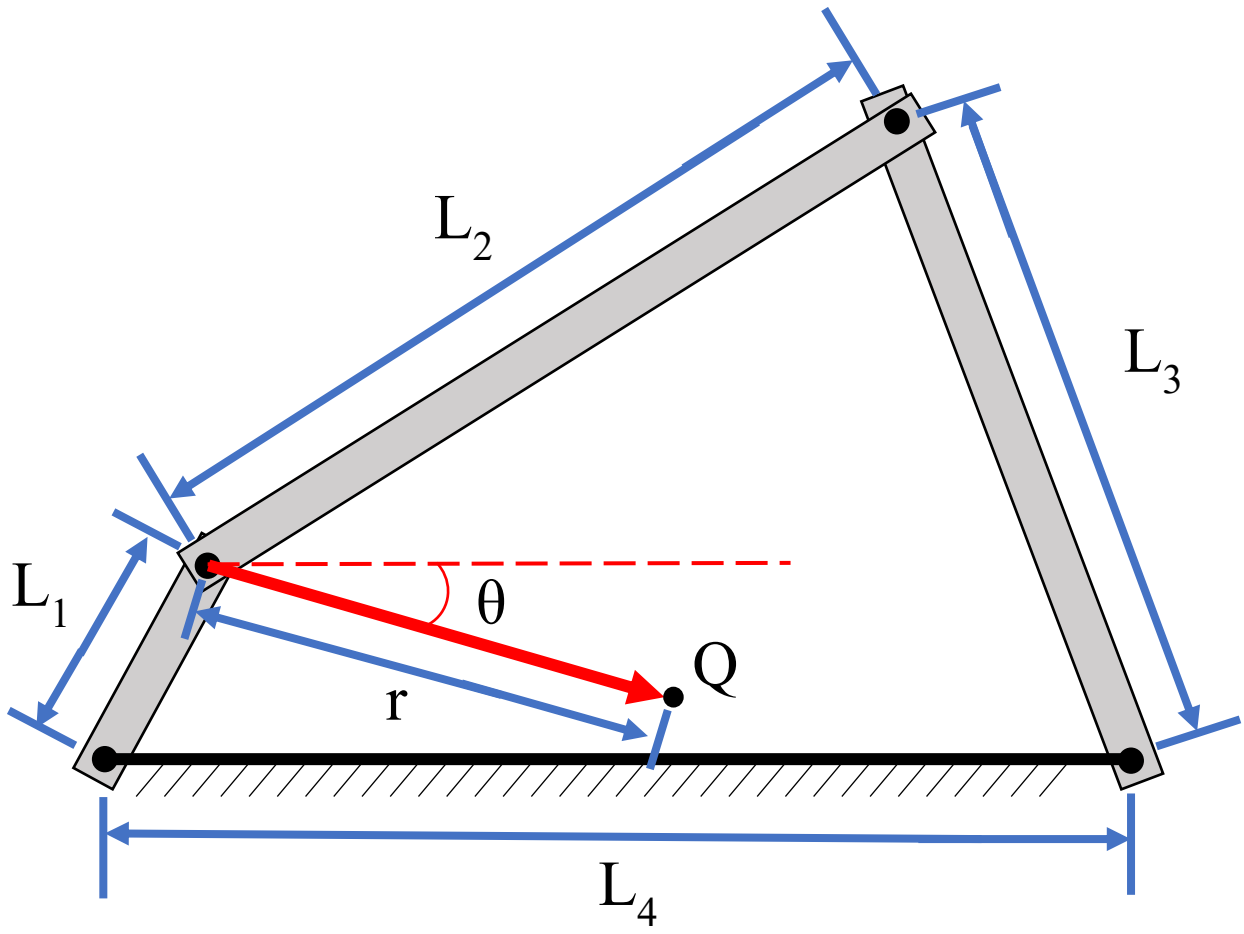

Figure 22: Configuration of four-bar linkage used to reproduce TMJ chewing motion at arbitrary point Q on center link.

The discrete Fréchet distance [315] is used to compare the isometry of two curves by quantifying the greatest distance between ordered points along those curves. For a range of r and θ values, the Fréchet distance between the observed chewing curve and the arbitrary point's motion along the four-bar linkage curve was calculated. MATLAB was used to determine the path of point Q for increments of r between 20 mm and 40 mm, and increments θ from 0° to 360°. The number of points defining the locations of point Q matched the number of points used from the ideal chewing motion. The discrete Fréchet distance was calculated for each r & θ combination and the combination which minimized the discrete Fréchet distance was identified. Using this approach,

the optimal values for r (24.33 mm) and θ (47°) resulted in a minimum discrete Fréchet distance of 3.19 mm. The curve associated with the finalized linkage design is shown in Figure 23.

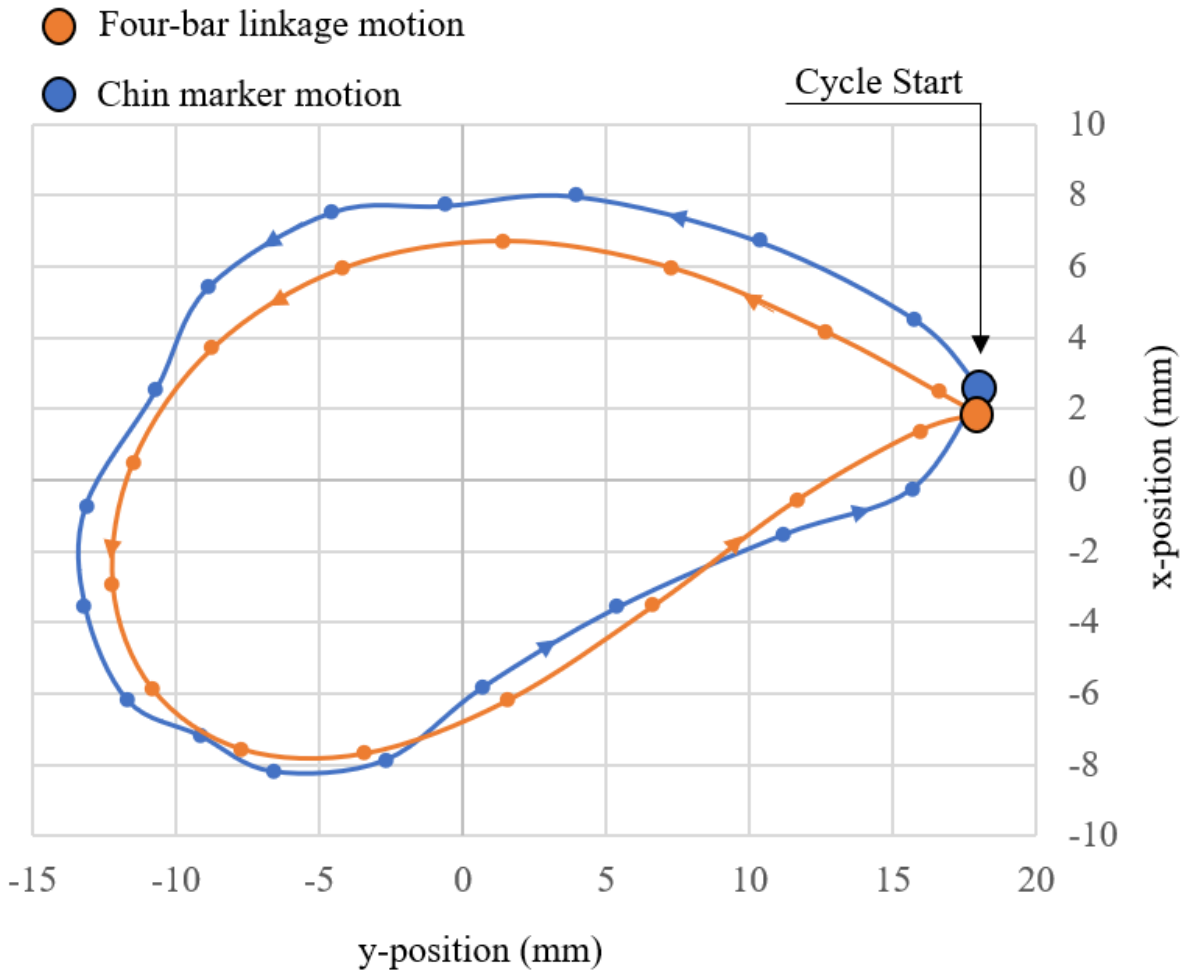

Figure 23: Comparison between measured mandible marker motion and optimized four-bar linkage motion.

Solidworks® was used for 3D modeling of a linkage based on the optimized theoretical linkage identified using MATLAB (Figure 24). The modeled four-bar linkage was manufactured using a combination of traditional and additive manufacturing techniques. This linkage was affixed to a rigid frame with integrated 6 degree-of-freedom load cell (AMTI, Watertown, MA) and driver motor (Model: AKM53H-ANCNC-00, National Instruments, Austin, TX). The SCA frame is

adjustable to allow for differently sized specimens to be used for analysis. Ovine cadaveric skulls are mounted in the SCA using wood screws inserted into the cranium and mandible, which are then embedded in a two-part epoxy in a cylindrical mold. Molded sections are secured in the apparatus using appropriately sized cylindrical grips and thumb screws, which provides rigid attachment to the load cell for the cranium, and four-bar linkage control point for the mandible. A compressive force up to 250 N can also be applied across the TMJ and load cell using an integrated set of springs attached to the SCA frame and angles of the mandible (Figure 25). A Labview (version 8.0, National Instruments Co., Austin, TX) program is used for motor speed control and to count revolutions and capture applied forces and moments across the integrated load cell. Implant strain is measured optically *post hoc* using fiducial markers on the implant surface. A maximum chewing rate of 3 revolutions/second allows for expedited analysis of high cycle fatigue failure. A misting humidifier was used to keep the artificial TMJ discs hydrated throughout the experiment.

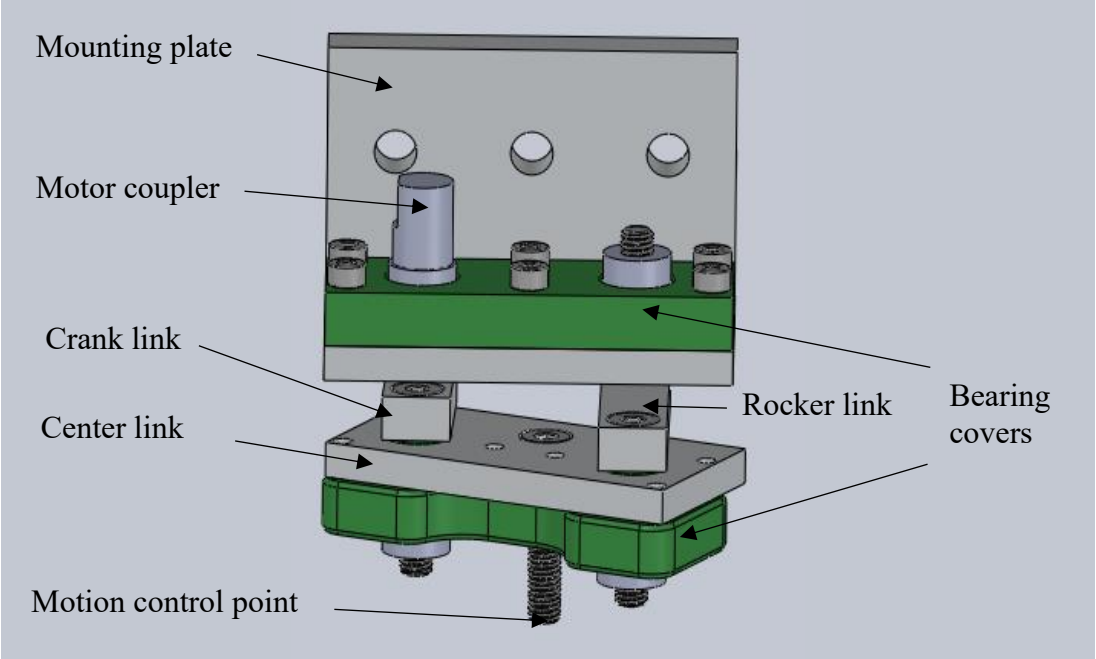

Figure 24: Four-bar linkage design assembled virtually with Solidworks®. The mounting plate serves as the link L_4, the crank link is L_1, the center link is L_1, and the rocker is L_3. Bearing covers were 3D printed and used to mount precision bearings (not pictured) at the link pivot points. The motor coupler is attached to the driver motor and rotates the crank link. The motion control point is coupled to the mandible with a fixture and two-part epoxy.

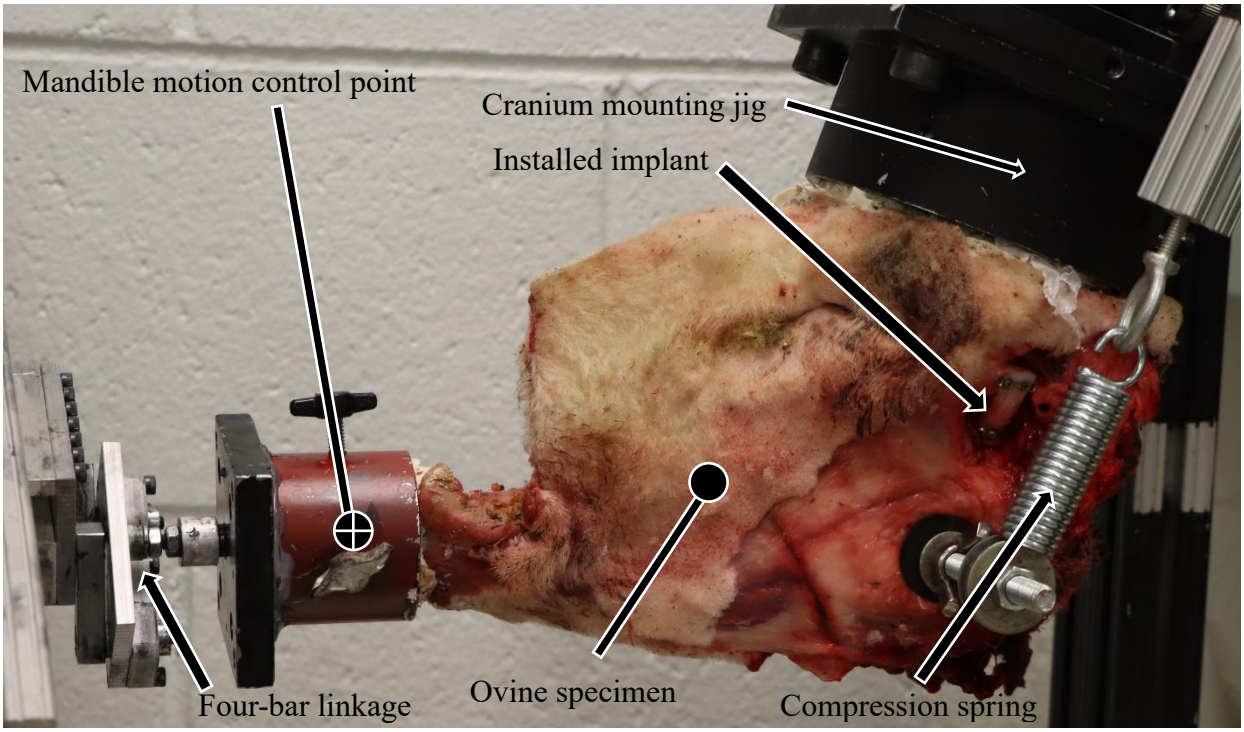

Figure 25: SCA configured for compressive failure analysis depicting mounted specimen with left artificial TMJ disc replacement.

2 Methods

To prepare both the tensile and compressive failure experiments, an artificial TMJ disc was molded from 25% PVA hydrogel and installed according to the surgical procedure that is described in Chapter 6. Briefly, an incision was made to expose the left TMJ capsule, and the capsule was cut circumferentially to release the TMJ disc. The TMJ disc was removed with care to prevent damage to the articular cartilage surfaces. The patient specific TMJ disc replacement was inserted into the disc space, and its superior and inferior flanges were affixed to the zygoma and condyle, respectively, using thin maxillofacial plates with 1.5 mm diameter titanium orthopedic screws. The cadaveric skull was mounted in the SCA using wood screws embedded in a two-part epoxy. The specimen was mounted with the linkage and mandible in the fully closed orientation, which was confirmed by the occurrence of tooth contact in each chewing cycle.

2.1 Tensile failure analysis

An experiment to cause implant failure due to cyclic tensile forces on the implant attachment was performed. The four-bar linkage was articulated at a rate of 3 revolutions/second for a total of 600,000 cycles. Hydration of the TMJ space was maintained with a misting humidifier. Incremental images of the artificial TMJ disc and videos of the articulating motion were captured throughout the experiment. The bulk tensile strain in the implant attachment flanges was measured optically *post hoc* from videos taken of the implant articulation for ten different chewing cycles. Based on these optical measurements, the attachment flange was subjected to an approximate cyclic tensile strain of 8 % ± 3 % due to the induced chewing motion.

2.2 Compressive failure analysis

Experiments to cause implant failure due to cyclic compressive loading on an artificial TMJ disc were performed on a 25% PVA hydrogel implant, and PVA hydrogel implant after thermal annealing. To create the annealed TMJ disc replacement, a 30% larger three-part mold was 3D printed to accommodate implant shrinkage due to thermal annealing. A 25% PVA hydrogel solution was created, injected into the scaled mold, and subjected to six freeze-thaw cycles. The completed implant was removed from the mold and dehydrated in a vacuum chamber. Once fully dry, the implant was placed in an oven at room temperature. The oven was heated to 150 °C over three hours, then held at 150 °C for one hour before removal. TMJ disc replacements were installed using the surgical procedure described in Chapter 6. Holes were drilled in the angles of the left and right mandible and a 9.53 mm diameter threaded rod was inserted through the holes to create a rigid attachment for the SCA springs. The springs were attached to the SCA frame and mandible-mounted threaded rod bilaterally to create a force of 50N (measured by the integrated load cell) across the joint spaces. The four-bar linkage was articulated at a rate of 1

revolution/second for a total of 10,000 cycles for both the 25% PVA and annealed hydrogel implants. Hydration of the TMJ space was maintained with a misting humidifier. Images were taken of the artificial TMJ disc component of the implants at 0, 1,000, and 10,000 cycles.

3 Results

3.1 Tensile failure analysis

Figure 26 shows the regions of crack initiation in the implant. Although catastrophic implant failure was not achieved in 600,000 cycles, the initiation and propagation of cracks in the implant flange predicts the mode of implant failure at high cycles. The initiation of cracks at the intersection between the plate and screw edges matches well with the mode of failure observed in the TMJ pilot experiment.

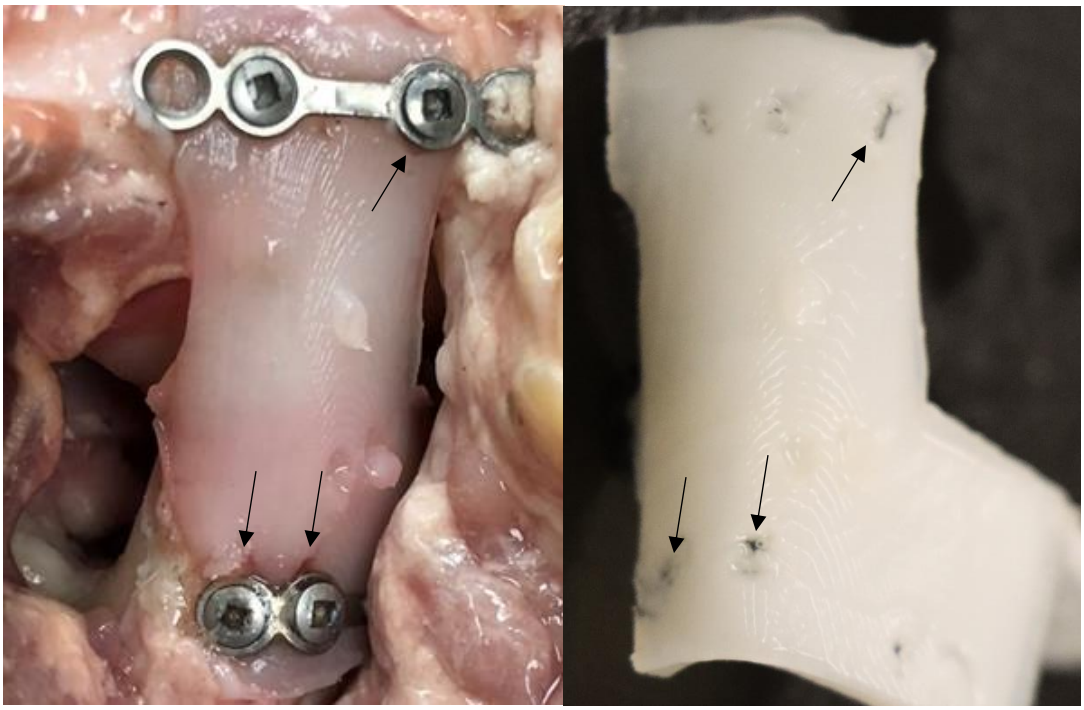

Figure 26: 25% PVA hydrogel TMJ disc replacement after 600,000 cycles in the SCA, arrows indicate locations of crack initiation and propagation.

3.2 Compressive failure analysis

Catastrophic failure occurred in less than 1,000 cycles in the compressive failure experiment on the untreated 25% PVA hydrogel implant, and in less than 10,000 cycles in the annealed PVA hydrogel experiment (Figure 27). Compressive stresses in the implant exceeded the hydrogel failure stress causing holes to form in the artificial TMJ disc. The holes created by the dynamic compressive stresses caused cracks to nucleate in the mediolateral direction near the crest of the TMJ condyle. This mode of failure was similar to the failure seen in the artificial TMJ disc components in the pilot study.

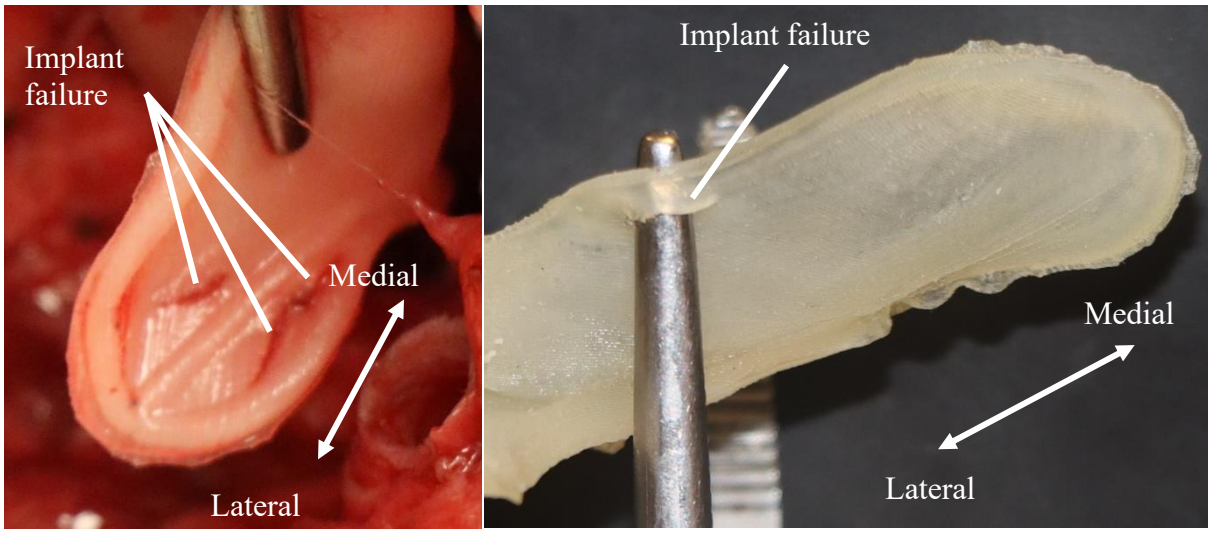

Figure 27: Image showing failed regions of the (left) 25% PVA hydrogel and (right) annealed PVA hydrogel TMJ disc replacements after completion of compressive failure analysis in the SCA.

4 Discussion

A method to replicate the *in vivo* loading conditions on an artificial TMJ disc replacement has been successfully created and will allow for expedited evaluation of artificial TMJ disc replacements. The system has been used to cause implant failure due to tensile stresses on the implant attachment flanges, and due to compressive forces through the TMJ disc component. Both

methods of failure matched the failure modes observed in the pilot study using the same patient specific artificial TMJ discs made with 25% PVA hydrogel.

Though catastrophic failure of the implant was not achieved, the tensile failure experiment helped to identify the location of crack nucleation at the interface between the PVA hydrogel and titanium plate. The bulk strain in the implant attachment flanges was 8% ± 3% which is only 3% of the failure strain (248% ± 27%) for 25% PVA hydrogels, a level at which the implant life may be nearly infinite. However, crack nucleation at the interface of the titanium plate and PVA flange is indicative of a stress concentration which may result in much higher local strains than those estimated by the bulk strain measurement, or the introduction of damage during installation of the titanium plate. Regardless of the means of nucleation, the formation and elongation of cracks was evident in the PVA attachment flanges after 600,000 cycles in the SCA tensile failure analysis. Though less rapid than the compressive failure, the initiation of tensile failure must be accounted for in further design to improve implant survivability.

Compressive failure in the artificial TMJ disc component of the 25% PVA and annealed TMJ disc replacements occurred rapidly (less than 10,000 cycles) in the SCA with an applied load of 50 N across the TMJs bilaterally. This suggests that the compressive forces through the TMJ disc component are the dominant contributor to implant failure with the current hydrogel formulation and implant design. It is clear that a 25% PVA hydrogel does not possess a sufficiently high compressive failure stress or wear resistance to withstand repeated loading of more than 25 N in the ovine TMJ. These findings underscore the need for structural reinforcement of the artificial TMJ disc structure to exceed the current, more biomimetic, mechanical behavior.

Ultimately, for an implant candidate to be considered successful it must be shown to survive for a number or loading cycles equal to decades of expected loading in the human TMJ space. In other articular joint replacements, these targets are typically of the order 10^6 or 10^7 [322], which greatly exceeds the lifetime of the current implant material and design. Implementation of the SCA has helped to refine the design targets for an artificial TMJ disc replacement, and redirect development towards even more durable, fatigue and wear resistant candidates. Additionally, methods for reducing stress concentrations in the attachment, and reducing or more effectively redistributing the stress on the artificial TMJ disc replacement must be investigated.

CHAPTER 6 - *IN VIVO* PILOT EXPERIMENT

In vivo preclinical studies are important evaluations in the path towards translation of artificial TMJ disc replacements to human clinical trials. This chapter describes the design, synthesis, and surgical procedure development of a patient specific, artificial TMJ disc replacement strategy and its implementation in an ovine preclinical pilot study. An implant design and surgical strategy was developed in collaboration with human maxillofacial and veterinarian surgeons, namely Dr. Ryan Dobbs, M.D., D.D.S. (Saddle Rock Institute, Aurora, Colorado); Dr. Jennifer Rawlinson, DVM (Colorado State University); and Dr. Jeremiah Easley, DVM, (Colorado State University). Implants were designed using geometry captured with clinical computed tomography scans and manufactured from 25% PVA hydrogel using 3D printed molds. The pilot experiment was designed to investigate the *in vivo* success of the implant in preventing joint degradation in comparison to disc excision alone. Body weight, body condition, and chewing behavior were monitored throughout the experiment. All *in vivo* experimental procedures were approved by the IACUC at Colorado State University (protocol #3999, approved November 28th, 2023). *Ex vivo* indentation-stress relaxation experiments were performed on the treated and contralateral articular cartilage surfaces, along with histological analysis of the TMJ cartilage surfaces and relevant organ tissues.

1 Artificial TMJ disc design and surgical strategy

An iterative approach to implant design, utilizing the expertise of surgeon partners Drs. Easley, Dobbs, Rawlinson, was implemented to develop a final implant design and surgical strategy. Initial implant development was focused on defining the overall implant geometry and synthesis method. Further development was focused on the implant attachment method. After each

iteration of implant redesign, the updated implant was tested in a practice surgery session using a cadaveric ovine skull.

1.1 Initial development

A patient specific TMJ disc replacement was developed to practice the surgical approach and refine the implant geometry. The TMJ disc geometry was captured using μCT of one left ovine TMJ soaked in a 30% Lugol's iodine solution as described in Chapter 4. Native tissue geometry was used to design a smoothed disc geometry using Solidworks®. Splines were used to define a surface following the curvature of the native TMJ disc. This surface was thickened to 0.75 mm, and a rounded edge with a radius of 1 mm was created to mimic the biconcave shape of the disc (Figure 28). The result of this approach was an artificial TMJ disc shape that closely replicated the physical geometry of the ovine TMJ disc in size and thickness, while also reducing the surface roughness inherent to the original .STL file geometry. Finally, a 0.33 mm thick circumferential flange was added to the TMJ disc superiorly and inferiorly to aid in its attachment to the fossa and condyle. The flange geometry of the molded disc could be easily modified during the practice surgeries to provide a range of attachment options for the maxillofacial surgeons during initial surgical development.

Once the patient-specific replacement geometry was complete, 3D printed molds for the artificial TMJ disc and attachment flange were designed in Solidworks®. The mirror image of the mold design was used to produce implants for the right TMJ disc. A 25% PVA hydrogel was created by dissolving an initial concentration of 25% PVA polymer in DI water at 80 °C for two hours. The liquid hydrogel was then poured into the 3D printed molds and subjected to six freeze-thaw cycles. After FT cycling, the hydrogels were removed from their molds and submerged in

PBS. Figure 28 depicts the stages of artificial disc creation; the circumferential flange is not pictured so that the disc geometry can be visualized.

Figure 28: Initial TMJ disc design created using patient-specific μCT of a left ovine TMJ disc.

Molded TMJ disc replacements were implanted in cadaveric sheep skulls (n=3) to test and refine the surgical strategy and method of attachment. In collaboration with Drs. Dobbs and Rawlinson, an updated implant design was created. The inferior circumferential flange was retained, but a patient-specific contoured plate was added to the superior lateral aspect of the artificial TMJ disc replacement to aid in more secure attachment to the zygoma. The flange and disc component thicknesses were increased to 2 mm and 1 mm, respectively. The disc geometry was also thickened to 1.5 mm along the crest of the condyle and around the TMJ disc periphery. A streamlined procedure for TMJ access, disc excision, and artificial TMJ disc implantation was developed in the first round of practice surgeries.

Further development focused on the design of the implant from clinical CT, and refinement of the artificial TMJ disc attachment methods. CT of ovine subjects was performed for an unrelated study and used to create patient specific left and right artificial TMJ disc replacements for four additional animals. Ovine skulls were harvested at the end of the study and used for practice

surgeries. The finalized surgical strategy and method of attachment was developed over three more practice surgery sessions. Two low profile, titanium maxillofacial plates (81-5724 – 19 mm 4-hole straight plate, Bioplate, Placentia, CA) and corresponding 1.5 mm diameter fixation screws (81-5741 – 5 mm low profile self-drilling screw, Bioplate, Placentia, CA) were used to attach the artificial TMJ disc to the TMJ fossa and condyle through the contoured flanges. Titanium plates were bent to match the condyle and zygoma geometry during surgery using a pair of Kelly hemostat forceps and a 3D printed guide. Only two of the four screw holes were used in the superior implant attachment, the unused section of the plate was removed during surgery. Two screws were used to affix the superior lateral flange to the patient zygoma, and four screws were used to fix the implant to the condylar neck using the inferior four-hole plate.

To design the patient specific TMJ discs, CT scan data were imported into Mimics (Mimics 25.0, Materialise, Leuven, Belgium) which was used to segment out the TMJ fossa and condyle bones. The TMJ bone geometry was then exported as a surface .STL file. The .STL was imported into Meshmixer to remove superfluous bone, reduce the overall file size, and create a manifold .STL geometry. The fossa and condyle geometries were then imported into Solidworks® which was used to define the TMJ disc shape. A smoothed surface following the contour of the TMJ condyle was created using evenly spaced (7.5 mm apart) splines following the condylar surface, and a spline connecting the spline endpoints along the periphery of the disc footprint (Figure 29).

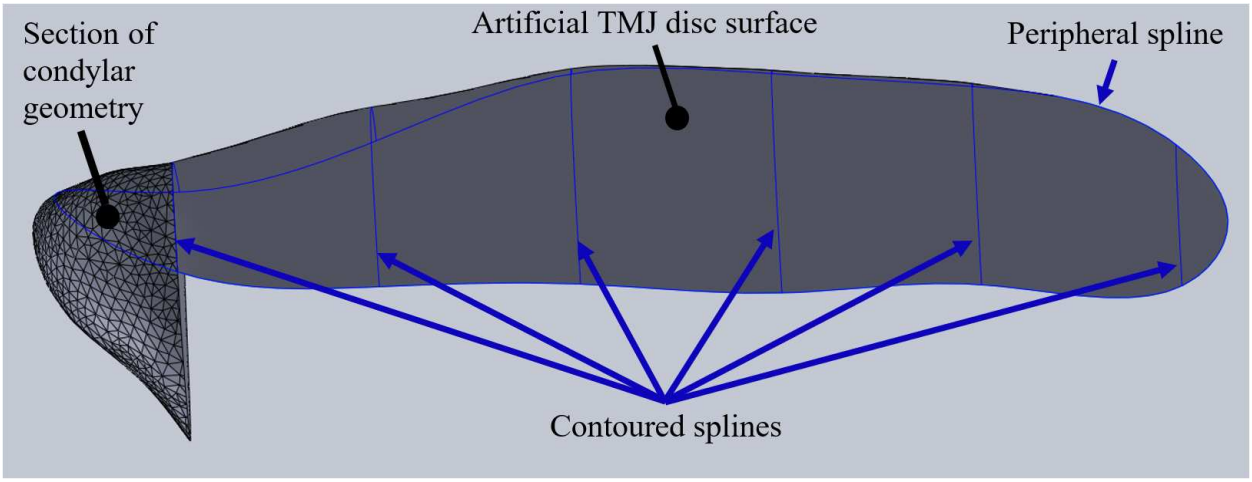

Figure 29: Construction of the TMJ disc surface geometry from contoured splines on the condylar articulating surface.

This surface was thickened to 1 mm in the center, 1.5 mm around the periphery, and 1.5 mm along the crest of the condyle. The internal surface of the superior-lateral TMJ disc attachment was defined using a similar approach to match the contour of the zygoma in the attachment location. An inferior attachment flange was designed to wrap around the neck of the condyle on the posterior and lateral faces using a similar method that also utilized the CT derived condylar geometry (Figure 29). Both flange geometries were created with a thickness of 2 mm.

Mold parting surfaces were created by extending surfaces from the edge of the attachment flanged and along the periphery of the TMJ disc component (Figure 30). An injection mold was created by performing a Boolean subtraction of the TMJ disc and parting surface geometry from a rectangular prism. An injection port was added to allow for injection molding on the external face of the implant attachment flanges. Three-part molds were manufactured from polylactic acid filament (Hatchbox 3D, Pomona, CA) using melt extrusion 3D printers (TAZ Workhorse and TAZ Pro, Lulzbot, Fargo, ND) with a 0.25 mm nozzle diameter. An example artificial TMJ disc geometry and three-part mold are shown in Figure 30.

To manufacture the patient specific TMJ discs, a liquid solution of 25% PVA was created by dissolving a concentration of 25% (by weight) PVA powder in deionized water at 80 °C while stirring. Three-part molds were sealed in advance of the molding stage using a silicon sealant. A male Luer lock adaptor was screwed into the exterior mold injection port. The 25% PVA solution was slowly injected into the mold using a Luer lock syringe to prevent the formation of bubbles in the molded part. The filled molds were subjected to 6 FT cycles prior to removal of the molded TMJ discs.

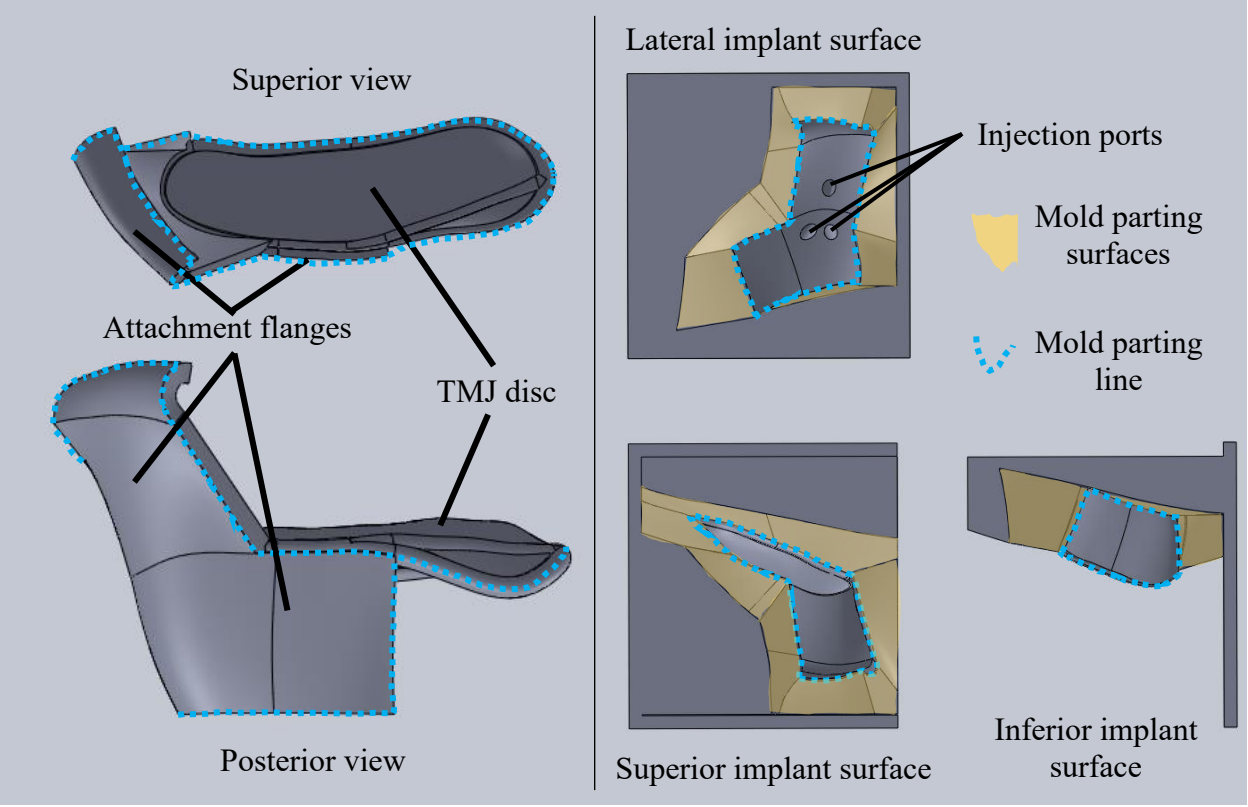

Figure 30: (left) Artificial TMJ disc design and (right) three-part mold geometry demonstrating mold parting line, parting surfaces, and injection ports.

1.2 Surgical procedure

The finalized surgical procedure was developed in conjunction with our clinical collaborators. A ~3-4 cm curvilinear pre-auricular skin incision was centered over the posterior

lateral aspect of the temporomandibular joint. Dissection was carried through the skin and subcutaneous tissues identifying the temporal fat pad superior to the zygomatic arch. Dissection was then carried down to the zygomatic arch and subperiosteal dissection was carried cranially, exposing the superior joint capsule. Tissues were retracted cranially and dissection with Metzenbaum scissors exposed the lateral and posterior aspect of the joint capsule. The condyle was retracted inferiorly to allow access for disc removal. An incision through the joint capsule exposed the superior and inferior joint compartments (Figure 31A). Sharp iris scissors and a #64 Beaver blade were used to dissect the TMJ disc from its circumferential attachments carefully avoiding the articular surfaces of the joint (Figure 31B). If necessary, the posterior aspect of the masseter insertion was elevated from the zygomatic arch to allow for increased access to the joint. The native TMJ disc tissue was then removed (Figure 31C), and the patient specific artificial replacement disc was inserted in the vacant joint space and aligned to the mandibular condyle and zygomatic arch (Figure 31D). A superior implant flange was secured to the posterior aspect of the zygomatic arch with a contoured titanium plate and two 1.5 mm diameter screws. The posterior inferior flange was secured to the mandibular condyle with a contoured titanium plate using four 1.5 mm diameter screws (Figure 31E). With the implant secure, the posterior insertion of the masseter muscle was reapproximated. The subcutaneous tissues and skin were closed in layers with resorbable sutures.

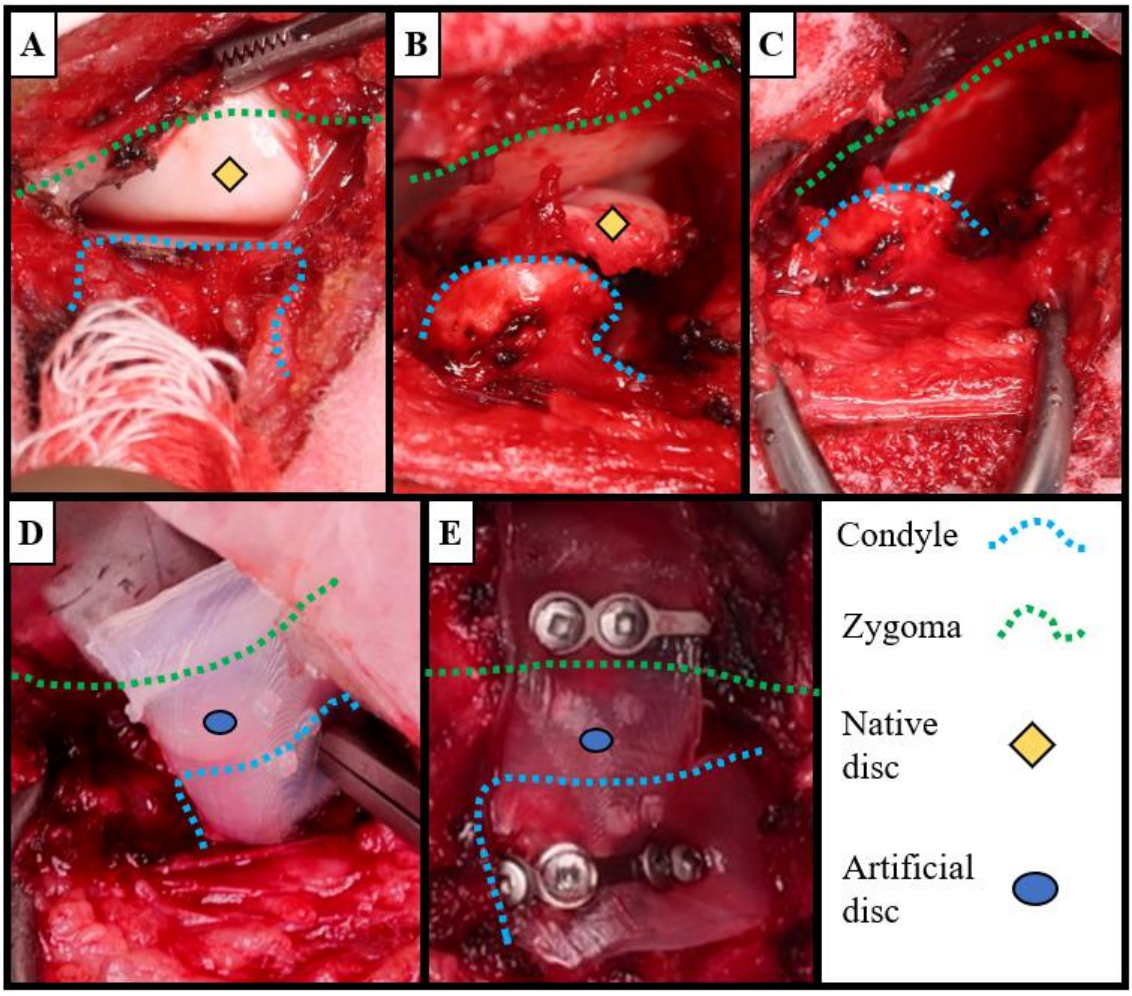

Figure 31: Stages of TMJ disc excision and replacement with a patient specific TMJ disc. (A) TMJ disc located, and inferior joint capsule resected, (B) superior joint capsule resected, (C) TMJ disc removed, (D) artificial TMJ disc inserted into vacant joint space, (E) completed installation of the artificial TMJ disc.

2 TMJ pilot study

2.1 Study design

The goal of the pilot study was to investigate *in vivo* and *ex vivo* outcomes of unilateral TMJ disc replacement in comparison to disc excision alone in an ovine preclinical model. A total of three animals underwent left TMJ disc excision (OTM01, OTM02, OTM03), and two of three animals received a patient specific artificial TMJ disc replacement made from 25% PVA hydrogel

using the previously described surgical procedure (OTM02, OTM03). The study duration was six weeks following surgical intervention ending in subject euthanasia. Table 4 shows a timeline of pilot study milestones focused on *in vivo* procedures. All experimental procedures were reviewed and approved by the CSU IACUC (#3999, approved November 28th, 2023).

Table 4: Summary and timeline of in vivo pilot study procedures relative to day 0, the date of surgical intervention.

	Day									
	-8	-7 to -1	0	7	14	21	28	35	41	42
Measure body weight		X		X	X	X	X	X		
Score body condition		X		X	X	X	X	X		
Measure consumption rate		X X X		X	X	X	X	X		
Record masticatory motions		X				X			X	
Head computed tomography scan	X									X
Surgery			X							
Sacrifice										X

2.2 Methods

2.2.1 In vivo procedures

Study animal health and chewing behavior were evaluated during the *in vivo* component of the pilot experiment by monitoring body weight (BW), body condition (BC), consumption rate (CR) and masticatory kinematics (MK). The goal of evaluating these parameters was to monitor subject welfare, and to examine which techniques may be used to assess the efficacy of TMJ treatments *ad hoc*.

Animal Care

Day-to-day animal care including feeding, watering, and bedding changes was performed by the Preclinical Surgical Research Laboratory (PSRL) team. Specialized animal care was also provided before, during, and after surgery. Prior to induction, a venous and an arterial catheter was

placed for administration of induction drugs, administration of fluids, and blood pressure monitoring. Anesthetic monitoring, including evaluation of electrocardiogram, arterial blood pressure, respiratory rate, pulse oximetry, capnography, and end-tidal carbon dioxide was performed by an anesthetist. Animals are placed in lateral recumbency following induction of general anesthesia. The wool was clipped from the regions external to the temporomandibular joint, masseter, and temporalis. The procedure site was prepped for aseptic surgery using alternating scrubs of povidone-iodine and alcohol. All instruments, gowns and drapes were properly sterilized prior to use. The surgeons donned masks and scrub caps prior to performing an aseptic prep and used a topical disinfectant before sterile gowning and gloving. Surgery was performed as described previously in this chapter. The animals were extubated and returned to the TMI holding pens. Animal recovery was continuously monitored by the PSRL staff until the sheep were completely conscious from anesthesia and able to accept food. Subsequently, all animals were moved to the research barn at the Veterinary Teaching Hospital at Colorado State University. For the duration of the study, animal BW and BC were monitored weekly, and any signs of severe/unexpected illness, discomfort, lameness, or evident fixation/implant failure were monitored daily. At the completion of the study, all subjects were euthanized with a fatal dose of pentobarbital intravenously.

Computed tomography

Clinical CT scans were taken of the skull of all three subjects eight days prior to surgery and once following euthanasia. CT scans prior to surgery were used to design patient specific implants for the two study animals receiving a TMJ disc replacement following disc excision.

Body weight monitoring

The BW and BC of each animal were monitored throughout the study. An initial BW was captured eight days prior to surgical intervention, and weekly following surgery until euthanasia. BW was measured at the same time of day to avoid capturing daily BW fluctuations. BC was also assessed by the professional animal care team at study onset and weekly during weighing using the 5-point scale described by *Thompson and Meyer* [316].

Consumption rate

Consumption rate (CR) was measured three times in the week prior to surgery, and once weekly for the six weeks prior to euthanasia. Study animals were individually provided 100g of grain feed and the time to complete chewing was measured with a stopwatch. The consumption rate was calculated as the mass of grain consumed divided by the time to complete chewing.

Mastication kinematics

Masticatory motions were recorded using a multiple-camera stereophotogrammetry system once prior to surgical intervention, at three weeks post-surgery, and at six week post-surgery. Six 12.7 mm diameter spherical reflective markers were attached to the animal using cyanoacrylate-base glue and a flexible 3D printed structure. This structure allowed the reflective markers to be removed between data collection sessions to prevent damage to the markers and disruption of normal feeding habits. A triad of markers were attached to the subject nose and subject chin to capture the cranium and mandible translation and rotation separately. This configuration allows for the motion of the jaw markers to be isolated from whole skull movements. Cameras were calibrated prior to each session of data collection. Grain was provided *ad libitum* throughout recording sessions to encourage more frequent chewing. Subjects were

briefly restrained by the researcher to ensure chewing occurred in the observation volume of the motion capture cameras.

Post processing of captured motion was performed using the Motion Analysis software (Cortex-64 7.2.16.1839, Motion Analysis Corp., Santa Rosa, CA). Individual chewing cycles were identified in the software and the raw coordinates of the chewing motions were exported for each individual cycle. MATLAB was used to transform the raw motion into idealized chewing motions to compensate for differences in the camera calibration which was changed between recording sessions. All data were analyzed with respect to the central marker on the subject mandible. MATLAB was first used to remove superfluous translation and rotation due to whole skull movement from the selected mandible marker motion. Translation of the whole skull was measured directly from cranium marker movements, and the resultant motion due to whole skull translation was subtracted from the subsequent location of the mandible marker (Figure 32). The rotation of the cranium markers between subsequent frames was captured in the form of rotation matrix R. Which was calculated using the vectors between two cranium markers in the first (*a*) and second (*b*) frame (Figure 32) using *Equation 6.1* and *Equation 6.2*.

Equation 6.1

$$R = I + N + N^2 \frac{1}{1 + \boldsymbol{c}}$$

Equation 6.2

$$N = \begin{bmatrix} 0 & -\boldsymbol{n_3} & \boldsymbol{n_2} \\ \boldsymbol{n_3} & 0 & -\boldsymbol{n_1} \\ -\boldsymbol{n_2} & \boldsymbol{n_1} & 0 \end{bmatrix}$$

Where I is the 3-by-3 identity matrix, $\boldsymbol{n}$ is the vector cross product $\boldsymbol{a} \times \boldsymbol{b}$, and $\boldsymbol{c}$ is the vector dot product $\boldsymbol{a} \cdot \boldsymbol{b}$ vectors $\boldsymbol{a}$ and $\boldsymbol{b}$. The rotation matrix was used to calculate the change in position of the mandible marker due to whole skull rotation between each frame, and the projected change in position was removed from the subsequent mandible marker position (Figure 32). The result of

these two procedures was to capture only the motion of the central jaw-mounted marker that was associated with mastication.

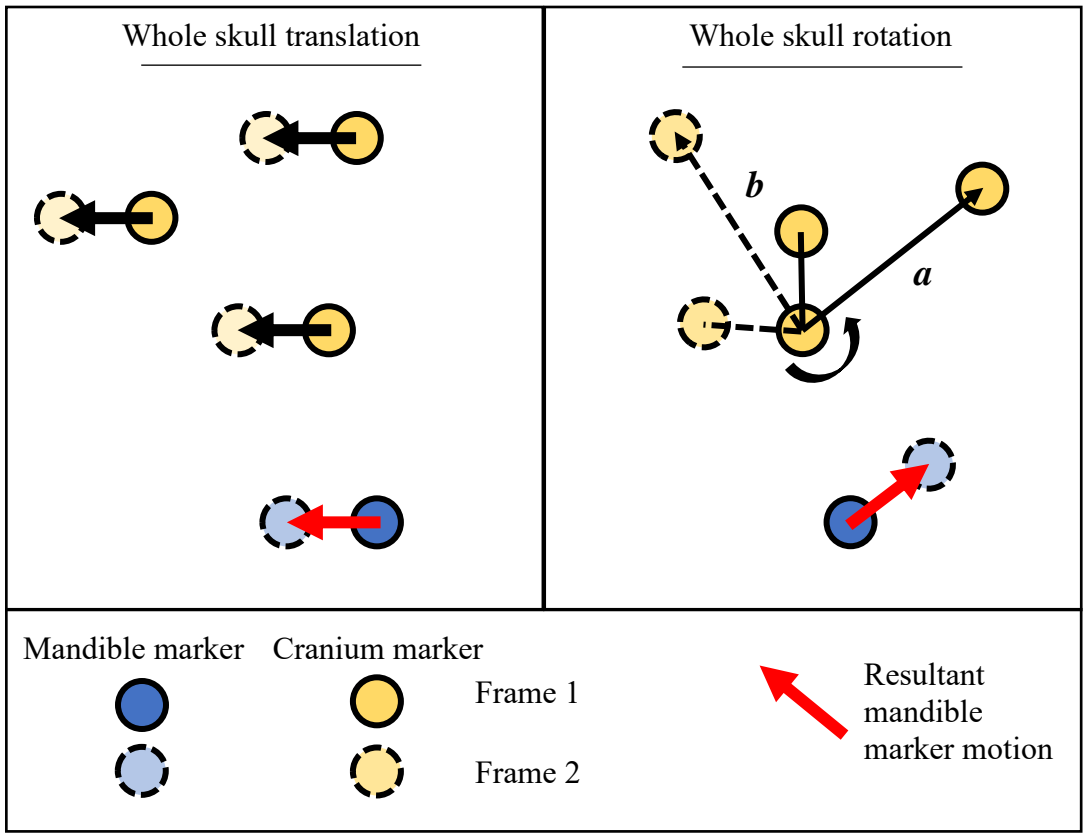

Figure 32: Diagram showing nature of mandible marker motion due to motion of the whole skull between two frames.

Six idealized chewing cycles were used to calculate a specimen range of motion (ROM) vector, maximum chewing velocity (v_{max}), and maximum chewing acceleration (a_{max}). Parameters were calculated for each time point, prior to surgery, at three weeks post-surgery, and at six weeks post-surgery prior to euthanasia. ROM was defined using *Equation 6.3*:

$$ROM = \sqrt{(X_{max} - X_{min})^2 + (Y_{max} - Y_{min})^2 + (Z_{max} - Z_{min})^2} \quad \textit{Equation 6.3}$$

Where X_{max} , Y_{max} , and Z_{max} are the maximum and X_{min} , Y_{min} , and Z_{min} are the minimum measured value of displacement in three orthogonal directions. The ROM was defined as the length of the largest vector bounded by the measured mandible marker motion due to mastication. *Equation 6.4* was used to define υ_{max} :

$$v_{max} = max\left[\sqrt{(v_x)^2 + \left(v_y\right)^2 + (v_z)^2}\right] \qquad \textit{Equation 6.4}$$

Where υ_x, υ_y, and υ_z are the values of velocity for each corresponding time point. Thus, the value of υ_{max} is the maximum velocity of the mandible marker during any given chewing cycle. *Equation 6.5* was used to define α_{max}:

$$a_{max} = max\left[\sqrt{(a_x)^2 + \left(a_y\right)^2 + (a_z)^2}\right] \qquad \textit{Equation 6.5}$$

where α_x, α_y, and α_z are the values of velocity for each corresponding time point. Thus, the value of α_{max} is the maximum acceleration of the mandible marker during any given chewing cycle. The calculated ROM, υ_{max}, and α_{max} were compared between time points for the individual study participants using one-way ANOVA with *post hoc* Tukey test. $p < 0.05$ was considered significant for this statistical evaluation.

2.2.2 Ex vivo procedures

Post-sacrifice dissection, x-ray imaging and photography, indentation of the cartilage surfaces, and histological analysis of the left and right TMJs and selected organ tissues was performed. These methods allow for direct observation of the implant and TMJ structures, as well as biomechanical and histological means to assess implant success in comparison to TMJ disc excision.

Ex vivo imaging and scoring

Sequential images and x-rays were taken of the pilot study skulls and TMJs throughout sample dissection following study termination. Example x-rays and images from each specimen are shown for visual analysis of the bony and cartilage features of the treated and contralateral TMJs.

Cartilage indentation

Indentation-stress relaxation experiments were performed on the left and right TMJ cartilage surfaces for all study animals. Indentation-stress relaxation testing followed the same protocol described in Chapter 2. Briefly, a stainless-steel indenter tip with a 0.4 mm radius was used to indent the cartilage surfaces surface in five locations spaced equally across the width of the sample surface. Specimens were indented to a depth of 0.2 mm at a rate of 0.2 mm/s, followed by a 100 s hold to allow for tissue relaxation before indenter retraction. Force and displacement data were collected and used to calculate the instantaneous and equilibrium elastic moduli using Hertzian contact mechanics (*Equation 2.4*). The instantaneous modulus was calculated using a least-squares fit of *Equation 2.4* to the loading portion of the force-displacement data. Force-displacement data from the end of the 100 s hold period was used to calculate the equilibrium modulus using *Equation 2.4*. Data were logarithmically transformed to satisfy the assumptions for normality and equal variance. A one-way ANOVA with *post hoc* Tukey test was implemented to compare the indentation results for instantaneous and equilibrium moduli separately. For these analyses, $p < 0.05$ was considered significant.

Histological analysis

The TMJ disc replacements were removed from the left TMJs of each specimen, and both left and right TMJs were fixed in a 10% neutral buffered formalin solution (Epredia, Kalamazoo, MI). A sample of the kidney, lungs, left submandibular lymph node, liver, spleen, and heart was also collected for toxicological assessment. Organ samples from each subject were fixed in a 10% neutral buffered formalin solution. After fixation, the TMJ fossas and condyles were separated and decalcified in a 10% formic acid solution. Total decalcification was confirmed by a loss of radiopacity on x-ray images. The decalcified TMJ bones, organs, and right TMJ discs were

infiltrated with paraffin wax using a tissue processor (Sakura Tissue-Tek VIP E300, Sakura Finetek USA, INC., Torrance, CA) and embedded in paraffin blocks using a tissue embedder (Shandon Histocentre 2, Thermo Shandon, Inc., Kalamazoo, MI). A microtome (Leica RM2255, Leica Biosystems, Wetzlar, Germany) was used to create 5 µm slices of each sample, which were mounted on microscope slides. At least one slide from each tissue was stained with Hematoxylin and Eosin (H&E). Additional slides of the TMJ bones and right TMJ discs were also stained with a combination of Safranin O and Fast-green. Unless otherwise stated, all chemicals were purchased from the Sigma Aldrich catalog (Merck KGaA, Darmstadt, Germany). All slides were reviewed by a trained veterinary pathologist (Dr. Dan Reagan, Colorado State University). The degree of periosteal proliferation, fibrosis, inflammation, synovial hyperplasia, and subintimal fibrosis in each sample was scored using the following scale: 0 = none, 1= minimal, 2 = mild, 3 = moderate, 4 = severe.

2.3 Results

2.3.1 *In vivo* procedures

Consumption rate

The food consumption rate for all animals generally increased throughout the study. There was no indication that the surgical intervention resulted in a demonstrable decrease in the consumption rate for any of the subjects. All subjects were able to participate in the consumption rate evaluations with no signs of pain or discomfort associated with chewing. Figure 33 shows a plot of the measured consumption rates throughout the experiment.

Body weight monitoring

Animal BW initially decreased following surgery (to a minimum of 89% of initial body weight) but recovered to within 5% of the initial body weight by study termination for all animals. A plot of the animal body weight percentage, normalized to initial body weight, is shown for the study duration in Figure 33. No change in animal body condition was observed for any subject during the experiment.

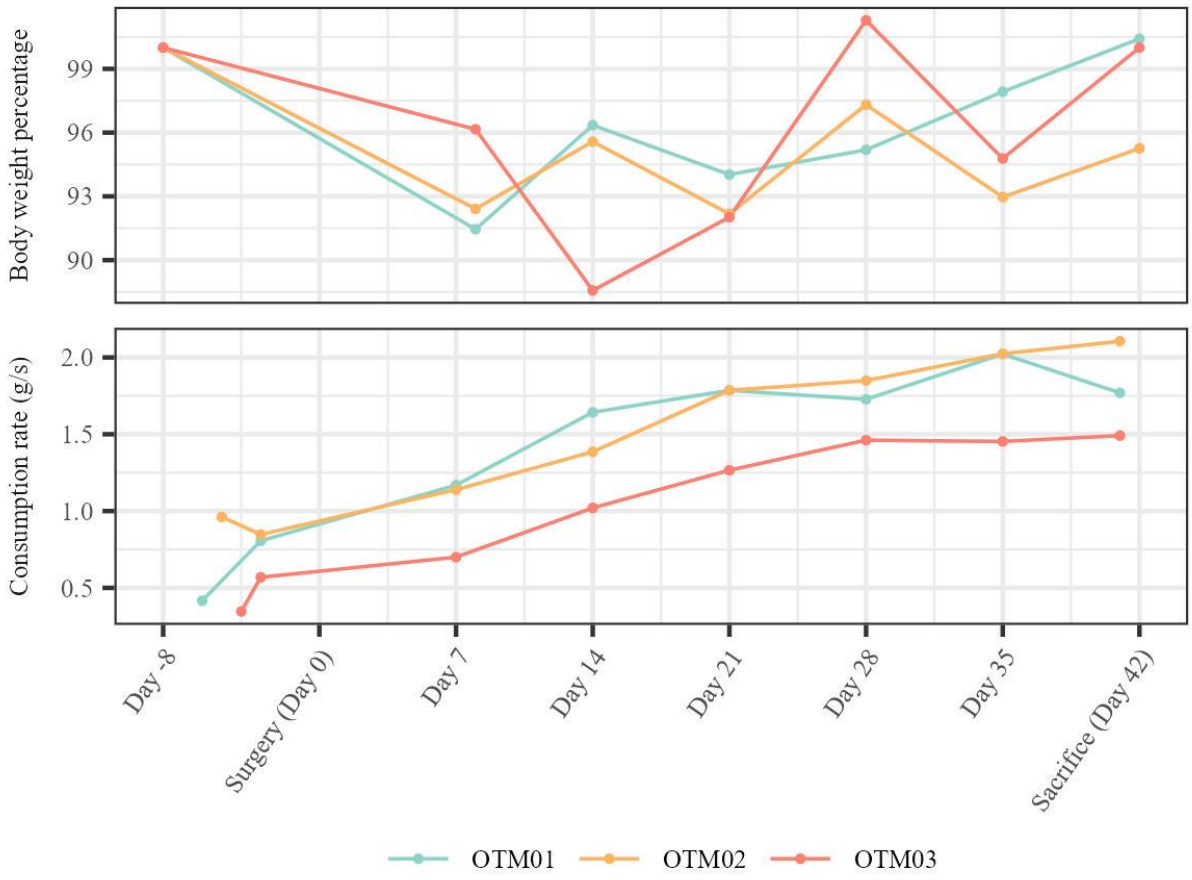

Figure 33: Body weight percentage and consumption rate over the in vivo portion of the pilot study.

Masticatory kinematics

Figure 34 shows the results of the MK evaluation, separated by individual and time point. There were no statistically significant differences in ROM, υ_{max}, and α_{max} across study timepoints for the untreated subject (discectomy only). There were statistically significant differences between the pre-surgery and mid-study v_{max} for the treated subjects (OTM02, OTM03), but no matching trends.

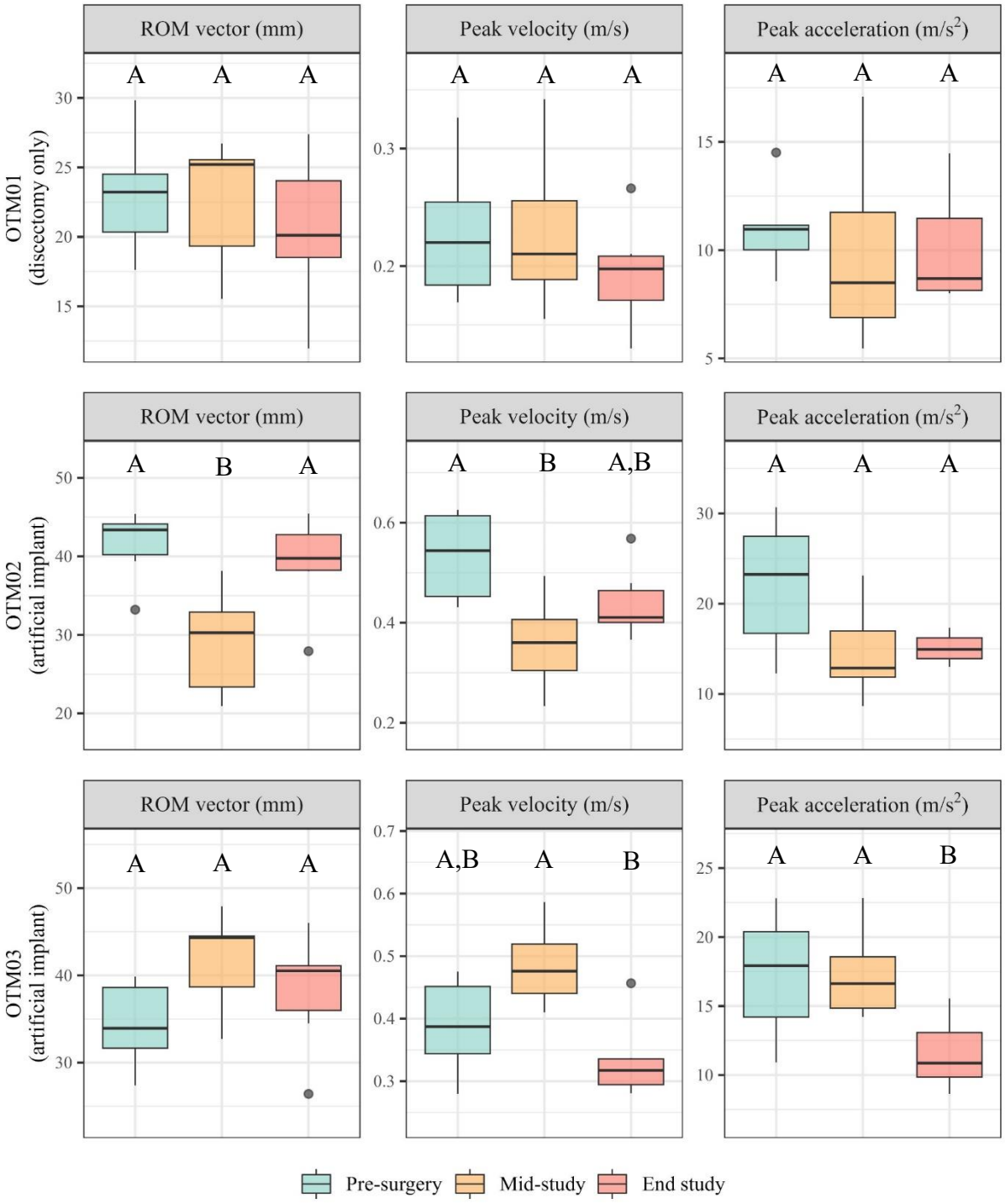

Figure 34: Results from kinematic motion analysis of the pilot study animals. Groups that do not share a letter were significantly different.

2.3.2 *Ex vivo* procedures

Imaging and dissection

In all left TMJs, the joint capsule was recapitulated in the form of a fibrous scar tissue layer surrounding and stabilizing the joint. Throughout dissection it was clear that there was no adhesion between the recapitulated joint capsule and PVA hydrogel for any of the specimens. Implant failure was observed in the disc component and attachment flange of both artificial TMJ disc replacements (Figure 35). X-rays did not reveal any evidence of failure in the titanium plate or screws used to secure the implant, there was also no apparent erosion or fracture in the TMJ bones on the left or right sides (Figure 36). Images show evidence of articular cartilage erosion in all left TMJ fossas (Figure 37) and condyles (Figure 38). The right TMJ discs and articular cartilage surfaces appeared normal.

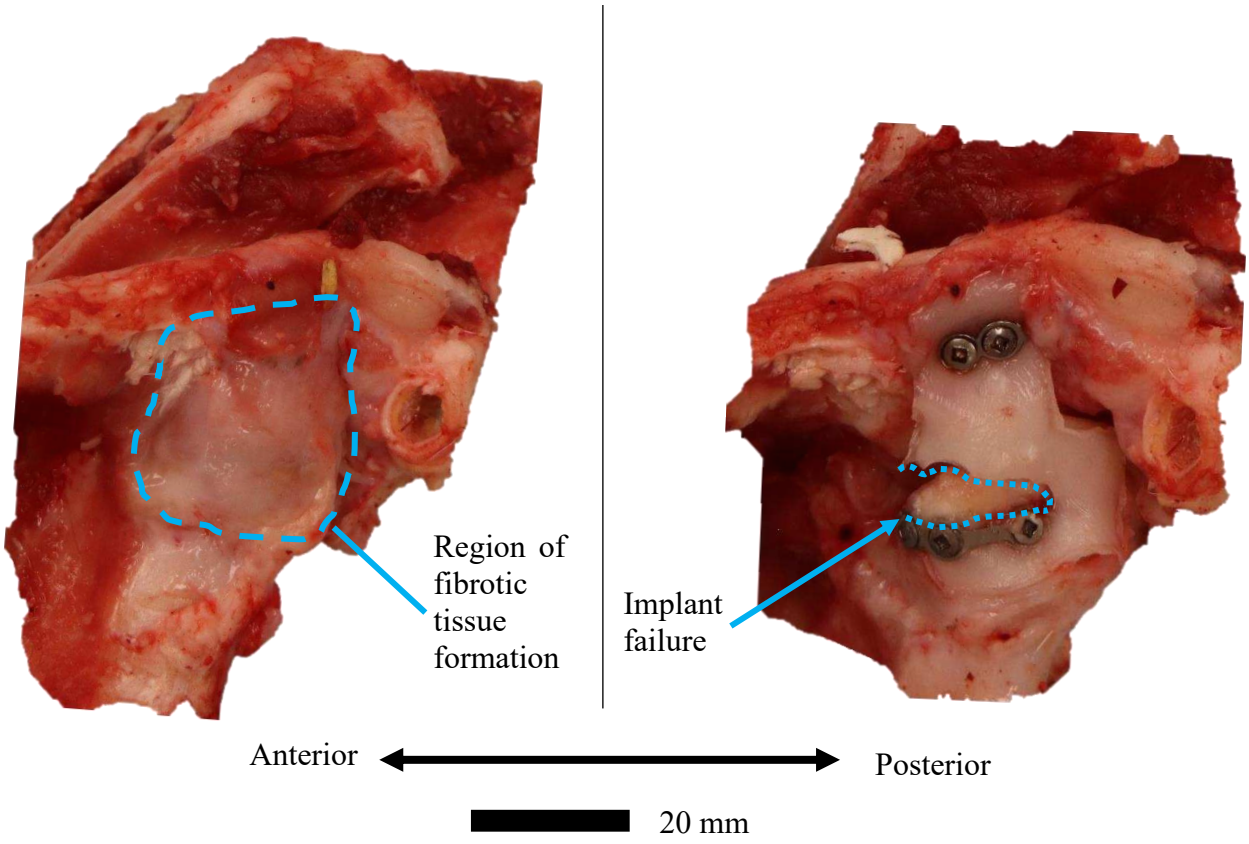

Figure 35: (left) Image of left TMJ showing fibrotic tissue formation surrounding the artificial TMJ disc replacement. (right) Image of left TMJ after removal of fibrotic tissue surrounding joint space, implant failure is evident along the edge of the inferior titanium plate.

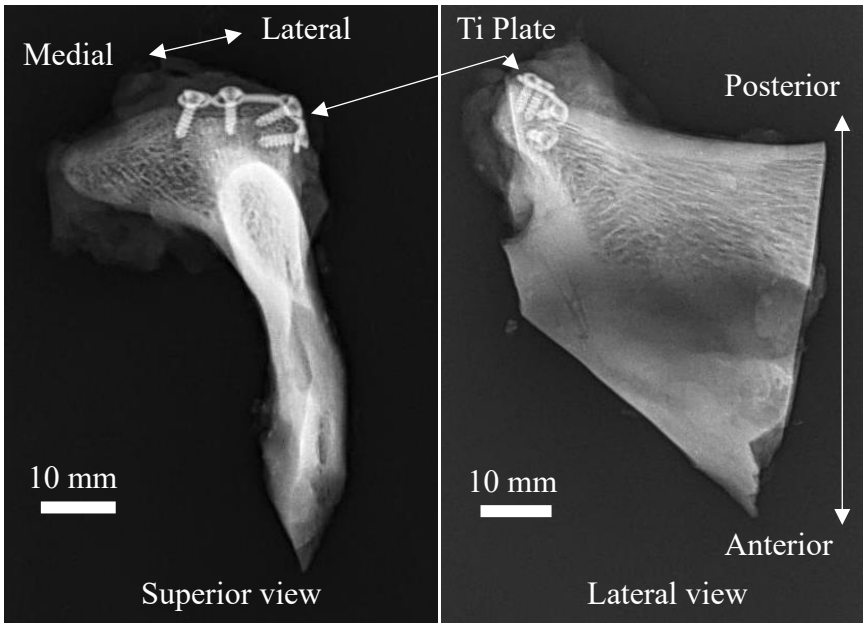

Figure 36: Example x-ray images showing a left TMJ condyle with titanium plate still installed following gross dissection.

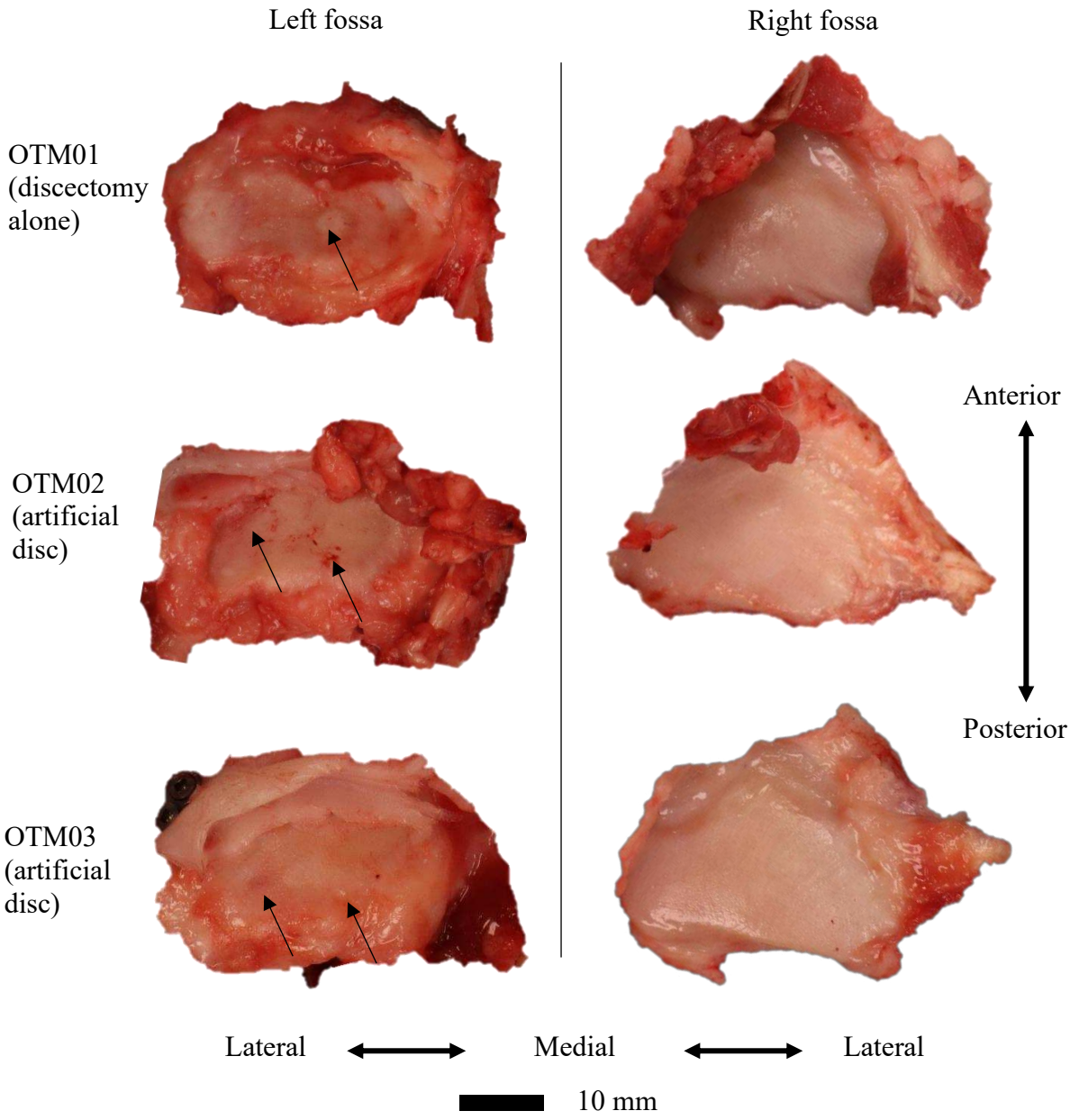

Figure 37: Images of the fossa articular cartilage surfaces of the pilot study subjects following gross dissection, arrows indicate regions of cartilage erosion. Right (contralateral) TMJ fossas appear visually normal.

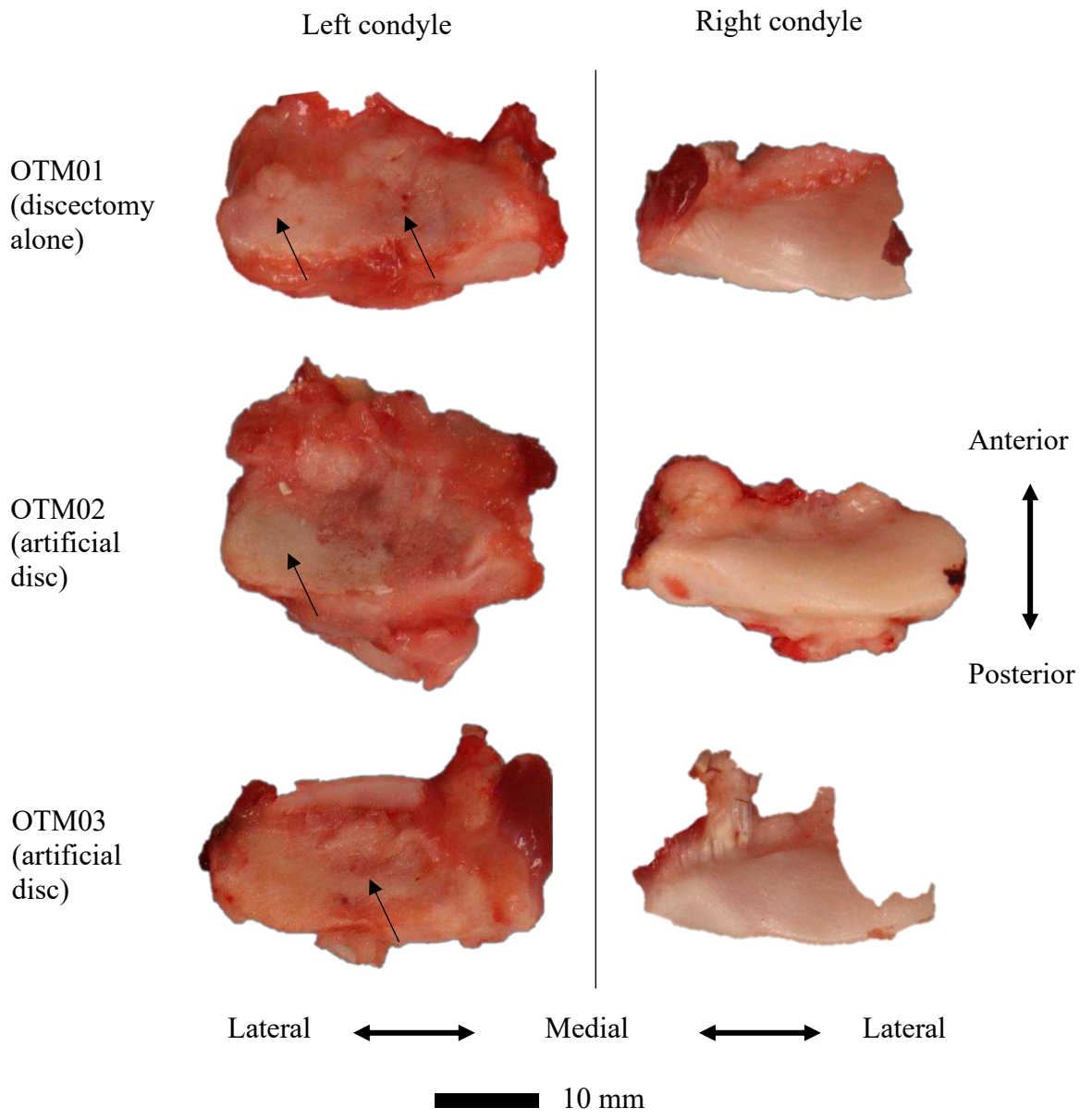

Figure 38: Images of the condyle articular cartilage surfaces of the pilot study subjects following gross dissection, arrows indicate regions of cartilage erosion. Right (contralateral) TMJ condyles appear visually normal.

Indentation

There were no statistically significant differences between the instantaneous or equilibrium moduli measured with indentation. The indentation moduli of the articular cartilage surfaces was

generally greater for animals that received an artificial TMJ disc replacement in both the left and right side (Figure 39).

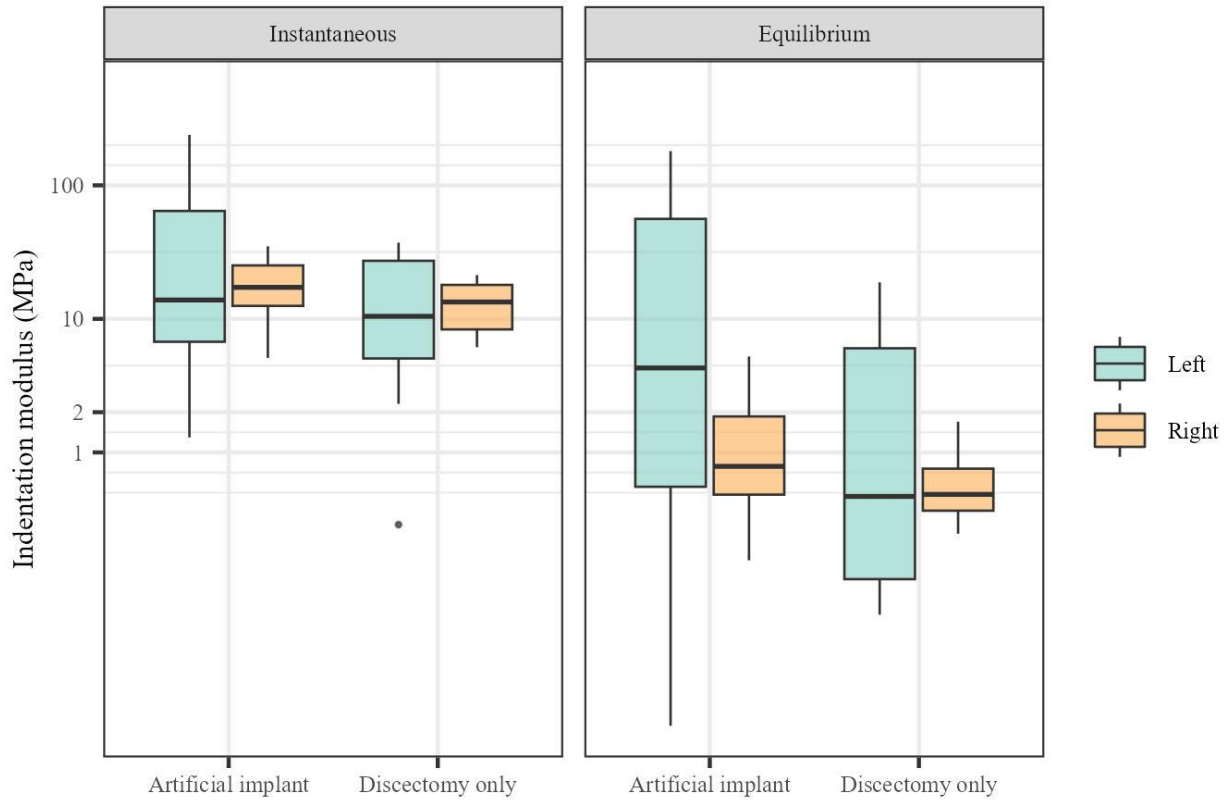

Figure 39: Results from indentation-stress relaxation experiments on the pilot study animal left and right TMJ articular cartilage surfaces. Bars indicate the measurement standard deviation.

Histological analysis

The kidney, lungs, left submandibular lymph node, liver, spleen, and heart tissues appeared histologically normal for all subjects. The right TMJ articular cartilage surfaces and TMJ discs also appeared histologically normal. Major changes in were observed in the left TMJs and were more prominent in the condyle than the fossa. These changes were characterized primarily by periosteal proliferation of a mixture of new woven bone and fibrosis/fibrocartilage. The synovium tissue was also moderately to markedly thickened by fibrosis with mild synovial hyperplasia.

Table 5: Results of histological scoring of TMJ articular surfaces, 0 = none, 1= minimal, 2 = mild, 3 = moderate, 4 = severe.

					Synovium		
Animal ID	**Tissue**	**Site**	**Periosteal proliferation**	**Fibrosis**	**Inflammation**	**Synovial hyperplasia**	**Subintimal Fibrosis**
OTM01 (discectomy only)	**Fossa**	**R**	0	0	--	--	--
	Fossa	**L**	1	3	--	--	--
	Condyle	**R**	0	0	0	0	0
	Condyle	**L**	2	2	0	1	3
OTM02 (artificial disc)	**Fossa**	**R**	0	0	--	--	--
	Fossa	**L**	3	2	--	--	--
	Condyle	**R**	0	0	0	0	0
	Condyle	**L**	4	3	0	2	2
OTM03 (artificial disc)	**Fossa**	**R**	0	0	--	--	--
	Fossa	**L**	1	1	0	2	1
	Condyle	**R**	0	0	0	0	0
	Condyle	**L**	3	3	0	3	3

2.4 Discussion

An abundance of evidence suggests that the artificial TMJ discs made from 25% PVA hydrogel were not successful in preventing TMJ degeneration following TMJ disc resection in this pilot experiment. There were no statistically significant results supporting the use of the 25% PVA hydrogel disc replacements as a treatment over TMJ disc excision alone. The artificial discs lacked the necessary mechanical strength to withstand the dynamic stresses over the study duration, despite the mechanical attributes that made the PVA hydrogels a promising candidate. However, the development and execution of this pilot study is helpful for refining *in vivo* and *ex vivo* procedures for future TMJ disc replacement development. Data collected during this pilot has also been used to bolster expedited *ex vivo* methods for evaluating the TMJ disc replacements investigation of implant failure allows for further refinement of the surgical procedure and implant geometry, and experience gained is useful in planning for in future *in vivo* studies.

Prior to returning to an *in vivo* model, a more robust TMJ disc replacement structure must be developed and appropriately evaluated. The 25% PVA hydrogels exhibited similar mechanical behavior in key areas, including friction and compression and exhibited high toughness and failure stress. Unfortunately, the implants were not sufficiently strong to withstand the *in vivo* joint forces for the duration of the study. If PVA hydrogels are to be used in future iterations of the TMJ disc replacement design, they must be mechanically reinforced. A preliminary investigation of thermally annealed PVA hydrogels showed an increased durability over the 25% PVA hydrogels. Additional investigation of annealed PVA, and PVA hydrogels reinforced with PP meshes produced using melt extrusion and melt electrowriting 3D printing is a promising area of future research. Future development of a TMJ disc replacement will focus on these methods to prevent premature implant failure and preserve TMJ articular cartilage health.

A limitation of this work is the low sample size, which makes it difficult to draw conclusions about the efficacy of TMJ disc replacement treatment in comparison to TMJ disc resection alone. However, the purpose of this pilot experiment was to develop and refine the techniques needed to assess success in a larger experiment. Though BW and BC were helpful in monitoring the health in the study animals, these methods were not sensitive enough to differentiate the outcome of TMJ disc replacement or discectomy alone throughout the *in vivo* portion of this pilot study. The author suggests that future experiments monitor body weight and body condition of the animals at a similar interval throughout the study, but only as a method for monitoring animal health, rather than long term implant success. Observation of the CR may also be helpful in future experiments if the onset of such observations precedes surgical intervention by a longer duration than eight days. Over the course of this pilot study the consumption rate generally increased, but this may also be due to acclimatization of the animals to hand feeding by

the research group. If CR observations began six weeks prior to surgical intervention, a more pronounced response in CR may be distinguished following surgery.

Indentation stress-relaxation experiments were performed similarly to the methods used in Chapter 2. This method was appropriate for evaluating the articular cartilage surfaces of the right TMJs but produced highly variable results for the left TMJs due to the inhomogeneity of the articulating surfaces. Indentation experiments will be valuable in future experiments if a more uniform articular cartilage remains in the treated TMJ throughout the study.

Measurement of the masticatory motions was useful in preparing *ex vivo* experiments to evaluate artificial TMJ disc replacement candidates as they are developed (described in Chapter 5). However, the fidelity of the MK parameters was insufficient for identifying statistical differences in the masticatory behavior throughout the study. Differences in the individual chewing cycles may be causation for the variance in MK parameters. As the bolus size and shape changes so do the individual chewing motions. Careful selection of chewing cycles, for instance by only analyzing the first or last chewing cycle in a sequence, may help to reduce the magnitude of the MK parameter variance. Increasing the number of cycles captured and included in the MK parameter evaluation is recommended to allow for a more robust analysis.

Histological evaluation was intended to be the primary variable for assessing the longer-term success of a TMJ disc replacement in preventing TMJ degradation following TMJ disc resection. For this to be accomplished, a larger number of animals will need to be used in the control group (discectomy alone) to quantify any differences with higher significance. In future *in vivo* experiments a larger cohort of control animals are recommended.

Right TMJs appeared unaffected by disc excision and disc excision with artificial disc replacement in the contralateral joint. This may be in part due to the short duration of the study (6 weeks), but in the case of this pilot study, the right TMJs were considered an untreated control group. If the study duration was increased, the health of the right TMJ may be adversely affected or undergo morphological changes. Thus, the author suggests that a group of untreated subjects be included in future analysis of both *in vivo* and *ex vivo* parameters.

Overall, this pilot experiment was successful in refining techniques for *in vivo* and *ex vivo* evaluation of an artificial TMJ disc replacement despite the premature failure of the implants used. Methods for improving and evaluating future implants candidates are informed by the results of this pilot experiment. Future TMJ disc replacement development will build on the procedures and results of this pilot to improve methods for evaluating implant success.

CHAPTER 7 - SUMMARY AND CONCLUSIONS

The primary goal for artificial TMJ disc replacement is to arrest degenerative changes in the TMJ after disc excision by protecting the diseased TMJ with a robust replacement. Previous failures to successfully replace the TMJ disc emphasize both the urgency and the difficulty in accomplishing this task. There are currently no artificial TMJ disc replacements on the market, despite the fact that disc excision fails to prevent further disease progression in up to 25% of patients [142]. Thus, methods for TMJ disc replacement must be reevaluated on a fundamental level, focusing first on the basic science and material evaluation before implementation of *in vivo* experiments. We endeavored to explore PVA hydrogels as a suitable material for a patient specific artificial TMJ disc replacement through a series of mechanical tests, an ovine preclinical model, and *ex vivo* and *in silico* simulations.

These efforts began with an in-depth characterization of the ovine TMJ soft tissues to measure design targets for the artificial TMJ disc replacement. A survey of literature paired with a panel of mechanical tests lead to the identification of PVA hydrogels as an excellent candidate for a non-degradable TMJ disc replacement due to its biocompatibility and mechanical tunability in the range of the native TMJ discs. A FE model of jaw clenching in the ovine TMJ was also developed and validated as a means to investigate TMJ disc replacement candidates *in silico*. Next, a method for designing and implanting an artificial TMJ disc replacement was developed with the help of orthopedic and maxillofacial surgeons. This strategy was implemented in a pilot experiment to develop *in vivo* and *post hoc ex vivo* methods for assessing the outcomes of TMJ disc excision and artificial TMJ disc replacement in ovine specimens. Finally, a SCA was designed to reproduce chewing motions in ovine cadaveric specimens, using data collected during the pilot experiment, to study the modes of implant failure. Although PVA hydrogels were identified as an

excellent candidate for TMJ disc replacement through literature review and mechanical evaluation, the implants were not sufficiently strong to withstand the TMJ mechanical environment in the pilot experiment or the *ex vivo* chewing apparatus. However, a range of useful methods for evaluating the implant material candidates, surgical approach, and implant design were developed that will support future TMJ disc replacement research. The development of these new methods lays the foundation for success in the future of TMJ disc replacement design.

A rigorous evaluation of the ovine TMJ biomechanics was performed in order to set the initial design targets for an artificial TMJ disc replacement. This assessment included indentation on the articular cartilage surfaces of the TMJ and tensile evaluation of the circumferential joint capsule. The mechanical properties of freshly harvested ovine TMJ discs were also characterized in unconfined compression and friction experiments. These tests informed not only the design targets of the artificial TMJ disc replacements, but also the mechanical properties used for the TMJ disc in the clenching FE model. This broad characterization of the native ovine TMJ disc establishes a basis for future mechanical evaluation that may be applied to the human TMJ disc, including a suite of testing procedures that are repeatable for implant material candidates.

PVA hydrogels were initially identified as a candidate material for the artificial TMJ disc replacement through literature review. Subsequent mechanical characterization confirmed their candidacy due to their biocompatibility and mechanical tunability in the range of the native TMJ disc. Several PVA hydrogel concentrations were evaluated, of which the 25% PVA hydrogels were the most promising. At this concentration, the hydrogels possessed biomimetic frictional and compressive properties, as well as high toughness and failure stretch. However, the 25% PVA hydrogel implants lacked sufficient fatigue strength to withstand the stresses imposed during both the *ex vivo* SCA experiments and the *in vivo* pilot study. Thus, a reevaluation of the implant

material candidates should be expanded to include long-term wear and fatigue properties. We propose that for PVA hydrogels to be a successful candidate for an artificial TMJ disc replacement, they must be reinforced by thermal annealing [311, 312, 317] or with an embedded fiber scaffold [318-320]. Thermal annealing is a method that has been shown to increase toughness and elastic modulus by heating crosslinked PVA hydrogels to a temperature between the glass transition and melting temperatures [321]. The resulting constructs must remain biocompatible, manufacturable, and implantable in the TMJ disc space. PVA hydrogels remain a promising option for TMJ disc replacement, but only if their long-term performance can be improved while retaining their current advantages. The mechanical characterization of PVA hydrogels performed by the author will support future refinement of PVA hydrogels for TMJ disc replacement.

A FE model of ovine jaw clenching was created to support the development of an artificial TMJ disc replacement. This model was validated by *ex vivo* measurements of TMJ contact stresses during simulated jaw clenching in freshly harvested TMJs. A comparison between the model predictions for native TMJ disc and 25% PVA hydrogels showed no difference in the disc component stress response in comparison to the validation data. These results suggest that the PVA hydrogels mimic the natural tissue behavior during clenching. However, due to the quasi-static nature of the experiment, these findings cannot be extrapolated to other activities such as chewing. A dynamic model, including both the left and right TMJs, is necessary for more rigorous evaluation of implant candidates moving forward. Including left and right TMJs is more appropriate for chewing analysis as the motion of the left and right TMJs is not symmetric. Motion in the chewing model can be defined based on the measured masticatory motion of the pilot study animals. A chewing FE model can be used to identify regions of the artificial implants that require reinforcement or geometry modification. Ultimately, the current clenching model can be used for

cursory evaluation of implant material candidates in a clenching simulation, but future modeling should focus on the stress response to dynamic motions of the TMJs.

Ex vivo analysis of TMJ disc replacement candidates was performed using a simulated chewing apparatus. By using a cadaveric skull and measured masticatory motion, the *in vivo* mechanical environment of the TMJ can be more effectively reproduced than by discretized experiments such as compression or indentation. The SCA is meant to be used for evaluation of the entire TMJ disc replacement strategy to predict the mode of implant failure that may occur *in vivo*. The SCA was used to replicate the modes of failure observed in both the TMJ disc component and attachment flange of the 25% PVA hydrogel implants used in the pilot study. Future implants should be evaluated using the SCA as a final investigation before returning to *in vivo* experiments. The target number of cycles before implant failure should safely exceed the expected number of chewing cycles over the *in vivo* implant lifespan (30,000 to 50,000 chewing cycles per day in sheep). It is common for these design targets to be on the order of 10^6 to 10^7 loading cycles [322], particularly for the frequently used TMJ. Thus, future implant candidates must be shown to withstand a sufficiently high number of cycles for the expected loading modality. Future implant development will implement the SCA as a more efficient means for analyzing TMJ disc replacements prior to use *in vivo*.

Iterative development of an artificial TMJ disc replacement has helped to refine the design and manufacturing pathway for future advancements. The current design iteration is molded using a three-part injection mold that is generated using patient-specific CT scans. The implant geometry approximates the native TMJ disc, while also providing a surgically accessible method for securing the implant in place through contoured flanges. Titanium maxillofacial plates and screws are used to fix the implant in the subject TMJ and can be modified during surgery to match the bone

contours more appropriately. The method of implant attachment must be more rigorously evaluated based on catastrophic implant failure in the *in vivo* pilot study and *ex vivo* SCA experiments. Methods focused on eventual integration of the attachment flanges into the host tissue, particularly into the recapitulated TMJ capsule, may allow for a more effective long-term attachment. In the pilot experiment, no adhesion between the PVA hydrogel and host tissue was achieved. This was an expected outcome for PVA hydrogels, which are known for their low tissue and cell adhesive properties [323]. In the disc component of the replacement, this feature of PVA hydrogels is considered an advantage. However, increased adhesion between the implant flanges and the host tissue may provide additional support to the implant, which would reduce implant stresses and increase *in vivo* lifespan. This goal may be accomplished by creating a porous attachment flange or by including a degradable or bioactive component to the implant flange.

An *in vivo* pilot study was carried out to compare disc excision (n = 1) to disc excision with artificial TMJ disc replacement (n = 2) in an ovine preclinical model. The subject body weight, body condition, consumption rate, and masticatory kinematics were recorded during the *in vivo* portion of the study before and after surgical intervention. Dissection and visual inspection, indentation of the cartilage surfaces, and histological evaluation of the TMJ tissues was also performed following subject termination. Failure of the TMJ disc replacements was evident during *post hoc* evaluation, but there was no external evidence of implant failure during the *in vivo* component of the study. In fact, all study subjects recovered normally following surgery and showed no signs of TMJ pain or dysfunction according to the *in vivo* evaluation methods. These findings suggest that more acute diagnostic methods for assessing the health of the TMJ disc replacement are necessary in future experiments. Current methods for evaluation TMJ health in human patients utilize MRI as a diagnostic criterion for TMJ dysfunction [324]. Inclusion of MRI

as an *in vivo* method for assessing implant health is recommended in future experiments. Overall, the pilot experiment was helpful in procedural development for future *in vivo* experiments and demonstrated a pronounced response to TMJ disc excision in all subjects. Prevention of joint degradation in comparison to TMJ disc excision alone was not achieved with the implant and surgical strategy described in this body of work. However, the process for design and manufacture of PVA hydrogel implants has been refined, and numerous methods of implant attachment have been investigated. The pilot experiment reinforced the need for more rigorous evaluation of the artificial TMJ disc constructs and emphasized the importance of TMJ disc replacement over TMJ disc excision.

The completion of this body of work is an essential step towards creating a successful TMJ disc replacement strategy. Evaluation of the ovine TMJ disc, investigation of material candidates for disc replacement, and the development of *in vivo, ex vivo*, and *in silico* methods for assessing TMJ disc replacement strategies in the ovine preclinical model will be essential building blocks for the future of TMJ research.

REFERENCES

[1] E. J. Van der Linden, A. R. Burdi, and H. J. de Jongh, "Critical periods in the prenatal morphogenesis of the human lateral pterygoid muscle, the mandibular condyle, the articular disk, and medial articular capsule," *Am J Orthod Dentofacial Orthop,* vol. 91, no. 1, pp. 22-8, Jan 1987, doi: 10.1016/0889-5406(87)90205-8.

[2] D. A. Keith, "Development of the human temporomandibular joint," *Br J Oral Surg,* vol. 20, no. 3, pp. 217-24, Sep 1982, doi: 10.1016/s0007-117x(82)80042-5.

[3] T. Humphrey, "The development of mouth opening and related reflexes involving the oral area of human fetuses," *Ala J Med Sci,* vol. 5, no. 2, pp. 126-57, Apr 1968. [Online]. Available: https://www.ncbi.nlm.nih.gov/pubmed/5675826.

[4] M. E. Bender, R. B. Lipin, and S. L. Goudy, "Development of the Pediatric Temporomandibular Joint," *Oral Maxillofac Surg Clin North Am,* vol. 30, no. 1, pp. 1-9, Feb 2018, doi: 10.1016/j.coms.2017.09.002.

[5] D. L. Stocum and W. E. Roberts, "Part I: Development and Physiology of the Temporomandibular Joint," *Curr Osteoporos Rep,* vol. 16, no. 4, pp. 360-368, Aug 2018, doi: 10.1007/s11914-018-0447-7.

[6] J. C. Nickel, L. R. Iwasaki, Y. M. Gonzalez, L. M. Gallo, and H. Yao, "Mechanobehavior and Ontogenesis of the Temporomandibular Joint," *J Dent Res,* vol. 97, no. 11, pp. 1185-1192, Oct 2018, doi: 10.1177/0022034518786469.

[7] R. J. Hinton, J. Jing, and J. Q. Feng, "Genetic Influences on Temporomandibular Joint Development and Growth," *Curr Top Dev Biol,* vol. 115, pp. 85-109, 2015, doi: 10.1016/bs.ctdb.2015.07.008.

[8] D. Tamimi, E. Jalali, and D. Hatcher, "Temporomandibular Joint Imaging," *Radiol Clin North Am,* vol. 56, no. 1, pp. 157-175, Jan 2018, doi: 10.1016/j.rcl.2017.08.011.

[9] W. E. Roberts and D. L. Stocum, "Part II: Temporomandibular Joint (TMJ)-Regeneration, Degeneration, and Adaptation," *Curr Osteoporos Rep,* vol. 16, no. 4, pp. 369-379, Aug 2018, doi: 10.1007/s11914-018-0462-8.

[10] X. Alomar *et al.*, "Anatomy of the temporomandibular joint," *Semin Ultrasound CT MR,* vol. 28, no. 3, pp. 170-83, Jun 2007, doi: 10.1053/j.sult.2007.02.002.

[11] S. Standring and H. Gray, *Gray's anatomy : the anatomical basis of clinical practice*, Forty-second edition / ed. Amsterdam: Elsevier, 2021, pp. xvii, 1588 pages.

[12] F. H. Netter, *Atlas of human anatomy*, Sixth edition. ed. Philadelphia, PA: Saunders/Elsevier, 2014.

[13] A. J. Thirunavukarasu *et al.*, "Temporomandibular joint anatomy: Ultrasonographic appearances and sexual dimorphism," *Clin Anat,* vol. 34, no. 7, pp. 1043-1049, Oct 2021, doi: 10.1002/ca.23719.

[14] E. Piette, "Anatomy of the human temporomandibular joint. An updated comprehensive review," *Acta Stomatol Belg,* vol. 90, no. 2, pp. 103-27, Jun 1993. [Online]. Available: https://www.ncbi.nlm.nih.gov/pubmed/8237635.

[15] A. Tuncer, "Chapter 14 - Kinesiology of the temporomandibular joint," in *Comparative Kinesiology of the Human Body*, S. Angin and I. E. Şimşek Eds.: Academic Press, 2020, pp. 285-302.

[16] X. She *et al.*, "Three-dimensional temporomandibular joint muscle attachment morphometry and its impacts on musculoskeletal modeling," *J Biomech,* vol. 79, pp. 119-128, Oct 5 2018, doi: 10.1016/j.jbiomech.2018.08.010.

[17] L. F. Rodella, B. Buffoli, M. Labanca, and R. Rezzani, "A review of the mandibular and maxillary nerve supplies and their clinical relevance," *Arch Oral Biol,* vol. 57, no. 4, pp. 323-34, Apr 2012, doi: 10.1016/j.archoralbio.2011.09.007.

[18] P. L. Westesson, L. Eriksson, and J. Liedberg, "The risk of damage to facial nerve, superficial temporal vessels, disk, and articular surfaces during arthroscopic examination of the temporomandibular joint," *Oral Surg Oral Med Oral Pathol,* vol. 62, no. 2, pp. 124-7, Aug 1986, doi: 10.1016/0030-4220(86)90028-9.

[19] S. Weinberg and B. Kryshtalskyj, "Analysis of facial and trigeminal nerve function after arthroscopic surgery of the temporomandibular joint," *J Oral Maxillofac Surg,* vol. 54, no. 1, pp. 40-3; discussion 43-4, Jan 1996, doi: 10.1016/s0278-2391(96)90301-8.

[20] A. M. Cuccia *et al.*, "The arterial blood supply of the temporomandibular joint: an anatomical study and clinical implications," *Imaging Sci Dent,* vol. 43, no. 1, pp. 37-44, Mar 2013, doi: 10.5624/isd.2013.43.1.37.

[21] M. S. Detamore *et al.*, "Cell type and distribution in the porcine temporomandibular joint disc," *J Oral Maxillofac Surg,* vol. 64, no. 2, pp. 243-8, Feb 2006, doi: 10.1016/j.joms.2005.10.009.

[22] B. K. Berkovitz and J. Pacy, "Age changes in the cells of the intra-articular disc of the temporomandibular joints of rats and marmosets," *Arch Oral Biol,* vol. 45, no. 11, pp. 987-95, Nov 2000, doi: 10.1016/s0003-9969(00)00067-4.

[23] R. Landesberg, E. Takeuchi, and J. E. Puzas, "Cellular, biochemical and molecular characterization of the bovine temporomandibular joint disc," *Arch Oral Biol,* vol. 41, no. 8-9, pp. 761-7, Aug-Sep 1996, doi: 10.1016/s0003-9969(96)00068-4.

[24] P. C. Verdonk *et al.*, "Characterisation of human knee meniscus cell phenotype," *Osteoarthritis Cartilage,* vol. 13, no. 7, pp. 548-60, Jul 2005, doi: 10.1016/j.joca.2005.01.010.

[25] D. I. Paegle, A. B. Holmlund, and F. P. Reinholt, "Characterization of tissue components in the temporomandibular joint disc and posterior disc attachment region: internal derangement and control autopsy specimens compared by morphometry," *J Oral Maxillofac Surg,* vol. 60, no. 9, pp. 1032-7, Sep 2002, doi: 10.1053/joms.2002.34416.

[26] I. Mizoguchi, N. Toriya, and Y. Nakao, "Growth of the mandible and biological characteristics of the mandibular condylar cartilage," *Japanese Dental Science Review,* vol. 49, no. 4, pp. 139-150, 2013/11/01/ 2013, doi: https://doi.org/10.1016/j.jdsr.2013.07.004.

[27] L. Wang, M. Lazebnik, and M. S. Detamore, "Hyaline cartilage cells outperform mandibular condylar cartilage cells in a TMJ fibrocartilage tissue engineering application," *Osteoarthritis Cartilage,* vol. 17, no. 3, pp. 346-53, Mar 2009, doi: 10.1016/j.joca.2008.07.004.

[28] K. Nozawa-Inoue, N. Amizuka, N. Ikeda, A. Suzuki, Y. Kawano, and T. Maeda, "Synovial membrane in the temporomandibular joint--its morphology, function and development," *Arch Histol Cytol,* vol. 66, no. 4, pp. 289-306, Oct 2003, doi: 10.1679/aohc.66.289.

[29] S. Kuroda, K. Tanimoto, T. Izawa, S. Fujihara, J. H. Koolstra, and E. Tanaka, "Biomechanical and biochemical characteristics of the mandibular condylar cartilage," *Osteoarthritis Cartilage,* vol. 17, no. 11, pp. 1408-15, Nov 2009, doi: 10.1016/j.joca.2009.04.025.

[30] J. J. Tse, "Analysis of Subchondral Bone and Microvessels Using a Novel Vascular Perfusion Contrast Agent and Optimized Dual-Energy Computed Tomography," *Electronic Thesis and Dissertation Repository. 5301,* 2018.

[31] J. Kuo, C. Shi, S. Cisewski, L. Zhang, M. J. Kern, and H. Yao, "Regional cell density distribution and oxygen consumption rates in porcine TMJ discs: an explant study," *Osteoarthritis Cartilage,* vol. 19, no. 7, pp. 911-8, Jul 2011, doi: 10.1016/j.joca.2011.03.002.

[32] L. R. Iwasaki *et al.*, "TMJ energy densities in healthy men and women," *Osteoarthritis Cartilage,* vol. 25, no. 6, pp. 846-849, Jun 2017, doi: 10.1016/j.joca.2016.12.027.

[33] K. N. Kalpakci, V. P. Willard, M. E. Wong, and K. A. Athanasiou, "An interspecies comparison of the temporomandibular joint disc," *J Dent Res,* vol. 90, no. 2, pp. 193-8, Feb 2011, doi: 10.1177/0022034510381501.

[34] A. J. Almarza, A. C. Bean, L. S. Baggett, and K. A. Athanasiou, "Biochemical analysis of the porcine temporomandibular joint disc," *Br J Oral Maxillofac Surg,* vol. 44, no. 2, pp. 124-8, Apr 2006, doi: 10.1016/j.bjoms.2005.05.002.

[35] M. S. Detamore and K. A. Athanasiou, "Structure and function of the temporomandibular joint disc: implications for tissue engineering," *J Oral Maxillofac Surg,* vol. 61, no. 4, pp. 494-506, Apr 2003, doi: 10.1053/joms.2003.50096.

[36] F. Behzadi, J. C. Mandell, S. E. Smith, and J. P. Guenette, "Temporomandibular joint imaging: current clinical applications, biochemical comparison with the intervertebral disc and knee meniscus, and opportunities for advancement," *Skeletal Radiol,* vol. 49, no. 8, pp. 1183-1193, Aug 2020, doi: 10.1007/s00256-020-03412-0.

[37] L. C. Dijkgraaf, L. G. de Bont, G. Boering, and R. S. Liem, "The structure, biochemistry, and metabolism of osteoarthritic cartilage: a review of the literature," *J Oral Maxillofac Surg,* vol. 53, no. 10, pp. 1182-92, Oct 1995, doi: 10.1016/0278-2391(95)90632-0.

[38] L. C. Dijkgraaf, L. G. De Bont, G. Boering, and R. S. Liem, "Function, biochemistry, and metabolism of the normal synovial membrane of the temporomandibular joint: a review of the literature," *J Oral Maxillofac Surg,* vol. 54, no. 1, pp. 95-100, Jan 1996, doi: 10.1016/s0278-2391(96)90313-4.

[39] V. P. Willard, B. Arzi, and K. A. Athanasiou, "The attachments of the temporomandibular joint disc: a biochemical and histological investigation," *Arch Oral Biol,* vol. 57, no. 6, pp. 599-606, Jun 2012, doi: 10.1016/j.archoralbio.2011.10.004.

[40] M. S. Detamore, J. G. Orfanos, A. J. Almarza, M. M. French, M. E. Wong, and K. A. Athanasiou, "Quantitative analysis and comparative regional investigation of the extracellular matrix of the porcine temporomandibular joint disc," *Matrix Biol,* vol. 24, no. 1, pp. 45-57, Feb 2005, doi: 10.1016/j.matbio.2004.11.006.

[41] A. K. Bag *et al.*, "Imaging of the temporomandibular joint: An update," *World J Radiol,* vol. 6, no. 8, pp. 567-82, Aug 28 2014, doi: 10.4329/wjr.v6.i8.567.

[42] S. C. Woodford, D. L. Robinson, A. Mehl, P. V. S. Lee, and D. C. Ackland, "Measurement of normal and pathological mandibular and temporomandibular joint kinematics: A systematic review," *J Biomech,* vol. 111, p. 109994, Oct 9 2020, doi: 10.1016/j.jbiomech.2020.109994.

[43] S. E. Nishi, R. Basri, and M. K. Alam, "Uses of electromyography in dentistry: An overview with meta-analysis," (in eng), no. 1305-7456 (Print).

[44] K. Hiraba, K. Hibino K Fau - Hiranuma, T. Hiranuma K Fau - Negoro, and T. Negoro, "EMG activities of two heads of the human lateral pterygoid muscle in relation to mandibular condyle movement and biting force," (in eng), no. 0022-3077 (Print).

[45] in *Temporomandibular Disorders: Priorities for Research and Care*, O. Yost, C. T. Liverman, R. English, S. Mackey, and E. C. Bond Eds., (The National Academies Collection: Reports funded by National Institutes of Health. Washington (DC), 2020.

[46] A. Matsumoto, R. M. Celar, A. Celar, S. Sato, Y. Suzuki, and R. Slavicek, "An analysis of hinge axis translation and rotation during opening and closing in dentulous and edentulous subjects," *Cranio,* vol. 13, no. 4, pp. 238-41, Oct 1995, doi: 10.1080/08869634.1995.11682215.

[47] R. P. Lewis, P. H. Buschang, and G. S. Throckmorton, "Sex differences in mandibular movements during opening and closing," *Am J Orthod Dentofacial Orthop,* vol. 120, no. 3, pp. 294-303, Sep 2001, doi: 10.1067/mod.2001.115612.

[48] K. H. Travers, P. H. Buschang, H. Hayasaki, and G. S. Throckmorton, "Associations between incisor and mandibular condylar movements during maximum mouth opening in humans," *Archives of Oral Biology,* vol. 45, no. 4, pp. 267-275, 2000/04/01/ 2000, doi: https://doi.org/10.1016/S0003-9969(99)00140-5.

[49] L. M. Gallo, "Modeling of temporomandibular joint function using MRI and jaw-tracking technologies--mechanics," *Cells Tissues Organs,* vol. 180, no. 1, pp. 54-68, 2005, doi: 10.1159/000086199.

[50] J. C. Nickel, L. R. Iwasaki, L. M. Gallo, S. Palla, and D. B. Marx, "Tractional Forces, Work and Energy Densities in the Human TMJ," *Craniofac Growth Ser,* vol. 46, pp. 427-450, Mar 2009. [Online]. Available: https://www.ncbi.nlm.nih.gov/pubmed/26549916.

[51] L. R. Iwasaki *et al.*, "Temporomandibular joint loads in subjects with and without disc displacement," *Orthop Rev (Pavia),* vol. 1, no. 2, pp. 90-93, 2009, doi: 10.4081/or.2009.e29.

[52] S. Palla, L. M. Gallo, and D. Gossi, "Dynamic stereometry of the temporomandibular joint," *Orthod Craniofac Res,* vol. 6 Suppl 1, pp. 37-47, 2003, doi: 10.1034/j.1600-0544.2003.233.x.

[53] N. Celebi *et al.*, "Development of a mandibular motion simulator for total joint replacement," *J Oral Maxillofac Surg,* vol. 69, no. 1, pp. 66-79, Jan 2011, doi: 10.1016/j.joms.2010.05.085.

[54] J. J. Huddleston Slater, F. Visscher Cm Fau - Lobbezoo, M. Lobbezoo F Fau - Naeije, and M. Naeije, "The intra-articular distance within the TMJ during free and loaded closing movements," (in eng), no. 0022-0345 (Print).

[55] M. Beek, M. P. Aarnts, J. H. Koolstra, A. J. Feilzer, and T. M. van Eijden, "Dynamic properties of the human temporomandibular joint disc," *J Dent Res,* vol. 80, no. 3, pp. 876-80, Mar 2001, doi: 10.1177/00220345010800030601.

[56] E. Barrientos, F. Pelayo, E. Tanaka, M. J. Lamela-Rey, and A. Fernandez-Canteli, "Dynamic and stress relaxation properties of the whole porcine temporomandibular joint disc under compression," *J Mech Behav Biomed Mater,* vol. 57, pp. 109-15, Apr 2016, doi: 10.1016/j.jmbbm.2015.12.003.

[57] M. Singh and M. S. Detamore, "Tensile properties of the mandibular condylar cartilage," *J Biomech Eng,* vol. 130, no. 1, p. 011009, Feb 2008, doi: 10.1115/1.2838062.

[58] M. K. Murphy, B. Arzi, J. C. Hu, and K. A. Athanasiou, "Tensile characterization of porcine temporomandibular joint disc attachments," *J Dent Res,* vol. 92, no. 8, pp. 753-8, Aug 2013, doi: 10.1177/0022034513494817.

[59] G. J. Wright *et al.*, "Tensile biomechanical properties of human temporomandibular joint disc: Effects of direction, region and sex," *J Biomech,* vol. 49, no. 16, pp. 3762-3769, Dec 8 2016, doi: 10.1016/j.jbiomech.2016.09.033.
[60] J. Middendorf, S. Albahrani, and L. J. Bonassar, "Stribeck Curve Analysis of Temporomandibular Joint Condylar Cartilage and Disc," *J Biomech Eng,* Mar 1 2019, doi: 10.1115/1.4045283.
[61] K. M. Labus, J. P. Kuiper, J. Rawlinson, and C. M. Puttlitz, "Mechanical characterization and viscoelastic model of the ovine temporomandibular joint Disc in indentation, uniaxial tension, and biaxial tension," *J Mech Behav Biomed Mater,* vol. 116, p. 104300, Apr 2021, doi: 10.1016/j.jmbbm.2020.104300.
[62] N. Vapniarsky, A. Aryaei, B. Arzi, D. C. Hatcher, J. C. Hu, and K. A. Athanasiou, "The Yucatan Minipig Temporomandibular Joint Disc Structure-Function Relationships Support Its Suitability for Human Comparative Studies," *Tissue Eng Part C Methods,* vol. 23, no. 11, pp. 700-709, Nov 2017, doi: 10.1089/ten.TEC.2017.0149.
[63] H. Kang, G. J. Bao, and S. N. Qi, "Biomechanical responses of human temporomandibular joint disc under tension and compression," *Int J Oral Maxillofac Surg,* vol. 35, no. 9, pp. 817-21, Sep 2006, doi: 10.1016/j.ijom.2006.03.005.
[64] S. Gutman, D. Kim, S. Tarafder, S. Velez, J. Jeong, and C. H. Lee, "Regionally variant collagen alignment correlates with viscoelastic properties of the disc of the human temporomandibular joint," *Arch Oral Biol,* vol. 86, pp. 1-6, Feb 2018, doi: 10.1016/j.archoralbio.2017.11.002.
[65] K. D. Allen and K. A. Athanasiou, "Viscoelastic characterization of the porcine temporomandibular joint disc under unconfined compression," *J Biomech,* vol. 39, no. 2, pp. 312-22, 2006, doi: 10.1016/j.jbiomech.2004.11.012.
[66] M. J. Lamela, Y. Prado, P. Fernández, A. Fernández-Canteli, and E. Tanaka, "Non-linear Viscoelastic Model for Behaviour Characterization of Temporomandibular Joint Discs," *Experimental Mechanics,* vol. 51, no. 8, pp. 1435-1440, 2011/10/01 2011, doi: 10.1007/s11340-011-9465-4.
[67] E. Tanaka, M. S. Detamore, K. Tanimoto, and N. Kawai, "Lubrication of the Temporomandibular Joint," *Annals of Biomedical Engineering,* vol. 36, no. 1, pp. 14-29, 2008/01/01 2008, doi: 10.1007/s10439-007-9401-z.
[68] B. K. Zimmerman *et al.*, "Role of interstitial fluid pressurization in TMJ lubrication," *J Dent Res,* vol. 94, no. 1, pp. 85-92, Jan 2015, doi: 10.1177/0022034514553626.
[69] E. Tanaka *et al.*, "The effect of removal of the disc on the friction in the temporomandibular joint," *J Oral Maxillofac Surg,* vol. 64, no. 8, pp. 1221-4, Aug 2006, doi: 10.1016/j.joms.2006.04.017.
[70] E. Tanaka *et al.*, "The frictional coefficient of the temporomandibular joint and its dependency on the magnitude and duration of joint loading," *J Dent Res,* vol. 83, no. 5, pp. 404-7, May 2004, doi: 10.1177/154405910408300510.
[71] H. Forster and J. Fisher, "The influence of continuous sliding and subsequent surface wear on the friction of articular cartilage," *Proc Inst Mech Eng H,* vol. 213, no. 4, pp. 329-45, 1999, doi: 10.1243/0954411991535167.
[72] J. Katta, Z. Jin, E. Ingham, and J. Fisher, "Biotribology of articular cartilage--a review of the recent advances," *Med Eng Phys,* vol. 30, no. 10, pp. 1349-63, Dec 2008, doi: 10.1016/j.medengphy.2008.09.004.

[73] P. Fernandez, M. Jesus Lamela, A. Ramos, A. Fernandez-Canteli, and E. Tanaka, "The region-dependent dynamic properties of porcine temporomandibular joint disc under unconfined compression," *J Biomech,* vol. 46, no. 4, pp. 845-8, Feb 22 2013, doi: 10.1016/j.jbiomech.2012.11.035.

[74] L. K. Tappert, A. Baldit, R. Rahouadj, and P. Lipinski, "Local elastic properties characterization of the temporo-mandibular joint disc through macro-indentation," *Comput Methods Biomech Biomed Engin,* vol. 20, no. sup1, pp. 201-202, Oct 2017, doi: 10.1080/10255842.2017.1382932.

[75] M. Singh and M. S. Detamore, "Biomechanical properties of the mandibular condylar cartilage and their relevance to the TMJ disc," *J Biomech,* vol. 42, no. 4, pp. 405-17, Mar 11 2009, doi: 10.1016/j.jbiomech.2008.12.012.

[76] L. Ruggiero *et al.*, "Roles of the Fibrous Superficial Zone in the Mechanical Behavior of TMJ Condylar Cartilage," *Ann Biomed Eng,* vol. 43, no. 11, pp. 2652-62, Nov 2015, doi: 10.1007/s10439-015-1320-9.

[77] P. Chandrasekaran *et al.*, "Biomechanical properties of murine TMJ articular disc and condyle cartilage via AFM-nanoindentation," *J Biomech,* vol. 60, pp. 134-141, Jul 26 2017, doi: 10.1016/j.jbiomech.2017.06.031.

[78] F. Ben Amor, P. Carpentier, J. M. Foucart, and A. Meunier, "Anatomic and mechanical properties of the lateral disc attachment of the temporomandibular joint," *J Oral Maxillofac Surg,* vol. 56, no. 10, pp. 1164-7; discussion 1168-9, Oct 1998, doi: 10.1016/s0278-2391(98)90763-7.

[79] X. D. Wang, J. N. Zhang, Y. H. Gan, and Y. H. Zhou, "Current understanding of pathogenesis and treatment of TMJ osteoarthritis," *J Dent Res,* vol. 94, no. 5, pp. 666-73, May 2015, doi: 10.1177/0022034515574770.

[80] E. Tanaka, M. S. Detamore, and L. G. Mercuri, "Degenerative disorders of the temporomandibular joint: etiology, diagnosis, and treatment," *J Dent Res,* vol. 87, no. 4, pp. 296-307, Apr 2008, doi: 10.1177/154405910808700406.

[81] J. Palmer and J. Durham, "Temporomandibular disorders," *BJA Educ,* vol. 21, no. 2, pp. 44-50, Feb 2021, doi: 10.1016/j.bjae.2020.11.001.

[82] H.-S. Roh, W. Kim, Y.-K. Kim, and J.-Y. Lee, "Relationships between disk displacement, joint effusion, and degenerative changes of the TMJ in TMD patients based on MRI findings," *Journal of Cranio-Maxillofacial Surgery,* vol. 40, no. 3, pp. 283-286, 2012/04/01/ 2012, doi: https://doi.org/10.1016/j.jcms.2011.04.006.

[83] R. B. Ross, "Developmental anomalies of the temporomandibular joint," *J Orofac Pain,* vol. 13, no. 4, pp. 262-72, Fall 1999. [Online]. Available: https://www.ncbi.nlm.nih.gov/pubmed/10823040.

[84] B. Stegenga, "Nomenclature and classification of temporomandibular joint disorders," *J Oral Rehabil,* vol. 37, no. 10, pp. 760-5, Oct 2010, doi: 10.1111/j.1365-2842.2010.02146.x.

[85] H. Sale and A. Isberg, "Delayed temporomandibular joint pain and dysfunction induced by whiplash trauma: a controlled prospective study," *J Am Dent Assoc,* vol. 138, no. 8, pp. 1084-91, Aug 2007, doi: 10.14219/jada.archive.2007.0320.

[86] E. Yucel, U. Borkan, N. Mollaoglu, E. Erkmen, and O. Gunhan, "Histological evaluation of changes in the temporomandibular joint after direct and indirect trauma: an experimental study," *Dent Traumatol,* vol. 18, no. 4, pp. 212-6, Aug 2002, doi: 10.1034/j.1600-9657.2001.00088.x.

[87] T. List and R. H. Jensen, "Temporomandibular disorders: Old ideas and new concepts," *Cephalalgia,* vol. 37, no. 7, pp. 692-704, Jun 2017, doi: 10.1177/0333102416686302.
[88] A. Sójka, B. Stelcer, M. A.-O. Roy, E. Mojs, and M. Pryliński, "Is there a relationship between psychological factors and TMD?," (in eng), no. 2162-3279 (Electronic).
[89] C. G. da Silva *et al.*, "Prevalence of clinical signs of intra-articular temporomandibular disorders in children and adolescents: A systematic review and meta-analysis," *J Am Dent Assoc,* vol. 147, no. 1, pp. 10-18 e8, Jan 2016, doi: 10.1016/j.adaj.2015.07.017.
[90] G. D. Slade *et al.*, "Summary of findings from the OPPERA prospective cohort study of incidence of first-onset temporomandibular disorder: implications and future directions," *J Pain,* vol. 14, no. 12 Suppl, pp. T116-24, Dec 2013, doi: 10.1016/j.jpain.2013.09.010.
[91] G. Slade and J. Durham, "Prevalence, impact, and costs of treatment for temporomandibular disorders.," Committee on Temporomandibular Disorders (TMDs): From Research Discoveries to Clinical Treatment, 2020.
[92] A. M. Velly *et al.*, "The effect of catastrophizing and depression on chronic pain--a prospective cohort study of temporomandibular muscle and joint pain disorders," *Pain,* vol. 152, no. 10, pp. 2377-2383, Oct 2011, doi: 10.1016/j.pain.2011.07.004.
[93] B. J. Bielajew *et al.*, "Knee orthopedics as a template for the temporomandibular joint," *Cell Rep Med,* vol. 2, no. 5, p. 100241, May 18 2021, doi: 10.1016/j.xcrm.2021.100241.
[94] D. M. Laskin, "Putting order into temporomandibular disorders," (in eng), no. 0278-2391 (Print).
[95] G. Dimitroulis, "Management of temporomandibular joint disorders: A surgeon's perspective," *Aust Dent J,* vol. 63 Suppl 1, pp. S79-S90, Mar 2018, doi: 10.1111/adj.12593.
[96] G. Dimitroulis, "Temporomandibular disorders: a clinical update," *BMJ,* vol. 317, no. 7152, pp. 190-4, Jul 18 1998, doi: 10.1136/bmj.317.7152.190.
[97] K. Herb, S. Cho, and M. A. Stiles, "Temporomandibular joint pain and dysfunction," *Curr Pain Headache Rep,* vol. 10, no. 6, pp. 408-14, Dec 2006, doi: 10.1007/s11916-006-0070-7.
[98] M. Kalladka, A. Young, and J. Khan, "Myofascial pain in temporomandibular disorders: Updates on etiopathogenesis and management," *J Bodyw Mov Ther,* vol. 28, pp. 104-113, Oct 2021, doi: 10.1016/j.jbmt.2021.07.015.
[99] D. Manfredini, L. Guarda-Nardini, E. Winocur, F. Piccotti, J. Ahlberg, and F. Lobbezoo, "Research diagnostic criteria for temporomandibular disorders: a systematic review of axis I epidemiologic findings," *Oral Surg Oral Med Oral Pathol Oral Radiol Endod,* vol. 112, no. 4, pp. 453-62, Oct 2011, doi: 10.1016/j.tripleo.2011.04.021.
[100] M. Miernik and W. Więckiewicz, "The Basic Conservative Treatment of Temporomandibular Joint Anterior Disc Displacement Without Reduction--Review," (in eng), no. 1899-5276 (Print).
[101] A. L. Young, "Internal derangements of the temporomandibular joint: A review of the anatomy, diagnosis, and management," *J Indian Prosthodont Soc,* vol. 15, no. 1, pp. 2-7, Jan-Mar 2015, doi: 10.4103/0972-4052.156998.
[102] S. Barkin and S. Weinberg, "Internal derangements of the temporomandibular joint: the role of arthroscopic surgery and arthrocentesis," *J Can Dent Assoc,* vol. 66, no. 4, pp. 199-203, Apr 2000. [Online]. Available: https://www.ncbi.nlm.nih.gov/pubmed/10789172.
[103] R. W. Katzberg, P. L. Westesson, R. H. Tallents, and C. M. Drake, "Anatomic disorders of the temporomandibular joint disc in asymptomatic subjects," *J Oral Maxillofac Surg,* vol. 54, no. 2, pp. 147-53; discussion 153-5, Feb 1996, doi: 10.1016/s0278-2391(96)90435-8.

[104] C. H. Wilkes, "Internal derangements of the temporomandibular joint. Pathological variations," *Northwest Dent,* vol. 69, no. 2, pp. 25-32, Mar-Apr 1990. [Online]. Available: https://www.ncbi.nlm.nih.gov/pubmed/2381794.

[105] G. Dimitroulis, "A new surgical classification for temporomandibular joint disorders," *Int J Oral Maxillofac Surg,* vol. 42, no. 2, pp. 218-22, Feb 2013, doi: 10.1016/j.ijom.2012.11.004.

[106] A. F. Hegab, H. I. Al Hameed, and K. S. Karam, "Classification of temporomandibular joint internal derangement based on magnetic resonance imaging and clinical findings of 435 patients contributing to a nonsurgical treatment protocol," *Sci Rep,* vol. 11, no. 1, p. 20917, Oct 22 2021, doi: 10.1038/s41598-021-00456-7.

[107] J. Nyberg, R. Adell, and B. Svensson, "Temporomandibular joint discectomy for treatment of unilateral internal derangements--a 5 year follow-up evaluation," *Int J Oral Maxillofac Surg,* vol. 33, no. 1, pp. 8-12, Jan 2004, doi: 10.1054/ijom.2002.0453.

[108] S. J. McKenna, "Discectomy for the treatment of internal derangements of the temporomandibular joint," *J Oral Maxillofac Surg,* vol. 59, no. 9, pp. 1051-6, Sep 2001, doi: 10.1053/joms.2001.26682.

[109] E. F. Wright and G. D. Klasser, *Manual of temporomandibular disorders*, Fourth edition. ed. Hoboken, NJ: Wiley-Blackwell, 2020, p. pages cm.

[110] R. Schiffman E Fau - Ohrbach *et al.*, "Diagnostic Criteria for Temporomandibular Disorders (DC/TMD) for Clinical and Research Applications: recommendations of the International RDC/TMD Consortium Network* and Orofacial Pain Special Interest Group†," (in eng), no. 2333-0384 (Print).

[111] R. M. Rodhen, T. A. de Holanda, F. J. Barbon, W. L. de Oliveira da Rosa, and N. Boscato, "Invasive surgical procedures for the management of internal derangement of the temporomandibular joint: a systematic review and meta-analysis regarding the effects on pain and jaw mobility," *Clin Oral Investig,* vol. 26, no. 4, pp. 3429-3446, Apr 2022, doi: 10.1007/s00784-022-04428-7.

[112] M. Miernik and W. Wieckiewicz, "The Basic Conservative Treatment of Temporomandibular Joint Anterior Disc Displacement Without Reduction--Review," *Adv Clin Exp Med,* vol. 24, no. 4, pp. 731-5, Jul-Aug 2015, doi: 10.17219/acem/35165.

[113] H. A. Israel, J. D. Ward, B. Horrell, and S. J. Scrivani, "Oral and maxillofacial surgery in patients with chronic orofacial pain," *J Oral Maxillofac Surg,* vol. 61, no. 6, pp. 662-7, Jun 2003, doi: 10.1053/joms.2003.50133.

[114] R. L. Gauer and M. J. Semidey, "Diagnosis and treatment of temporomandibular disorders," (in eng), no. 1532-0650 (Electronic).

[115] S. Ghurye and R. McMillan, "Pain-Related Temporomandibular Disorder - Current Perspectives and Evidence-Based Management," *Dent Update,* vol. 42, no. 6, pp. 533-6, 539-42, 545-6, Jul-Aug 2015, doi: 10.12968/denu.2015.42.6.533.

[116] O. Breik, V. Devrukhkar, and G. Dimitroulis, "Temporomandibular joint (TMJ) arthroscopic lysis and lavage: Outcomes and rate of progression to open surgery," *J Craniomaxillofac Surg,* vol. 44, no. 12, pp. 1988-1995, Dec 2016, doi: 10.1016/j.jcms.2016.09.017.

[117] A. Ouanounou, M. Goldberg, and D. A. Haas, "Pharmacotherapy in Temporomandibular Disorders: A Review," *J Can Dent Assoc,* vol. 83, p. h7, Jul 2017. [Online]. Available: https://www.ncbi.nlm.nih.gov/pubmed/29513209.

[118] T. Haketa, K. Kino, M. Sugisaki, M. Takaoka, and T. Ohta, "Randomized clinical trial of treatment for TMJ disc displacement," *J Dent Res,* vol. 89, no. 11, pp. 1259-63, Nov 2010, doi: 10.1177/0022034510378424.

[119] M. L. McNeely, S. Armijo Olivo, and D. J. Magee, "A systematic review of the effectiveness of physical therapy interventions for temporomandibular disorders," *Phys Ther,* vol. 86, no. 5, pp. 710-25, May 2006. [Online]. Available: https://www.ncbi.nlm.nih.gov/pubmed/16649894.

[120] Z. Al-Ani, R. J. Gray, S. J. Davies, P. Sloan, and A. M. Glenny, "Stabilization splint therapy for the treatment of temporomandibular myofascial pain: a systematic review," *J Dent Educ,* vol. 69, no. 11, pp. 1242-50, Nov 2005. [Online]. Available: https://www.ncbi.nlm.nih.gov/pubmed/16275687.

[121] N. Christidis, E. Lindström Ndanshau, A. Sandberg, and G. Tsilingaridis, "Prevalence and treatment strategies regarding temporomandibular disorders in children and adolescents—A systematic review," *Journal of Oral Rehabilitation,* https://doi.org/10.1111/joor.12759 vol. 46, no. 3, pp. 291-301, 2019/03/01 2019, doi: https://doi.org/10.1111/joor.12759.

[122] B. E. Cairns, "Pathophysiology of TMD pain--basic mechanisms and their implications for pharmacotherapy," *J Oral Rehabil,* vol. 37, no. 6, pp. 391-410, May 2010, doi: 10.1111/j.1365-2842.2010.02074.x.

[123] A. Alqutaibi and A. Aboalrejal, "Types of occlusal splint in management of temporomandibular disorders (TMD)," *J Arthritis,* vol. 4, no. 176, p. 2, 2015.

[124] C. Zhang *et al.*, "Efficacy of splint therapy for the management of temporomandibular disorders: a meta-analysis," *Oncotarget,* vol. 7, no. 51, pp. 84043-84053, Dec 20 2016, doi: 10.18632/oncotarget.13059.

[125] E. A. Al-Moraissi, R. Farea, K. A. Qasem, M. S. Al-Wadeai, M. E. Al-Sabahi, and G. M. Al-Iryani, "Effectiveness of occlusal splint therapy in the management of temporomandibular disorders: network meta-analysis of randomized controlled trials," *Int J Oral Maxillofac Surg,* vol. 49, no. 8, pp. 1042-1056, Aug 2020, doi: 10.1016/j.ijom.2020.01.004.

[126] M. Eliassen, C. Hjortsjo, H. Olsen-Bergem, and T. Bjornland, "Self-exercise programmes and occlusal splints in the treatment of TMD-related myalgia-Evidence-based medicine?," *J Oral Rehabil,* vol. 46, no. 11, pp. 1088-1094, Nov 2019, doi: 10.1111/joor.12856.

[127] K. Murakami, "Current role of arthrocentesis, arthroscopy and open surgery for temporomandibular joint internal derangement with inflammatory/degenerative disease; -pitfalls and pearls," *Journal of Oral and Maxillofacial Surgery, Medicine, and Pathology,* vol. 34, no. 1, pp. 1-11, 2022/01/01/ 2022, doi: https://doi.org/10.1016/j.ajoms.2021.06.009.

[128] M. Bengtsson and P. Fransson, "Do patient-reported outcome measures correlate with clinical follow-up after arthroscopic treatment of internal derangement of the temporomandibular joint?," (in eng), no. 2468-7855 (Electronic).

[129] I. Q. Gutierrez, H. Sabado-Bundo, and C. Gay-Escoda, "Intraarticular injections of platelet rich plasma and plasma rich in growth factors with arthrocenthesis or arthroscopy in the treatment of temporomandibular joint disorders: A systematic review," *J Stomatol Oral Maxillofac Surg,* Dec 11 2021, doi: 10.1016/j.jormas.2021.12.006.

[130] H. Sàbado-Bundó, M. Sánchez-Garcés, O. Camps-Font, and C. Gay-Escoda, "Intraarticular injections of hyaluronic acid in arthrocentesis and arthroscopy as a treatment of

temporomandibular joint disorders: A systematic review," (in eng), no. 2151-0903 (Electronic).

[131] T. S. Santos, L. E. C. Pagotto, E. Santos Nascimento, L. Rezende da Cunha, D. Serra Cassano, and J. R. Goncalves, "Effectiveness of disk repositioning and suturing comparing open-joint versus arthroscopic techniques: a systematic review and meta-analysis," *Oral Surg Oral Med Oral Pathol Oral Radiol,* vol. 132, no. 5, pp. 506-513, Nov 2021, doi: 10.1016/j.oooo.2021.02.015.

[132] S. Abramowicz and M. F. Dolwick, "20-year follow-up study of disc repositioning surgery for temporomandibular joint internal derangement," *J Oral Maxillofac Surg,* vol. 68, no. 2, pp. 239-42, Feb 2010, doi: 10.1016/j.joms.2009.09.051.

[133] S. Zhang *et al.*, "Temporomandibular joint disc repositioning using bone anchors: an immediate post surgical evaluation by Magnetic Resonance Imaging," *BMC Musculoskeletal Disorders,* vol. 11, no. 1, p. 262, 2010/11/12 2010, doi: 10.1186/1471-2474-11-262.

[134] J. P. McCain, R. H. Hossameldin, S. Srouji, and A. Maher, "Arthroscopic Discopexy Is Effective in Managing Temporomandibular Joint Internal Derangement in Patients With Wilkes Stage II and III," *Journal of Oral and Maxillofacial Surgery,* vol. 73, no. 3, pp. 391-401, 2015/03/01/ 2015, doi: https://doi.org/10.1016/j.joms.2014.09.004.

[135] J. R. Gonçalves, D. S. Cassano, L. Rezende, and L. M. Wolford, "Disc repositioning: does it really work?," *Oral and Maxillofacial Surgery Clinics,* vol. 27, no. 1, pp. 85-107, 2015.

[136] R. Curry Jt Fau - Alexander, C. Alexander R Fau - Walker, T. Walker C Fau - Goksel, and T. Goksel, "Discectomy as the primary surgical option for internal derangement of the temporomandibular joint," (in eng), no. 1531-5053 (Electronic).

[137] M. DeMerle, O. O. Nafiu, and S. Aronovich, "Temporomandibular Joint Discectomy With Abdominal Fat Graft Versus Temporalis Myofascial Flap: A Comparative Study," *J Oral Maxillofac Surg,* vol. 75, no. 6, pp. 1137-1143, Jun 2017, doi: 10.1016/j.joms.2016.11.028.

[138] D. F. Ângelo, D. Sanz, and H. J. Cardoso, "Unilateral temporomandibular joint discectomy without interposal material in patients with disc perforation or fragmentation: A prospective study," *Journal of Oral and Maxillofacial Surgery, Medicine, and Pathology,* vol. 34, no. 4, pp. 375-380, 2022/07/01/ 2022, doi: https://doi.org/10.1016/j.ajoms.2021.12.005.

[139] G. Dimitroulis, "A critical review of interpositional grafts following temporomandibular joint discectomy with an overview of the dermis-fat graft," *Int J Oral Maxillofac Surg,* vol. 40, no. 6, pp. 561-8, Jun 2011, doi: 10.1016/j.ijom.2010.11.020.

[140] H. Miyamoto, K. Kurita, N. Ogi, J. I. Ishimaru, and A. N. Goss, "The role of the disk in sheep temporomandibular joint ankylosis," *Oral Surg Oral Med Oral Pathol Oral Radiol Endod,* vol. 88, no. 2, pp. 151-8, Aug 1999, doi: 10.1016/s1079-2104(99)70109-5.

[141] N. De Meurechy and M. Y. Mommaerts, "Alloplastic temporomandibular joint replacement systems: a systematic review of their history," *Int J Oral Maxillofac Surg,* vol. 47, no. 6, pp. 743-754, Jun 2018, doi: 10.1016/j.ijom.2018.01.014.

[142] O. G. Ellis, S. Tocaciu, D. P. McKenzie, M. J. McCullough, and G. Dimitroulis, "Risk Factors Associated With Poor Outcomes Following Temporomandibular Joint Discectomy and Fat Graft," *J Oral Maxillofac Surg,* vol. 79, no. 12, pp. 2448-2454, Dec 2021, doi: 10.1016/j.joms.2021.05.018.

[143] W. Minston *et al.*, "Pre-surgical radiographic and clinical features as predictors for temporomandibular joint discectomy prognosis," *Oral Dis,* May 25 2021, doi: 10.1111/odi.13923.
[144] L. G. Mercuri, "Considering total temporomandibular joint replacement," *Cranio,* vol. 17, no. 1, pp. 44-8, Jan 1999, doi: 10.1080/08869634.1999.11746076.
[145] T. Yoda *et al.*, "Clinical guidelines for total temporomandibular joint replacement," *Jpn Dent Sci Rev,* vol. 56, no. 1, pp. 77-83, Nov 2020, doi: 10.1016/j.jdsr.2020.03.001.
[146] E. Bach, N. Sigaux, M. Fauvernier, and A. S. Cousin, "Reasons for failure of total temporomandibular joint replacement: a systematic review and meta-analysis," *Int J Oral Maxillofac Surg,* vol. 51, no. 8, pp. 1059-1068, Aug 2022, doi: 10.1016/j.ijom.2021.12.012.
[147] S. W. Herring, "TMJ anatomy and animal models," *J Musculoskelet Neuronal Interact,* vol. 3, no. 4, pp. 391-4; discussion 406-7, Dec 2003. [Online]. Available: https://www.ncbi.nlm.nih.gov/pubmed/15758330.
[148] Y. Zhao *et al.*, "Animal Models of Temporomandibular Joint Osteoarthritis: Classification and Selection," *Front Physiol,* vol. 13, p. 859517, 2022, doi: 10.3389/fphys.2022.859517.
[149] M. A. Martinez-Garcia, B. C. Miguelanez-Medran, and C. Goicoechea, "Animal models in the study and treatment of orofacial pain," *J Clin Exp Dent,* vol. 11, no. 4, pp. e382-e390, Apr 2019, doi: 10.4317/jced.55429.
[150] A. Suzuki and J. Iwata, "Mouse genetic models for temporomandibular joint development and disorders," *Oral Dis,* vol. 22, no. 1, pp. 33-8, Jan 2016, doi: 10.1111/odi.12353.
[151] F. E. Artuzi *et al.*, "Rabbit model for osteoarthrosis of the temporomandibular joint as a basis for assessment of outcomes after intervention," *Br J Oral Maxillofac Surg,* vol. 54, no. 5, pp. e33-7, Jun 2016, doi: 10.1016/j.bjoms.2016.01.022.
[152] M. C. Embree *et al.*, "Soft tissue ossification and condylar cartilage degeneration following TMJ disc perforation in a rabbit pilot study," *Osteoarthritis Cartilage,* vol. 23, no. 4, pp. 629-39, Apr 2015, doi: 10.1016/j.joca.2014.12.015.
[153] F. Bryndahl, G. Warfvinge, L. Eriksson, and A. Isberg, "Cartilage changes link retrognathic mandibular growth to TMJ disc displacement in a rabbit model," *Int J Oral Maxillofac Surg,* vol. 40, no. 6, pp. 621-7, Jun 2011, doi: 10.1016/j.ijom.2011.01.004.
[154] N. H. Dormer, K. Busaidy, C. J. Berkland, and M. S. Detamore, "Osteochondral interface regeneration of rabbit mandibular condyle with bioactive signal gradients," *J Oral Maxillofac Surg,* vol. 69, no. 6, pp. e50-7, Jun 2011, doi: 10.1016/j.joms.2010.12.049.
[155] R. Dantuma and W. A. Weijs, "Functional Anatomy of the Masticatory Apparatus in the Rabbit (Oryctolagus Cuniculus L.)," (in English), *Netherlands Journal of Zoology,* vol. 31, no. 1, pp. 99-147, 01 Jan. 1980 1980, doi: https://doi.org/10.1163/002829680X00212.
[156] R. P. Donahue, J. C. Hu, and K. A. Athanasiou, "Remaining Hurdles for Tissue-Engineering the Temporomandibular Joint Disc," *Trends Mol Med,* vol. 25, no. 3, pp. 241-256, Mar 2019, doi: 10.1016/j.molmed.2018.12.007.
[157] J. D. Lee, J. I. Becker, L. M. Larkin, A. J. Almarza, and S. D. Kapila, "Morphologic and histologic characterization of sheep and porcine TMJ as large animal models for tissue engineering applications," *Clin Oral Investig,* vol. 26, no. 7, pp. 5019-5027, Jul 2022, doi: 10.1007/s00784-022-04472-3.
[158] A. J. Almarza *et al.*, "Preclinical Animal Models for Temporomandibular Joint Tissue Engineering," *Tissue Eng Part B Rev,* vol. 24, no. 3, pp. 171-178, Jun 2018, doi: 10.1089/ten.TEB.2017.0341.

[159] A. Bermejo, O. González, and J. M. González, "The pig as an animal model for experimentation on the temporomandibular articular complex," *Oral Surgery, Oral Medicine, Oral Pathology,* vol. 75, no. 1, pp. 18-23, 1993/01/01/ 1993, doi: https://doi.org/10.1016/0030-4220(93)90399-O.
[160] S. G. Cone, P. B. Warren, and M. B. Fisher, "Rise of the Pigs: Utilization of the Porcine Model to Study Musculoskeletal Biomechanics and Tissue Engineering During Skeletal Growth," *Tissue Eng Part C Methods,* vol. 23, no. 11, pp. 763-780, Nov 2017, doi: 10.1089/ten.TEC.2017.0227.
[161] J. C. Nickel, L. R. Iwasaki, M. W. Beatty, and D. B. Marx, "Tractional forces on porcine temporomandibular joint discs," *J Dent Res,* vol. 88, no. 8, pp. 736-40, Aug 2009, doi: 10.1177/0022034509340161.
[162] M. S. Detamore and K. A. Athanasiou, "Tensile properties of the porcine temporomandibular joint disc," *J Biomech Eng,* vol. 125, no. 4, pp. 558-65, Aug 2003, doi: 10.1115/1.1589778.
[163] C. M. Juran, M. F. Dolwick, and P. S. McFetridge, "Shear mechanics of the TMJ disc: relationship to common clinical observations," *J Dent Res,* vol. 92, no. 2, pp. 193-8, Feb 2013, doi: 10.1177/0022034512468749.
[164] S. W. Herring, J. D. Decker, Z. J. Liu, and T. Ma, "Temporomandibular joint in miniature pigs: anatomy, cell replication, and relation to loading," *Anat Rec,* vol. 266, no. 3, pp. 152-66, Mar 1 2002, doi: 10.1002/ar.10049.
[165] L. Wang and M. S. Detamore, "Effects of growth factors and glucosamine on porcine mandibular condylar cartilage cells and hyaline cartilage cells for tissue engineering applications," *Arch Oral Biol,* vol. 54, no. 1, pp. 1-5, Jan 2009, doi: 10.1016/j.archoralbio.2008.06.002.
[166] M. S. Detamore and K. A. Athanasiou, "Evaluation of three growth factors for TMJ disc tissue engineering," *Ann Biomed Eng,* vol. 33, no. 3, pp. 383-90, Mar 2005, doi: 10.1007/s10439-005-1741-y.
[167] W. M. H. Kaduk, H. R. Metelmann, and K. K. H. Gundlach, "[Development, standardisation and evaluation of a model for arthroscopic surgery of the joint. An experimental study in pigs]," (in ger), *Mund Kiefer Gesichtschir,* vol. 7, no. 4, pp. 235-240, 2003/07// 2003, doi: 10.1007/s10006-003-0488-6.
[168] J. Štembírek, M. Kyllar, I. Putnová, L. Stehlík, and M. Buchtová, "The pig as an experimental model for clinical craniofacial research," *Laboratory Animals,* vol. 46, no. 4, pp. 269-279, 2012/10/01 2012, doi: 10.1258/la.2012.012062.
[169] B. N. Brown *et al.*, "Inductive Remodeling of Extracellular Matrix Scaffolds in the Temporomandibular Joint of Pigs," *Tissue Eng Part A,* vol. 28, no. 9-10, pp. 447-457, May 2022, doi: 10.1089/ten.TEA.2021.0123.
[170] J. Liang *et al.*, "Acellular matrix hydrogel for repair of the temporomandibular joint disc," *J Biomed Mater Res B Appl Biomater,* vol. 108, no. 7, pp. 2995-3007, Oct 2020, doi: 10.1002/jbm.b.34629.
[171] D. Chen, "Regenerative Engineering of the Temporomandibular Joint in a Porcine Model," Ph.D., Columbia University, Ann Arbor, 28265123, 2021. [Online]. Available: https://ezproxy2.library.colostate.edu/login?url=https://www.proquest.com/dissertations-theses/regenerative-engineering-temporomandibular-joint/docview/2488007836/se-2?accountid=10223

https://colostate.primo.exlibrisgroup.com/openurl/01COLSU_INST/01COLSU_INST:01COLSU?url_ver=Z39.88-2004&rft_val_fmt=info:ofi/fmt:kev:mtx:dissertation&genre=dissertations&sid=ProQ:ProQuest+Dissertations+%26+Theses+Global&atitle=&title=Regenerative+Engineering+of+the+Temporomandibular+Joint+in+a+Porcine+Model&issn=&date=2021-01-01&volume=&issue=&spage=&au=Chen%2C+David&isbn=9798569963157&jtitle=&btitle=&rft_id=info:eric/&rft_id=info:doi/

[172] D. F. Angelo *et al.*, "Choosing sheep (Ovis aries) as animal model for temporomandibular joint research: Morphological, histological and biomechanical characterization of the joint disc," *Morphologie,* vol. 100, no. 331, pp. 223-233, Dec 2016, doi: 10.1016/j.morpho.2016.06.002.

[173] M. Kaske, M. Beyerbach, Y. Hailu, W. Gobel, and S. Wagner, "The assessment of the frequency of chews during rumination enables an estimation of rumination activity in hay-fed sheep," *J Anim Physiol Anim Nutr (Berl),* vol. 86, no. 3-4, pp. 83-9, Apr 2002, doi: 10.1046/j.1439-0396.2002.00360.x.

[174] Y. B. Yan, Y. Zhang, Y. H. Gan, J. G. An, J. M. Li, and E. Xiao, "Surgical induction of TMJ bony ankylosis in growing sheep and the role of injury severity of the glenoid fossa on the development of bony ankylosis," *J Craniomaxillofac Surg,* vol. 41, no. 6, pp. 476-86, Sep 2013, doi: 10.1016/j.jcms.2012.03.011.

[175] O. Guven, M. Metin, and A. Keskin, "Remodelling in young sheep: a histological study of experimentally produced defects in TMJ," *Swiss Med Wkly,* vol. 133, no. 29-30, pp. 423-6, Jul 26 2003, doi: 2003/29/smw-10179.

[176] N. De Meurechy, D. Verwilghen, Y. De Brucker, B. Van Thielen, and M. Y. Mommaerts, "Lateral pterygoid muscle enthesis reconstruction in total temporomandibular joint replacement: An animal experiment with radiological correlation," *J Craniomaxillofac Surg,* vol. 49, no. 4, pp. 256-268, Apr 2021, doi: 10.1016/j.jcms.2021.01.029.

[177] D. F. Angelo *et al.*, "Preclinical randomized controlled trial of bilateral discectomy versus bilateral discopexy in Black Merino sheep temporomandibular joint: TEMPOJIMS - Phase 1- histologic, imaging and body weight results," *J Craniomaxillofac Surg,* vol. 46, no. 4, pp. 688-696, Apr 2018, doi: 10.1016/j.jcms.2018.01.006.

[178] P. Shen, S. Y. Zhang, C. Yang, and B. Yun, "Stability study of total temporomandibular joint replacement on sheep," *J Craniomaxillofac Surg,* vol. 42, no. 7, pp. 1265-70, Oct 2014, doi: 10.1016/j.jcms.2014.03.008.

[179] A. Erdemir, T. M. Guess, J. Halloran, S. C. Tadepalli, and T. M. Morrison, "Considerations for reporting finite element analysis studies in biomechanics," *J Biomech,* vol. 45, no. 4, pp. 625-33, Feb 23 2012, doi: 10.1016/j.jbiomech.2011.11.038.

[180] M. Cerrolaza, S. Shefelbine, and D. Garzón-Alvarado, *Numerical methods and advanced simulation in biomechanics and biological processes*. London, United Kingdom: Academic Press, an imprint of Elsevier, 2018, pp. xviii, 442 pages.

[181] E. L. Carniel, I. Toniolo, and C. G. Fontanella, "Computational Biomechanics: In-Silico Tools for the Investigation of Surgical Procedures and Devices," *Bioengineering (Basel),* vol. 7, no. 2, May 30 2020, doi: 10.3390/bioengineering7020048.

[182] W. M. S. Al Qahtani and M. I. El-Anwar, "Advanced Computational Methods in Bio-Mechanics," *Open Access Maced J Med Sci,* vol. 6, no. 4, pp. 742-746, Apr 15 2018, doi: 10.3889/oamjms.2018.149.

[183] S. C. Dogru, E. Cansiz, and Y. Z. Arslan, "A REVIEW OF FINITE ELEMENT APPLICATIONS IN ORAL AND MAXILLOFACIAL BIOMECHANICS," *Journal of Mechanics in Medicine and Biology,* vol. 18, no. 02, p. 1830002, 2018/03/01 2018, doi: 10.1142/S0219519418300028.
[184] Y. L. Rodrigues, M. T. Mathew, L. G. Mercuri, J. S. P. da Silva, B. Henriques, and J. C. M. Souza, "Biomechanical simulation of temporomandibular joint replacement (TMJR) devices: a scoping review of the finite element method," *Int J Oral Maxillofac Surg,* vol. 47, no. 8, pp. 1032-1042, Aug 2018, doi: 10.1016/j.ijom.2018.02.005.
[185] Y. Wu *et al.*, "Fluid pressurization and tractional forces during TMJ disc loading: A biphasic finite element analysis," *Orthod Craniofac Res,* vol. 20 Suppl 1, pp. 151-156, Jun 2017, doi: 10.1111/ocr.12147.
[186] E. Tanaka *et al.*, "Three-dimensional finite element analysis of human temporomandibular joint with and without disc displacement during jaw opening," *Medical Engineering & Physics,* vol. 26, no. 6, pp. 503-511, 2004/07/01/ 2004, doi: https://doi.org/10.1016/j.medengphy.2004.03.001.
[187] Z. Liu, Y. Qian, Y. Zhang, and Y. Fan, "Effects of several temporomandibular disorders on the stress distributions of temporomandibular joint: a finite element analysis," (in eng), no. 1476-8259 (Electronic).
[188] E. Hattori-Hara *et al.*, "The influence of unilateral disc displacement on stress in the contralateral joint with a normally positioned disc in a human temporomandibular joint: an analytic approach using the finite element method," (in eng), no. 1878-4119 (Electronic).
[189] R. del Pozo *et al.*, "Influence of friction at articular surfaces of the temporomandibular joint on stresses in the articular disk: a theoretical approach with the finite element method," (in eng), no. 0003-3219 (Print).
[190] M. Beek, J. H. Koolstra, L. J. van Ruijven, and T. M. van Eijden, "Three-dimensional finite element analysis of the cartilaginous structures in the human temporomandibular joint," *J Dent Res,* vol. 80, no. 10, pp. 1913-8, Oct 2001, doi: 10.1177/00220345010800101001.
[191] J. Ortún-Terrazas, J. Cegoñino, and A. Pérez del Palomar, "Biomechanical impact of the porous-fibrous tissue behaviour in the temporomandibular joint movements. An in silico approach," *Journal of the Mechanical Behavior of Biomedical Materials,* vol. 120, p. 104542, 2021/08/01/ 2021, doi: https://doi.org/10.1016/j.jmbbm.2021.104542.
[192] M. Beek, J. H. Koolstra, L. J. van Ruijven, and T. M. van Eijden, "Three-dimensional finite element analysis of the human temporomandibular joint disc," *J Biomech,* vol. 33, no. 3, pp. 307-16, Mar 2000, doi: 10.1016/s0021-9290(99)00168-2.
[193] P. S. Donzelli, R. L. Gallo Lm Fau - Spilker, S. Spilker Rl Fau - Palla, and S. Palla, "Biphasic finite element simulation of the TMJ disc from in vivo kinematic and geometric measurements," (in eng), no. 0021-9290 (Print), 2004.
[194] E. L. Bortel, B. Charbonnier, and R. Heuberger, "Development of a Synthetic Synovial Fluid for Tribological Testing," *Lubricants,* vol. 3, no. 4, 2015, doi: 10.3390/lubricants3040664.
[195] L. M. Gallo, L. R. Nickel Jc Fau - Iwasaki, S. Iwasaki Lr Fau - Palla, and S. Palla, "Stress-field translation in the healthy human temporomandibular joint," (in eng), no. 0022-0345 (Print), 2000.
[196] J. M. Middendorf, S. A. Albahrani, and L. J. Bonassar, "Stribeck Curve Analysis of Temporomandibular Joint Condylar Cartilage and Disc," *Journal of Biomechanical Engineering,* vol. 141, no. 12, 2019, doi: 10.1115/1.4045283.

[197] C. K. Hagandora, T. W. Chase, and A. J. Almarza, "A comparison of the mechanical properties of the goat temporomandibular joint disc to the mandibular condylar cartilage in unconfined compression," *J Dent Biomech,* vol. 2011, p. 212385, 2011, doi: 10.4061/2011/212385.
[198] S. Fazaeli, S. Ghazanfari, V. Everts, T. H. Smit, and J. H. Koolstra, "The contribution of collagen fibers to the mechanical compressive properties of the temporomandibular joint disc," *Osteoarthritis Cartilage,* vol. 24, no. 7, pp. 1292-301, Jul 2016, doi: 10.1016/j.joca.2016.01.138.
[199] G. Wu, C. Wang, and W. Zhang, "The factors of speeds and loads on the tribological properties of PVA-H/HA composites," *Journal of Applied Polymer Science,* vol. 106, no. 6, pp. 3908-3914, 2007, doi: https://doi.org/10.1002/app.27031.
[200] R. Ma, D. Xiong, F. Miao, J. Zhang, and Y. Peng, "Novel PVP/PVA hydrogels for articular cartilage replacement," *Materials Science and Engineering: C,* vol. 29, no. 6, pp. 1979-1983, 2009/08/01/ 2009, doi: https://doi.org/10.1016/j.msec.2009.03.010.
[201] S. E. Martinez Choy, J. Lenz, K. Schweizerhof, M. Schmitter, and H. J. Schindler, "Realistic kinetic loading of the jaw system during single chewing cycles: a finite element study," *J Oral Rehabil,* vol. 44, no. 5, pp. 375-384, May 2017, doi: 10.1111/joor.12501.
[202] J. H. Koolstra and T. M. van Eijden, "Combined finite-element and rigid-body analysis of human jaw joint dynamics," *J Biomech,* vol. 38, no. 12, pp. 2431-9, Dec 2005, doi: 10.1016/j.jbiomech.2004.10.014.
[203] C.-E. Wu, K.-H. Lin, and J.-Y. Juang, "Hertzian load–displacement relation holds for spherical indentation on soft elastic solids undergoing large deformations," *Tribology International,* vol. 97, pp. 71-76, 2016/05/01/ 2016, doi: https://doi.org/10.1016/j.triboint.2015.12.034.
[204] R. J. Young and P. A. Lovell, *Introduction to polymers*, 3rd ed. Boca Raton: CRC Press, 2011, pp. xx, 668.
[205] V. K. Stokes, *Introduction to plastics engineering*, Hoboken, NJ Chichester, West Sussex: Wiley ; ASME Press,, 2020, p. 1 online resource.
[206] N. Vapniarsky *et al.*, "Tissue engineering toward temporomandibular joint disc regeneration," *Sci Transl Med,* vol. 10, no. 446, Jun 20 2018, doi: 10.1126/scitranslmed.aaq1802.
[207] Y. Choi, M. H. Park, and K. Lee, "Tissue Engineering Strategies for Intervertebral Disc Treatment Using Functional Polymers," *Polymers (Basel),* vol. 11, no. 5, May 13 2019, doi: 10.3390/polym11050872.
[208] J. D. Drews *et al.*, "Spontaneous reversal of stenosis in tissue-engineered vascular grafts," *Sci Transl Med,* vol. 12, no. 537, Apr 1 2020, doi: 10.1126/scitranslmed.aax6919.
[209] Z. Z. Zhang *et al.*, "Orchestrated biomechanical, structural, and biochemical stimuli for engineering anisotropic meniscus," *Sci Transl Med,* vol. 11, no. 487, Apr 10 2019, doi: 10.1126/scitranslmed.aao0750.
[210] X. Li *et al.*, "Nanofiber-hydrogel composite-mediated angiogenesis for soft tissue reconstruction," *Sci Transl Med,* vol. 11, no. 490, May 1 2019, doi: 10.1126/scitranslmed.aau6210.
[211] S. E. Gullbrand *et al.*, "Long-term mechanical function and integration of an implanted tissue-engineered intervertebral disc," *Sci Transl Med,* vol. 10, no. 468, Nov 21 2018, doi: 10.1126/scitranslmed.aau0670.

[212] A. S. Hoffman, "Hydrogels for biomedical applications," *Adv Drug Deliv Rev,* vol. 54, no. 1, pp. 3-12, Jan 17 2002, doi: 10.1016/s0169-409x(01)00239-3.
[213] F. Asghari, M. Samiei, K. Adibkia, A. Akbarzadeh, and S. Davaran, "Biodegradable and biocompatible polymers for tissue engineering application: a review," *Artif Cells Nanomed Biotechnol,* vol. 45, no. 2, pp. 185-192, Mar 2017, doi: 10.3109/21691401.2016.1146731.
[214] D. Wu *et al.*, "Nanoengineered on-demand drug delivery system improves efficacy of pharmacotherapy for epilepsy," *Sci Adv,* vol. 8, no. 2, p. eabm3381, Jan 14 2022, doi: 10.1126/sciadv.abm3381.
[215] A. George, P. A. Shah, and P. S. Shrivastav, "Natural biodegradable polymers based nano-formulations for drug delivery: A review," *Int J Pharm,* vol. 561, pp. 244-264, Apr 20 2019, doi: 10.1016/j.ijpharm.2019.03.011.
[216] S. K. Prajapati, A. Jain, A. Jain, and S. Jain, "Biodegradable polymers and constructs: A novel approach in drug delivery," *European Polymer Journal,* vol. 120, p. 109191, 2019/11/01/ 2019, doi: https://doi.org/10.1016/j.eurpolymj.2019.08.018.
[217] A. R. Johnson *et al.*, "Drug eluting implants in pharmaceutical development and clinical practice," *Expert Opin Drug Deliv,* vol. 18, no. 5, pp. 577-593, May 2021, doi: 10.1080/17425247.2021.1856072.
[218] C. T. Laurencin, H. M. Pierre-Jacques, and R. Langer, "Toxicology and biocompatibility considerations in the evaluation of polymeric materials for biomedical applications," *Clin Lab Med,* vol. 10, no. 3, pp. 549-70, Sep 1990. [Online]. Available: https://www.ncbi.nlm.nih.gov/pubmed/2253450.
[219] J. Black, *Biological performance of materials : fundamentals of biocompatibility*, 4th ed. Boca Raton: CRC Taylor & Francis, 2006, p. 497 p.
[220] D. F. Williams, "On the mechanisms of biocompatibility," *Biomaterials,* vol. 29, no. 20, pp. 2941-53, Jul 2008, doi: 10.1016/j.biomaterials.2008.04.023.
[221] A. Remes and D. F. Williams, "Immune response in biocompatibility," *Biomaterials,* vol. 13, no. 11, pp. 731-43, 1992, doi: 10.1016/0142-9612(92)90010-l.
[222] D. F. Williams, "Specifications for Innovative, Enabling Biomaterials Based on the Principles of Biocompatibility Mechanisms," *Front Bioeng Biotechnol,* vol. 7, p. 255, 2019, doi: 10.3389/fbioe.2019.00255.
[223] K. F. Bowman, Jr., J. Fox, and J. K. Sekiya, "A clinically relevant review of hip biomechanics," *Arthroscopy,* vol. 26, no. 8, pp. 1118-29, Aug 2010, doi: 10.1016/j.arthro.2010.01.027.
[224] S. L. Woo, S. D. Abramowitch, R. Kilger, and R. Liang, "Biomechanics of knee ligaments: injury, healing, and repair," *J Biomech,* vol. 39, no. 1, pp. 1-20, 2006, doi: 10.1016/j.jbiomech.2004.10.025.
[225] J. C. Quarterman, S. M. Geary, and A. K. Salem, "Evolution of drug-eluting biomedical implants for sustained drug delivery," *Eur J Pharm Biopharm,* vol. 159, pp. 21-35, Feb 2021, doi: 10.1016/j.ejpb.2020.12.005.
[226] L. Yildirimer and A. M. Seifalian, "Three-dimensional biomaterial degradation - Material choice, design and extrinsic factor considerations," *Biotechnol Adv,* vol. 32, no. 5, pp. 984-99, Sep-Oct 2014, doi: 10.1016/j.biotechadv.2014.04.014.
[227] D. Umuhoza, F. Yang, D. Long, Z. Hao, J. Dai, and A. Zhao, "Strategies for Tuning the Biodegradation of Silk Fibroin-Based Materials for Tissue Engineering Applications," *ACS Biomater Sci Eng,* vol. 6, no. 3, pp. 1290-1310, Mar 9 2020, doi: 10.1021/acsbiomaterials.9b01781.

[228] B. Singh and N. Sharma, "Mechanistic implications of plastic degradation," *Polymer Degradation and Stability,* vol. 93, no. 3, pp. 561-584, 2008/03/01/ 2008, doi: https://doi.org/10.1016/j.polymdegradstab.2007.11.008.
[229] A. Gopferich, "Mechanisms of polymer degradation and erosion," *Biomaterials,* vol. 17, no. 2, pp. 103-14, Jan 1996, doi: 10.1016/0142-9612(96)85755-3.
[230] R. R. Pagar, S. R. Musale, G. Pawar, D. Kulkarni, and P. S. Giram, "Comprehensive Review on the Degradation Chemistry and Toxicity Studies of Functional Materials," *ACS Biomater Sci Eng,* vol. 8, no. 6, pp. 2161-2195, Jun 13 2022, doi: 10.1021/acsbiomaterials.1c01304.
[231] C. H. Bamford and C. F. H. Tipper, *Degradation of polymers* (Their Comprehensive chemical kinetics, no. 14). Amsterdam ; New York: Elsevier Scientific Pub. Co., 1975, pp. xv, 562 p.
[232] A. Imel, T. Malmgren, M. Dadmun, S. Gido, and J. Mays, "In vivo oxidative degradation of polypropylene pelvic mesh," *Biomaterials,* vol. 73, pp. 131-41, Dec 2015, doi: 10.1016/j.biomaterials.2015.09.015.
[233] M. S. Hahn, L. J. Taite, J. J. Moon, M. C. Rowland, K. A. Ruffino, and J. L. West, "Photolithographic patterning of polyethylene glycol hydrogels," *Biomaterials,* vol. 27, no. 12, pp. 2519-24, Apr 2006, doi: 10.1016/j.biomaterials.2005.11.045.
[234] M. P. Cuchiara, A. C. Allen, T. M. Chen, J. S. Miller, and J. L. West, "Multilayer microfluidic PEGDA hydrogels," *Biomaterials,* vol. 31, no. 21, pp. 5491-7, Jul 2010, doi: 10.1016/j.biomaterials.2010.03.031.
[235] S. Nemir, H. N. Hayenga, and J. L. West, "PEGDA hydrogels with patterned elasticity: Novel tools for the study of cell response to substrate rigidity," *Biotechnol Bioeng,* vol. 105, no. 3, pp. 636-44, Feb 15 2010, doi: 10.1002/bit.22574.
[236] I. Tomatsu, K. Peng, and A. Kros, "Photoresponsive hydrogels for biomedical applications," *Adv Drug Deliv Rev,* vol. 63, no. 14-15, pp. 1257-66, Nov 2011, doi: 10.1016/j.addr.2011.06.009.
[237] J. R. Choi, K. W. Yong, J. Y. Choi, and A. C. Cowie, "Recent advances in photo-crosslinkable hydrogels for biomedical applications," *Biotechniques,* vol. 66, no. 1, pp. 40-53, Jan 2019, doi: 10.2144/btn-2018-0083.
[238] M. B. Browning, S. N. Cereceres, P. T. Luong, and E. M. Cosgriff-Hernandez, "Determination of the in vivo degradation mechanism of PEGDA hydrogels," *J Biomed Mater Res A,* vol. 102, no. 12, pp. 4244-51, Dec 2014, doi: 10.1002/jbm.a.35096.
[239] M. B. Browning and E. Cosgriff-Hernandez, "Development of a biostable replacement for PEGDA hydrogels," *Biomacromolecules,* vol. 13, no. 3, pp. 779-86, Mar 12 2012, doi: 10.1021/bm201707z.
[240] C. Warr *et al.*, "Biocompatible PEGDA Resin for 3D Printing," *ACS Appl Bio Mater,* vol. 3, no. 4, pp. 2239-2244, Apr 20 2020, doi: 10.1021/acsabm.0c00055.
[241] G. V. Rathna, "Gelatin hydrogels: enhanced biocompatibility, drug release and cell viability," *J Mater Sci Mater Med,* vol. 19, no. 6, pp. 2351-8, Jun 2008, doi: 10.1007/s10856-007-3334-9.
[242] S. Ullm *et al.*, "Biocompatibility and inflammatory response in vitro and in vivo to gelatin-based biomaterials with tailorable elastic properties," *Biomaterials,* vol. 35, no. 37, pp. 9755-9766, Dec 2014, doi: 10.1016/j.biomaterials.2014.08.023.

[243] H. Shirahama, B. H. Lee, L. P. Tan, and N. J. Cho, "Precise Tuning of Facile One-Pot Gelatin Methacryloyl (GelMA) Synthesis," *Sci Rep,* vol. 6, p. 31036, Aug 9 2016, doi: 10.1038/srep31036.
[244] K. Yue, G. Trujillo-de Santiago, M. M. Alvarez, A. Tamayol, N. Annabi, and A. Khademhosseini, "Synthesis, properties, and biomedical applications of gelatin methacryloyl (GelMA) hydrogels," *Biomaterials,* vol. 73, pp. 254-71, Dec 2015, doi: 10.1016/j.biomaterials.2015.08.045.
[245] Y. Dong *et al.*, "A high-performance GelMA-GelMA homogeneous double-network hydrogel assisted by 3D printing," *J Mater Chem B,* vol. 10, no. 20, pp. 3906-3915, May 25 2022, doi: 10.1039/d2tb00330a.
[246] A. C. Daly, P. Pitacco, J. Nulty, G. M. Cunniffe, and D. J. Kelly, "3D printed microchannel networks to direct vascularisation during endochondral bone repair," *Biomaterials,* vol. 162, pp. 34-46, Apr 2018, doi: 10.1016/j.biomaterials.2018.01.057.
[247] M. Sun, X. Sun, Z. Wang, S. Guo, G. Yu, and H. Yang, "Synthesis and Properties of Gelatin Methacryloyl (GelMA) Hydrogels and Their Recent Applications in Load-Bearing Tissue," *Polymers,* vol. 10, no. 11, 2018, doi: 10.3390/polym10111290.
[248] S. Xiao *et al.*, "Gelatin Methacrylate (GelMA)-Based Hydrogels for Cell Transplantation: an Effective Strategy for Tissue Engineering," *Stem Cell Rev Rep,* vol. 15, no. 5, pp. 664-679, Oct 2019, doi: 10.1007/s12015-019-09893-4.
[249] N. B. Halima, "Poly (vinyl alcohol): review of its promising applications and insights into biodegradation," *RSC advances,* vol. 6, no. 46, pp. 39823-39832, 2016.
[250] M. Aslam, M. A. Kalyar, and Z. A. Raza, "Polyvinyl alcohol: A review of research status and use of polyvinyl alcohol based nanocomposites," *Polymer Engineering & Science,* vol. 58, no. 12, pp. 2119-2132, 2018.
[251] C. M. Hassan and N. A. Peppas, "Structure and morphology of freeze/thawed PVA hydrogels," *Macromolecules,* vol. 33, no. 7, pp. 2472-2479, 2000.
[252] A. Kumar and S. S. Han, "PVA-based hydrogels for tissue engineering: A review," *International Journal of Polymeric Materials and Polymeric Biomaterials,* vol. 66, no. 4, pp. 159-182, 2017/03/04 2017, doi: 10.1080/00914037.2016.1190930.
[253] C. Borges, R. Colaço, and A. Paula Serro, "Poly(vinyl alcohol)-based hydrogels for joint prosthesis," *Annals of Medicine,* vol. 51, no. sup1, pp. 105-105, 2019/03/29 2019, doi: 10.1080/07853890.2018.1562711.
[254] V. M. Sardinha, L. L. Lima, W. D. Belangero, C. A. Zavaglia, V. P. Bavaresco, and J. R. Gomes, "Tribological characterization of polyvinyl alcohol hydrogel as substitute of articular cartilage," *Wear,* vol. 301, no. 1, pp. 218-225, 2013/04/01/ 2013, doi: https://doi.org/10.1016/j.wear.2012.11.054.
[255] G. Paradossi, F. Cavalieri, E. Chiessi, C. Spagnoli, and M. K. Cowman, "Poly(vinyl alcohol) as versatile biomaterial for potential biomedical applications," *Journal of Materials Science: Materials in Medicine,* vol. 14, no. 8, pp. 687-691, 2003/08/01 2003, doi: 10.1023/A:1024907615244.
[256] H. F. Wu, L. Z. Yue, S. L. Jiang, Y. Q. Lu, Y. X. Wu, and Z. Y. Wan, "Biodegradation of polyvinyl alcohol by different dominant degrading bacterial strains in a baffled anaerobic bioreactor," *Water Sci Technol,* vol. 79, no. 10, pp. 2005-2012, May 2019, doi: 10.2166/wst.2019.202.
[257] D. A. Bichara *et al.*, "Porous Poly(vinyl alcohol)-Alginate Gel Hybrid Construct for Neocartilage Formation Using Human Nasoseptal Cells," *Journal of Surgical Research,*

vol. 163, no. 2, pp. 331-336, 2010/10/01/ 2010, doi: https://doi.org/10.1016/j.jss.2010.03.070.
[258] T. Noguchi *et al.*, "Poly(vinyl alcohol) hydrogel as an artificial articular cartilage: Evaluation of biocompatibility," *Journal of Applied Biomaterials,* vol. 2, no. 2, pp. 101-107, 1991, doi: https://doi.org/10.1002/jab.770020205.
[259] N. Alexandre *et al.*, "Biocompatibility and hemocompatibility of polyvinyl alcohol hydrogel used for vascular grafting--In vitro and in vivo studies," *J Biomed Mater Res A,* vol. 102, no. 12, pp. 4262-75, Dec 2014, doi: 10.1002/jbm.a.35098.
[260] B. H. Wang and G. Campbell, "Formulations of polyvinyl alcohol cryogel that mimic the biomechanical properties of soft tissues in the natural lumbar intervertebral disc," (in eng), no. 1528-1159 (Electronic), 2009.
[261] M. Kobayashi, Y. S. Chang, and M. Oka, "A two year in vivo study of polyvinyl alcohol-hydrogel (PVA-H) artificial meniscus," *Biomaterials,* vol. 26, no. 16, pp. 3243-8, Jun 2005, doi: 10.1016/j.biomaterials.2004.08.028.
[262] N. Alexandre *et al.*, "Long term performance evaluation of small-diameter vascular grafts based on polyvinyl alcohol hydrogel and dextran and MSCs-based therapies using the ovine pre-clinical animal model," *Int J Pharm,* vol. 523, no. 2, pp. 515-530, May 25 2017, doi: 10.1016/j.ijpharm.2017.02.043.
[263] A. N. Suciu, T. Iwatsubo, M. Matsuda, and T. Nishino, "A Study upon Durability of the Artificial Knee Joint with PVA Hydrogel Cartilage," *JSME International Journal Series C Mechanical Systems, Machine Elements and Manufacturing,* vol. 47, no. 1, pp. 199-208, 2004, doi: 10.1299/jsmec.47.199.
[264] M. Kobayashi and H. S. Hyu, "Development and Evaluation of Polyvinyl Alcohol-Hydrogels as an Artificial Atrticular Cartilage for Orthopedic Implants," (in eng), *Materials (Basel),* vol. 3, no. 4, pp. 2753-2771, 2010, doi: 10.3390/ma3042753.
[265] M. I. Baker, Z. Walsh Sp Fau - Schwartz, B. D. Schwartz Z Fau - Boyan, and B. D. Boyan, "A review of polyvinyl alcohol and its uses in cartilage and orthopedic applications," (in eng), no. 1552-4981 (Electronic), 2006.
[266] N. Jiang, Y. Yang, L. Zhang, Y. Jiang, M. Wang, and S. Zhu, "3D-Printed Polycaprolactone Reinforced Hydrogel as an Artificial TMJ Disc," (in eng), no. 1544-0591 (Electronic).
[267] N. Siddiqui, S. Asawa, B. Birru, R. Baadhe, and S. Rao, "PCL-Based Composite Scaffold Matrices for Tissue Engineering Applications," *Mol Biotechnol,* vol. 60, no. 7, pp. 506-532, Jul 2018, doi: 10.1007/s12033-018-0084-5.
[268] E. H. Backes *et al.*, "Polycaprolactone usage in additive manufacturing strategies for tissue engineering applications: A review," *J Biomed Mater Res B Appl Biomater,* vol. 110, no. 6, pp. 1479-1503, Jun 2022, doi: 10.1002/jbm.b.34997.
[269] B. Shiroud Heidari, R. Ruan, E. M. De-Juan-Pardo, M. Zheng, and B. Doyle, "Biofabrication and Signaling Strategies for Tendon/Ligament Interfacial Tissue Engineering," *ACS Biomater Sci Eng,* vol. 7, no. 2, pp. 383-399, Feb 8 2021, doi: 10.1021/acsbiomaterials.0c00731.
[270] N. Poomathi *et al.*, "3D printing in tissue engineering: a state of the art review of technologies and biomaterials," *Rapid Prototyping Journal,* 2020.
[271] M. Labet and W. Thielemans, "Synthesis of polycaprolactone: a review," *Chem Soc Rev,* vol. 38, no. 12, pp. 3484-504, Dec 2009, doi: 10.1039/b820162p.

[272] M. Bartnikowski, T. R. Dargaville, S. Ivanovski, and D. W. Hutmacher, "Degradation mechanisms of polycaprolactone in the context of chemistry, geometry and environment," *Progress in Polymer Science,* vol. 96, pp. 1-20, 2019/09/01/ 2019, doi: https://doi.org/10.1016/j.progpolymsci.2019.05.004.
[273] J. Peña, T. Corrales, I. Izquierdo-Barba, A. L. Doadrio, and M. Vallet-Regí, "Long term degradation of poly(ε-caprolactone) films in biologically related fluids," *Polymer Degradation and Stability,* vol. 91, no. 7, pp. 1424-1432, 2006/07/01/ 2006, doi: https://doi.org/10.1016/j.polymdegradstab.2005.10.016.
[274] R. Dwivedi *et al.*, "Polycaprolactone as biomaterial for bone scaffolds: Review of literature," *Journal of oral biology and craniofacial research,* vol. 10, no. 1, pp. 381-388, 2020.
[275] C. Maier and T. Calafut, *Polypropylene : the definitive user's guide and databook* (PDL handbook series). Norwich, NY: Plastics Design Library, 1998, pp. xx, 432 p.
[276] S. Saxena *et al.*, "Development of a new polypropylene-based suture: plasma grafting, surface treatment, characterization, and biocompatibility studies," *Macromol Biosci,* vol. 11, no. 3, pp. 373-82, Mar 10 2011, doi: 10.1002/mabi.201000298.
[277] C. C. Chu, L. Pratt, L. Zhang, A. Hsu, and A. Chu, "A comparison of a new polypropylene suture with Prolene," *J Appl Biomater,* vol. 4, no. 2, pp. 169-81, Summer 1993, doi: 10.1002/jab.770040209.
[278] W. S. Cobb, K. W. Kercher, and B. T. Heniford, "The argument for lightweight polypropylene mesh in hernia repair," *Surg Innov,* vol. 12, no. 1, pp. 63-9, Mar 2005, doi: 10.1177/155335060501200109.
[279] N. Mangir, B. Aldemir Dikici, C. R. Chapple, and S. MacNeil, "Landmarks in vaginal mesh development: polypropylene mesh for treatment of SUI and POP," *Nat Rev Urol,* vol. 16, no. 11, pp. 675-689, Nov 2019, doi: 10.1038/s41585-019-0230-2.
[280] H. J. Oswald and E. Turi, "The deterioration of polypropylene by oxidative degradation," *Polymer Engineering & Science,* https://doi.org/10.1002/pen.760050312 vol. 5, no. 3, pp. 152-158, 1965/07/01 1965, doi: https://doi.org/10.1002/pen.760050312.
[281] F. H. Greca *et al.*, "The influence of differing pore sizes on the biocompatibility of two polypropylene meshes in the repair of abdominal defects. Experimental study in dogs," *Hernia,* vol. 5, no. 2, pp. 59-64, Jun 2001, doi: 10.1007/s100290100001.
[282] M. Kelly, K. Macdougall, O. Olabisi, and N. McGuire, "In vivo response to polypropylene following implantation in animal models: a review of biocompatibility," *Int Urogynecol J,* vol. 28, no. 2, pp. 171-180, Feb 2017, doi: 10.1007/s00192-016-3029-1.
[283] T. Saha *et al.*, "Surface-Functionalized Polypropylene Surgical Mesh for Enhanced Performance and Biocompatibility," *ACS Appl Bio Mater,* vol. 2, no. 12, pp. 5905-5915, Dec 16 2019, doi: 10.1021/acsabm.9b00849.
[284] K. Ragaert, I. De Baere, L. Cardon, and J. Degrieck, "Bulk mechanical properties of thermoplastic poly-e-caprolactone," in *6th Polymers & Mould Innovations International Conference*, 2014, pp. 339-344.
[285] "MatWeb : Material Property Data," (in English). [Online]. Available: https://www.matweb.com/.
[286] M. Parlato, S. Reichert, N. Barney, and W. L. Murphy, "Poly(ethylene glycol) hydrogels with adaptable mechanical and degradation properties for use in biomedical applications," *Macromol Biosci,* vol. 14, no. 5, pp. 687-98, May 2014, doi: 10.1002/mabi.201300418.

[287] V. B. Morris, S. Nimbalkar, M. Younesi, P. McClellan, and O. Akkus, "Mechanical Properties, Cytocompatibility and Manufacturability of Chitosan:PEGDA Hybrid-Gel Scaffolds by Stereolithography," *Ann Biomed Eng,* vol. 45, no. 1, pp. 286-296, Jan 2017, doi: 10.1007/s10439-016-1643-1.

[288] S. R. Shin *et al.*, "Reduced Graphene Oxide-GelMA Hybrid Hydrogels as Scaffolds for Cardiac Tissue Engineering," *Small,* vol. 12, no. 27, pp. 3677-89, Jul 2016, doi: 10.1002/smll.201600178.

[289] L. Gu *et al.*, "Preparation and characterization of methacrylated gelatin/bacterial cellulose composite hydrogels for cartilage tissue engineering," *Regen Biomater,* vol. 7, no. 2, pp. 195-202, Mar 2020, doi: 10.1093/rb/rbz050.

[290] B. Kong *et al.*, "Fiber reinforced GelMA hydrogel to induce the regeneration of corneal stroma," *Nat Commun,* vol. 11, no. 1, p. 1435, Mar 18 2020, doi: 10.1038/s41467-020-14887-9.

[291] Y. Shi and D. Xiong, "Microstructure and friction properties of PVA/PVP hydrogels for articular cartilage repair as function of polymerization degree and polymer concentration," *Wear,* vol. 305, no. 1, pp. 280-285, 2013/07/30/ 2013, doi: https://doi.org/10.1016/j.wear.2012.12.020.

[292] K. M. Labus and C. M. Puttlitz, "An anisotropic hyperelastic constitutive model of brain white matter in biaxial tension and structural-mechanical relationships," *J Mech Behav Biomed Mater,* vol. 62, pp. 195-208, Sep 2016, doi: 10.1016/j.jmbbm.2016.05.003.

[293] C. A. Schneider, W. S. Rasband, and K. W. Eliceiri, "NIH Image to ImageJ: 25 years of image analysis," *Nat Methods,* vol. 9, no. 7, pp. 671-5, Jul 2012, doi: 10.1038/nmeth.2089.

[294] J. L. Holloway, A. M. Lowman, and G. R. Palmese, "Mechanical evaluation of poly(vinyl alcohol)-based fibrous composites as biomaterials for meniscal tissue replacement," *Acta Biomaterialia,* vol. 6, no. 12, pp. 4716-4724, 2010/12/01/ 2010, doi: https://doi.org/10.1016/j.actbio.2010.06.025.

[295] S. Duan *et al.*, "Tendon-inspired anti-freezing tough gels," *iScience,* vol. 24, no. 9, p. 102989, 2021/09/24/ 2021, doi: https://doi.org/10.1016/j.isci.2021.102989.

[296] F. Yang *et al.*, "A Synthetic Hydrogel Composite with the Mechanical Behavior and Durability of Cartilage," *Advanced Functional Materials,* vol. 30, no. 36, p. 2003451, 2020, doi: https://doi.org/10.1002/adfm.202003451.

[297] J. P. Kuiper, C. M. Puttlitz, J. E. Rawlinson, R. Dobbs, and K. M. Labus, "A mechanical evaluation of polyvinyl alcohol hydrogels for temporomandibular joint disc replacement," *Frontiers in Physics,* vol. 10, p. 928579, 2022.

[298] L. Gu *et al.*, "Preparation and characterization of methacrylated gelatin/bacterial cellulose composite hydrogels for cartilage tissue engineering," *Regenerative Biomaterials,* vol. 7, no. 2, pp. 195-202, 2020, doi: 10.1093/rb/rbz050.

[299] L. Lin, Y. Xu, J. Qin, S. Wang, M. Xiao, and Y. Meng, "Correlation Between Crystallization Behavior and Mechanical Properties of Biodegradable Poly(Caprolactone-co-Cyclohexene Carbonate)," *Polymer-Plastics Technology and Engineering,* vol. 57, no. 15, pp. 1530-1541, 2018/10/13 2018, doi: 10.1080/03602559.2017.1410839.

[300] H. Kotturi *et al.*, "Evaluation of Polyethylene Glycol Diacrylate-Polycaprolactone Scaffolds for Tissue Engineering Applications. LID - 10.3390/jfb8030039 [doi] LID - 39," (in eng), no. 2079-4983 (Print), 2017.

[301] C. K. Hagandora, A. J. Chase Tw Fau - Almarza, and A. J. Almarza, "A comparison of the mechanical properties of the goat temporomandibular joint disc to the mandibular condylar cartilage in unconfined compression," (in eng), no. 1758-7360 (Electronic), 2011.
[302] S. Eshraghi and S. Das, "Mechanical and microstructural properties of polycaprolactone scaffolds with one-dimensional, two-dimensional, and three-dimensional orthogonally oriented porous architectures produced by selective laser sintering," *Acta Biomaterialia,* vol. 6, no. 7, pp. 2467-2476, 2010/07/01/ 2010, doi: https://doi.org/10.1016/j.actbio.2010.02.002.
[303] D. Tranchida and S. Piccarolo, "Relating morphology to nanoscale mechanical properties: from crystalline to mesomorphic iPP," *Polymer,* vol. 46, no. 12, pp. 4032-4040, 2005/05/26/ 2005, doi: https://doi.org/10.1016/j.polymer.2005.03.055.
[304] P. Tordjeman, C. Robert, G. Marin, and P. Gerard, "The effect of α, β crystalline structure on the mechanical properties of polypropylene," *The European Physical Journal E,* vol. 4, no. 4, pp. 459-465, 2001.
[305] M. S. Detamore, K. A. Athanasiou, and J. Mao, "A call to action for bioengineers and dental professionals: directives for the future of TMJ bioengineering," *Ann Biomed Eng,* vol. 35, no. 8, pp. 1301-11, Aug 2007, doi: 10.1007/s10439-007-9298-6.
[306] J. Sanchez-Adams, A. L. Leddy Ha Fau - McNulty, C. J. McNulty Al Fau - O'Conor, F. O'Conor Cj Fau - Guilak, and F. Guilak, "The mechanobiology of articular cartilage: bearing the burden of osteoarthritis," (in eng), no. 1534-6307 (Electronic), 2014.
[307] S. Teng, M. Xu Y Fau - Cheng, Y. Cheng M Fau - Li, and Y. Li, "Biomechanical properties and collagen fiber orientation of temporomandibular joint discs in dogs: 2. Tensile mechanical properties of the discs," (in eng), no. 0890-2739 (Print), 1991.
[308] S. Wu *et al.*, "Poly(vinyl alcohol) Hydrogels with Broad-Range Tunable Mechanical Properties via the Hofmeister Effect," *Advanced Materials,* vol. 33, no. 11, p. 2007829, 2021, doi: https://doi.org/10.1002/adma.202007829.
[309] B. K. Tan, Y. C. Ching, S. C. Poh, L. C. Abdullah, and S. N. Gan, "A Review of Natural Fiber Reinforced Poly(Vinyl Alcohol) Based Composites: Application and Opportunity," *Polymers,* vol. 7, no. 11, pp. 2205-2222, 2015. [Online]. Available: https://www.mdpi.com/2073-4360/7/11/1509.
[310] L. E. Beckett, J. T. Lewis, T. K. Tonge, and L. T. J. Korley, "Enhancement of the Mechanical Properties of Hydrogels with Continuous Fibrous Reinforcement," *ACS Biomaterials Science & Engineering,* vol. 6, no. 10, pp. 5453-5473, 2020/10/12 2020, doi: 10.1021/acsbiomaterials.0c00911.
[311] J. S. Gonzalez and V. A. Alvarez, "The effect of the annealing on the poly(vinyl alcohol) obtained by freezing–thawing," *Thermochimica Acta,* vol. 521, no. 1, pp. 184-190, 2011/07/10/ 2011, doi: https://doi.org/10.1016/j.tca.2011.04.022.
[312] W.-I. Cha, S.-H. Hyon, M. Oka, and Y. Ikada, "Mechanical and wear properties of poly(vinyl alcohol) hydrogels," *Macromolecular Symposia,* vol. 109, no. 1, pp. 115-126, 1996, doi: https://doi.org/10.1002/masy.19961090111.
[313] R. Balint, T. Lowe, and T. Shearer, "Optimal Contrast Agent Staining of Ligaments and Tendons for X-Ray Computed Tomography," *PLoS One,* vol. 11, no. 4, p. e0153552, 2016, doi: 10.1371/journal.pone.0153552.
[314] P. A. Yushkevich *et al.*, "User-guided 3D active contour segmentation of anatomical structures: Significantly improved efficiency and reliability," *NeuroImage,* vol. 31, no. 3, pp. 1116-1128, 2006/07/01/ 2006, doi: https://doi.org/10.1016/j.neuroimage.2006.01.015.

[315] T. Eiter and H. Mannila, "Computing discrete Fréchet distance," 1994.
[316] J. M. Thompson and H. H. Meyer, "Body condition scoring of sheep," 1994.
[317] K. Ou, X. Dong, C. Qin, X. Ji, and J. He, "Properties and toughening mechanisms of PVA/PAM double-network hydrogels prepared by freeze-thawing and anneal-swelling," *Mater Sci Eng C Mater Biol Appl,* vol. 77, pp. 1017-1026, Aug 1 2017, doi: 10.1016/j.msec.2017.03.287.
[318] M. Sun *et al.*, "Multifunctional tendon-mimetic hydrogels," *Sci Adv,* vol. 9, no. 7, p. eade6973, Feb 17 2023, doi: 10.1126/sciadv.ade6973.
[319] M. Page, K. Baer, B. Schon, N. Mekhileri, T. Woodfield, and C. Puttlitz, "Biaxial mechanics of 3D fiber deposited ply-laminate scaffolds for soft tissue engineering part I: Experimental evaluation," *J Mech Behav Biomed Mater,* vol. 98, pp. 317-326, Oct 2019, doi: 10.1016/j.jmbbm.2019.06.029.
[320] M. Page and C. Puttlitz, "Biaxial mechanics of 3D fiber deposited ply-laminate scaffolds for soft tissue engineering part II: Finite element analyses," *J Mech Behav Biomed Mater,* vol. 100, p. 103395, Dec 2019, doi: 10.1016/j.jmbbm.2019.103395.
[321] S. K. Mallapragada and N. A. Peppas, "Dissolution mechanism of semicrystalline poly(vinyl alcohol) in water," *Journal of Polymer Science Part B: Polymer Physics,* vol. 34, no. 7, pp. 1339-1346, 1996, doi: https://doi.org/10.1002/(SICI)1099-0488(199605)34:7<1339::AID-POLB15>3.0.CO;2-B.
[322] A. Kashi and S. Saha, "15 - Failure mechanisms of medical implants and their effects on outcomes," in *Biointegration of Medical Implant Materials (Second Edition)*, C. P. Sharma Ed.: Woodhead Publishing, 2020, pp. 407-432.
[323] M. I. Baker, S. P. Walsh, Z. Schwartz, and B. D. Boyan, "A review of polyvinyl alcohol and its uses in cartilage and orthopedic applications," *Journal of Biomedical Materials Research Part B: Applied Biomaterials,* vol. 100B, no. 5, pp. 1451-1457, 2012, doi: https://doi.org/10.1002/jbm.b.32694.
[324] T. A. Larheim, "Role of Magnetic Resonance Imaging in the Clinical Diagnosis of the Temporomandibular Joint," *Cells Tissues Organs,* vol. 180, no. 1, pp. 6-21, 2005, doi: 10.1159/000086194.